Dissertation

submitted to the

combined Faculties for the Natural Sciences and for Mathematics

of the Ruperto-Carola University of Heidelberg, Germany

for the degree of Doctor of Natural Sciences

Presented by

Mostafa Zedan, M.Sc. Bioscience
Born in Cairo, Egypt
Oral examination: 25.01.2018

Analysis of the role of N-terminal acetylation of newly synthesized proteins in *Saccharomyces cerevisiae*

Referees: Prof. Dr. Bernd Bukau
Prof. Dr. Marius Lemberg

Summary:

N-terminal acetylation is a conserved co-translational protein modification that is highly abundant among eukaryotes. In *Saccharomyces cerevisiae*, at least five enzymes with distinct substrate specificities (N-terminal acetyl transferase Nat A to E) act to acetylate 50–70% of the yeast proteins. Despite being one of the most common protein modifications, its biological significance remains largely ambiguous. I set out to study the role of N-terminal acetylation in yeast cells by employing quantitative proteomics and ribosome profiling for analysis of the consequences of failure of N-terminal acetylation in strains lacking specific N-terminal acetyl transferases. My results revealed a multi-faceted stress response in *natB* deletion mutant that modulates protein quality control machinery, protein biogenesis capacity, and energy regeneration pathways in order to establish protein homeostasis. Systematic analysis of proteome stability in the *natB* deletion mutant suggests no global effect of the loss of N-terminal acetylation on the turnover of NatB substrates, but an increase in the level of global protein aggregation. SILAC-based mass spectrometry analysis of aggregated proteins isolated from the *natB* deletion mutant shows no significant enrichment of NatB substrates, indicating that protein aggregation in the *natB* deletion mutant cannot be solely explained as a direct consequence of the loss of N-terminal acetylation. In contrast, these protein aggregates show strong enrichment for components of specific biological pathways, in particular of the translation apparatus, suggesting an underlying selective sequestration mechanism. Consistently, quantitative proteomics revealed that, on average, approximately 40% of each of the quantified ribosomal proteins is sequestered into protein aggregates in the *natB* deletion mutant. Moreover, the aggregated proteins showed significantly higher interaction between each other and overlapped with aggregated proteins generated upon environmental stress, suggesting a common mode of sequestration of proteins into aggregates. Interestingly, the aggregated proteins in the *natB* deletion mutant strongly overlap with those identified upon deletion of the genes encoding the ribosome-associated Hsp70 chaperone Ssb. In addition, deletion of *SSB* in the *natB* deletion mutant leads to synthetic growth defects. Moreover, isolation of radiolabeled protein aggregates after 5 min ^{35}S pulse labeling showed that a fraction of the newly synthesized proteins is readily sequestered into aggregates. These findings together suggest a new link between N-terminal acetylation by NatB and co-translational protein folding activity by Ssb. Parallel analysis of *natA* deletion mutant revealed similar protein aggregation patterns, suggesting a general role of N-terminal acetylation in the maintenance of proteome integrity.

Contents

1 Introduction

1.1 Maintenance of proteome homeostasis in the eukaryotic model organism *S. cerevisiae*

The yeast proteome is the result of continuous protein biogenesis by mRNA translation, and protein degradation. Ultimately, the balance between the two pathways optimizes protein steady state levels. Under nutrient availability, a yeast cell is predicted to produce as many as 13,000 proteins per second (Haar, 2008). The massive influx of proteins from the translation machinery demands efficient systems supporting protein folding, protein targeting to subcellular compartments, as well as enzymatic processing to ensure proper functionality of the newly synthesized proteins. Under challenging environmental conditions, yeast cells can mount an environmental stress response that aims to modulate proteome homoeostasis pathways by down-regulating protein biogenesis, while up-regulating the protein quality control machinery. Global analysis of the effects of genetic and environmental perturbations on proteome homoeostasis has become possible by recent developments in the field of deep sequencing and proteomics, as well as the power of yeast genetics.

1.1.1 Protein biogenesis

1.1.1.1 The yeast translation machinery

At the core of the yeast translation machinery is the ribosome. The core function of the ribosome is to translate the genetic code of the messenger RNA (mRNA) into a protein. On average, a yeast cell contains as many as 200,000 ribosomes (Warner, 1999). Translation of mRNA into protein by the ribosome is accomplished in coordination with specialized transfer RNA or tRNA. tRNAs are non-coding RNAs that act as adapter molecules that specifically recognize the triplet genetic code on the mRNA by their anticoding loop, while bearing the corresponding amino acid covalently attached to their 3' end. Twenty different aminoacyl tRNA synthetases (corresponding to the 20 different amino acids) catalyze the covalent modification of tRNAs with their corresponding amino acids depending of the anti-codon as well as other recognition elements of each tRNA (Pang et al., 2014). In addition, a group of proteins named "Translation Factors" act together with the translation apparatus to coordinate the different steps of the translation of the mRNA sequence into a polypeptide chain.

The ribosome is a ribonucleoprotein complex composed of one small subunit (40S), and one large subunit (60S). The yeast small subunit consists of 33 proteins as well as the18S RNA **(Figure 1A)**, while the yeast large subunit is composed of 46 proteins and three RNA molecules: 5S RNA, 5.8S RNA and 25S RNA **(Figure 1B)**. Recent reports revealed heterogeneous composition of ribosomes, suggesting potential functional specializations (Xue and Barna, 2012). The small subunit harbors the decoding

activity needed for tRNA selection based on the mRNA sequence **(Figure 1C)**, and its major functional sites are the mRNA path, as well as the decoding site where the codon-anticodon base pairing takes place, together establishing the fidelity of the translation process **(Figure 1C)**. On the other hand, the large subunit is responsible for peptide bond formation, and its major structural features are the peptidyl transferase center (PTC) which catalyzes peptide bond formation, as well as a 10-20°A wide peptide exit tunnel that spans the entire body of the 60S, where the nascent chain emerges during synthesis **(Figure 1D-E).** At the interface side of the two ribosomal subunits exist the tRNA binding sites: A-site (where the amoinoacyl tRNA binds), P-site (where the peptidyl tRNA binds) and E-site (where the de-acylated tRNA leaves the ribosome) (**Figure 1C**)**.** The two subunits assemble together through multiple contact points called “Bridges”, leading to the formation of the 80S ribosome (Ben-Shem et al., 2011; Jenner et al., 2012; Melnikov et al., 2012; Wilson and Doudna Cate, 2012; Yusupova and Yusupov, 2014).

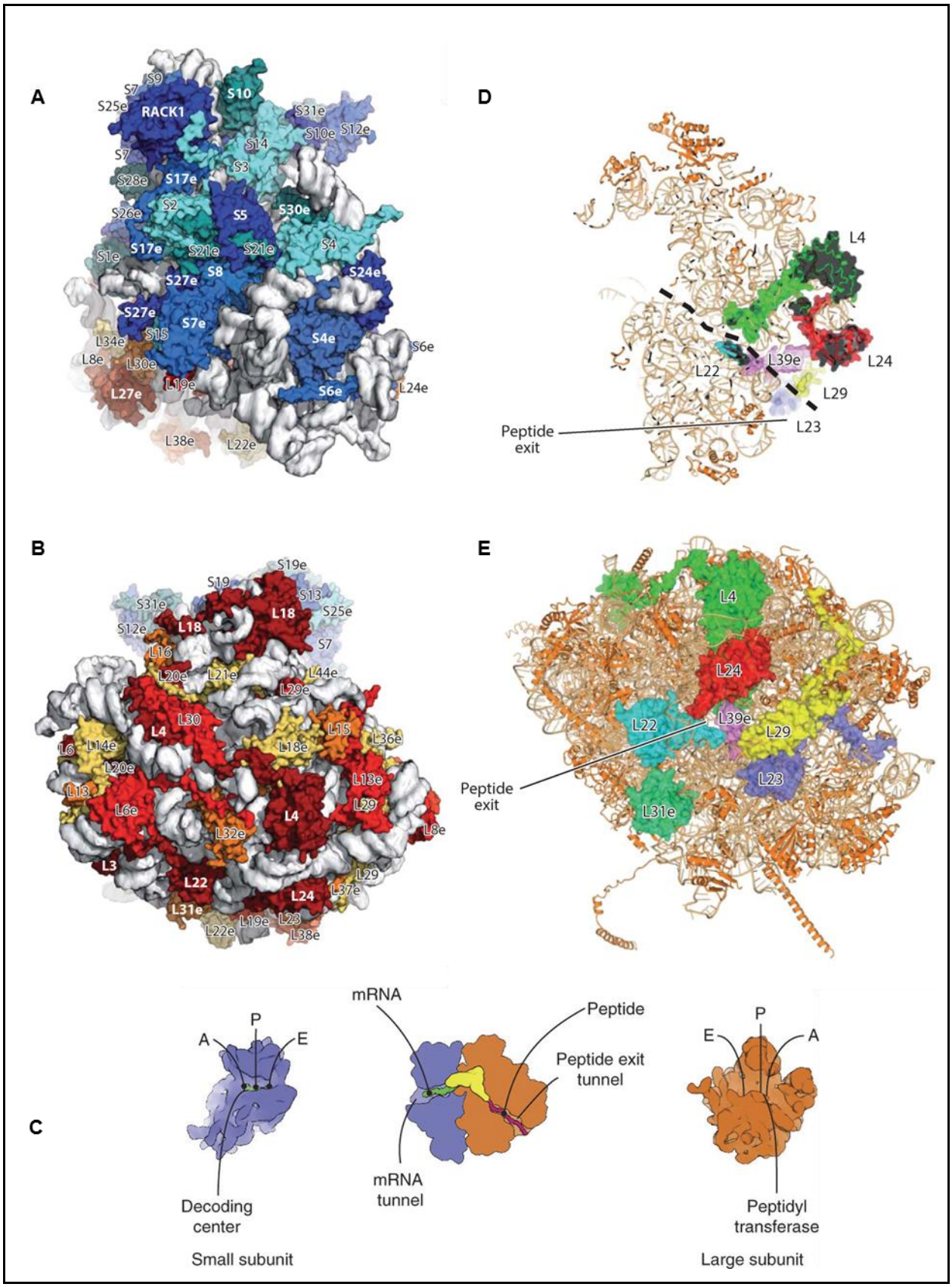
A
S9
S7
S25e
RACK1
S10
S31e
S10e
S12e
S14
S7
S3
S28e
S17e
S26e
S2
S5
S30e
S1e
S17e
S21e
S21e
S4
S8
S24e
S27e
S27e
S7e
S15
S4e
S6e
L34e
L8e
L30e
L19e
L27e
S6e
L24e
L38e
L22e
D
L4
L39e
L24
L22
L29
L23
Peptide exit
B
S19e
S19
S31e
S13
S25e
S12e
L18
L18
S7
L16
L20e
L21e
L44e
L29e
L30
L4
L15
L36e
L6
L14e
L18e
L20e
L13e
L13
L29
L6e
L4
L32e
L8e
L3
L29
L22
L24
L37e
L31e
L19e
L23
L22e
L38e
E
L4
L24
L22
L39e
L29
Peptide exit
L23
L31e
C
P
A
E
Decoding center
Small subunit
mRNA
Peptide
Peptide exit tunnel
mRNA tunnel
P
E
A
Peptidyl transferase
Large subunit

Figure 1: Structure and function of the yeast 80S ribosome.

A. Structure of the 40S subunit: Small subunit ribosomal proteins are colored blue, cyan and teal. Ribosomal RNA is colored in grey (Yusupova and Yusupov, 2014).
B. Structure of the 60S subunit: Large subunit ribosomal proteins are colored red, orange and yellow. Ribosomal RNA is colored in grey (Yusupova and Yusupov, 2014).
C. The functional centers of the ribosome: The small subunit harbors the decoding center of the ribosome and the mRNA tunnel. The large subunit harbors the PTC and the peptide exit tunnel (Melnikov et al., 2012).
D. The peptide exit tunnel viewed in a slice of the large ribosomal subunit (Yusupova and Yusupov, 2014).
E. Ribosomal proteins surrounding the outer rim of the peptide exit tunnel (Yusupova and Yusupov, 2014).

1.1.1.2 The mechanism of protein synthesis

Translation is multi-step process that can be divided into four major phases: Initiation, elongation, termination and recycling **(Figure 2)**. Translation initiation is the process during which the 40S bound to the initiator methionine tRNA scans along the mRNA starting at the 5' cap structure until it finds the start codon, and it is completed by the assembly of the 60S and 40S to form the 80S. Translation elongation is the process where the extension of the polypeptide takes places based on the genetic code of the mRNA. Translation termination starts when the ribosome encounters a stop codon, and it ends by the release of the polypeptide from the ribosome, followed by the dis-assembly of the 80S into 40S and 60S (ribosome recycling) (Dever et al., 2016; Dever and Green, 2012).

Translation initiation: Translation initiation starts with the binding of the initiation factors: eIF1, eIF1A, eIF3, and eIF5 to the 40S, followed by association with the ternary complex (TC) composed of GTP-bound eIF2 heterotrimeric complex and the initiator methionine tRNA, to form the 43S pre-initiation complex (PIC). On the other hand, initiation factors: eIF4G, eIF4E, and eIF4B, together with the poly-A binding protein “Pab1” bind to the mRNA thereby mediating its circularization and facilitating the PIC binding. The association of the PIC to the mRNA leads to the formation of the 48S complex. The 48S complex scans through the mRNA until it finds the start codon, which is mainly established by the correct base pairing between the initiator methionine anticodon and the AUG start codon, triggering GTP hydrolysis and release of eIF2. Eventually, eIF5B promotes the association of the 60S to the 40S leading to the formation of the 80S. Before elongation, most of the initiation factors are released from the ribosome. Recycling of GDP-bound eIF2 is mediated by eIF2B which allows regeneration of GTP-bound eIF2 for the next cycle of translation initiation. At the end of translation initiation, the ribosome P-site is occupied by the initiator methionine tRNA, while the A-site is vacant awaiting the first elongator tRNA.

Translation elongation: GTP-bound eEF1 associates with the aminoacyl-tRNA and facilitates its binding to an empty ribosome A-site. Base pairing between the anticodon of the aminoacyl-tRNA with the

corresponding code on the mRNA triggers GTP hydrolysis followed by release of the eEF1, which allows proper positioning of the aminoacyl-tRNA into the A-site. Recycling of the GDP-bound eEF1 into the GTP-bound eEF1 requires eEF1B, allowing repeated elongation cycles. Catalyzed by the peptidyl transferase center of the ribosome, peptide bond is formed between the two amino acids in the A and P site. Following peptide bond formation, the association and hydrolysis of the GTP-bound eEF2 facilitate the translocation of the peptidyl-tRNA into the P site, and the de-acylated tRNA into the E-site by re-positioning of the anticodon loops, followed by its release from the ribosome. eEF3 is a fungal specific elongation factor that presumably facilitates the release of the de-acylated tRNA from the exit site. Multiple ribosomes can translate a single mRNA simultaneously leading to the formation of large complexes called “Polysomes”. The cycle continues till the ribosome encounters one of the stop codons.

Translation termination and recycling: When the translating ribosome encounters a stop codon, eRF1 binds to the stop codon in association with GTP-bound eRF3, followed by GTP hydrolysis and release of eRF3 while eRF1 stays bound to the A-site. The association of eRF3 with eRF1 facilitates the stop codon selection. Following eRF3 release, Ril1 associates with eRF1 triggering hydrolysis of the peptidyl-tRNA and release of the polypeptide chain. Following termination of translation, dissociation of the 80S takes place mediated by Ril2, followed by tRNA and mRNA disassembly mediated by recycling factors, allowing recycling of the translation machinery for further rounds of translation.

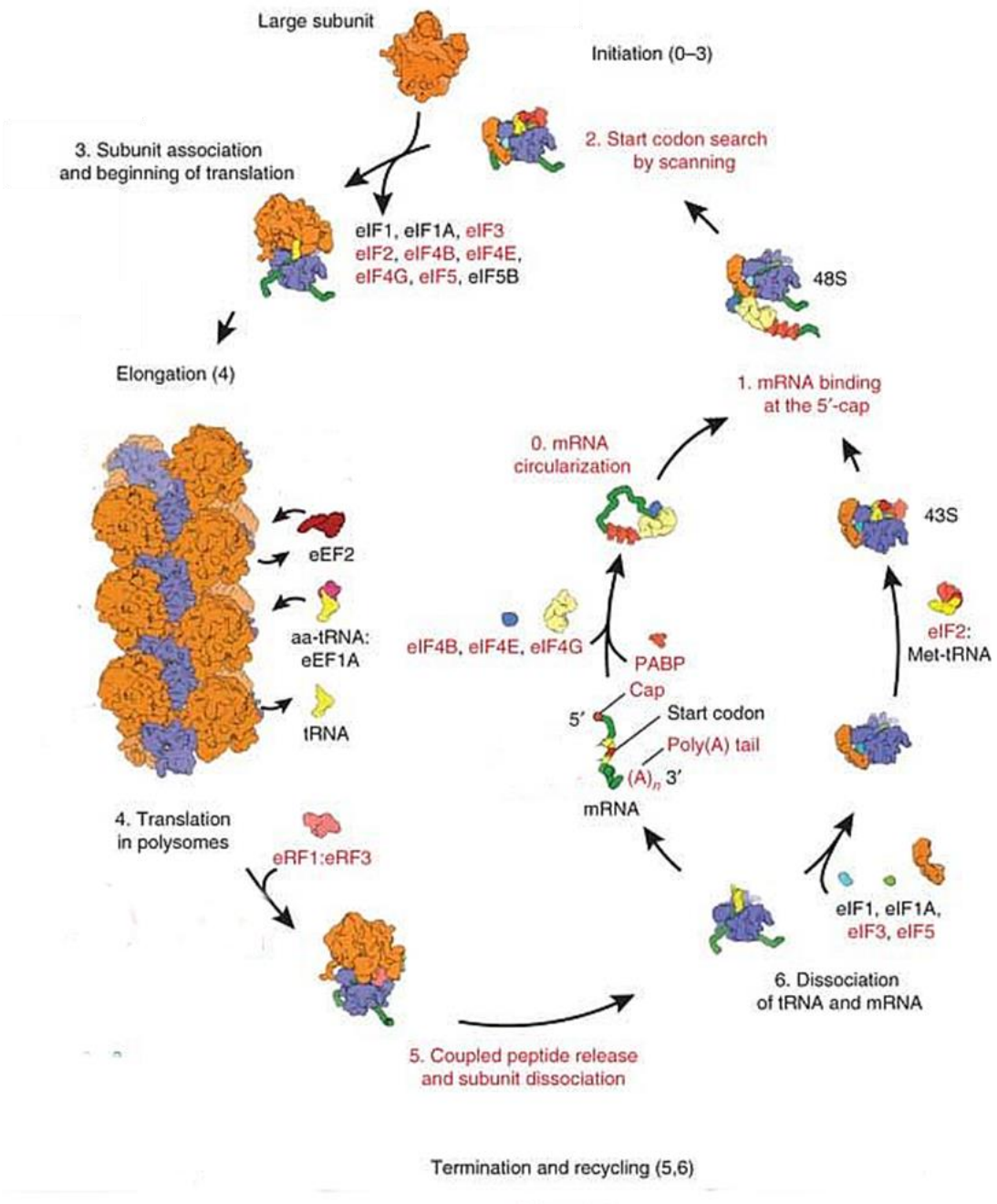

Figure 2: The mechanism of protein synthesis.

Translation is a multistep process that can be divided into four major phases: translation initiation (steps 0-3), translation elongation (step 4), termination and recycling (step 5 and 6) adapted from (Melnikov et al., 2012).

1.1.2 Maturation of nascent chains

As soon as the nascent chain starts to emerge from the ribosome exit tunnel, it undergoes different processing steps to ensure its proper folding, sorting, as well as enzymatic processing **(Figure 3)**. Protein folding is ensured by a network of ribosome associated chaperones that mainly guide co-translational folding steps of the nascent chain, as well as a network of chaperones acting independent of ribosome association and control both, *de novo* folding as well as re-folding of the misfolded proteins. In addition, both co-translational and post-translational pathways allow proper targeting of proteins to their corresponding compartments such as the endoplasmic reticulum (ER) and mitochondria. Furthermore, enzymatic processing of the nascent chains is accomplished co-translationally by a set of ribosome-associated enzymes, as a part of the nascent chain maturation process. Ultimately, proteins can be targeted for degradation via co/post-translational pathways (Pechmann et al., 2013).

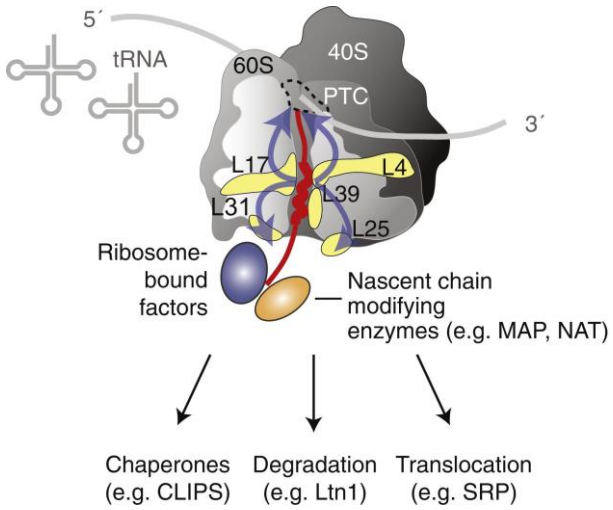

Figure 3: Maturation of nascnet chains into functional proteins.

Emerging nascent chains from the peptide exit tunnel undergo enzymatic proecessing, folding, translocation, and ultimately degradation either cotranslationally by ribosome associated factors or post-translationaly (Pechmann et al., 2013).

1.1.2.1 Enzymatic processing of the nascent chains

1.1.2.1.1 Methionine excision

Yeast encodes two methionine aminopeptidases (MAPs): Map1 and Map2 share 22% sequence identity, and show functional redundancy where Map1 is the dominant form. Both Map1 and Map2 interact with

the ribosome and target the nascent chains as they emerge from the ribosome exit tunnel. MAPs cleave the N-terminal methionine based on the identity of the N-terminal penultimate amino acid. MAPs cleave methionine followed by a small, uncharged amino acid with a gyration radius less than 1.29°A, while large hydrophobic or positively charged residues at the N-terminal penultimate position prevent MAP cleavage. Deletion of the genes encoding Map1 and Map2 in *S. cerevisiae* is lethal indicating an essential function for methionine excision (Chen et al., 2002; Li and Chang, 1995).

1.1.2.1.2 N-terminal acetylation

N-terminal acetylation of proteins is the process by which an acetyl group from “Acetyl-Coenzyme A” is transferred to the α-amino group of the N-terminal amino acid of a protein, catalyzed by a set of enzymes named N-terminal acetyl transferases (NATs) (Aksnes et al., 2016). NATs associate with the ribosome to co-translationally acetylate the nascent chains at their N-terminus, as they emerge from the ribosome exit tunnel (Gautschi et al., 2003a; Polevoda et al., 2008a). *S. cerevisiae* has five distinct NATs, NatA to E, which differ in their protein complex composition and substrate specificity **(Figure 4A)**, and together catalyze the N-terminal acetylation of the majority of yeast proteins **(Figure 4B)** (Aksnes et al., 2016; Starheim et al., 2012b).

The NatA complex consists of the catalytic subunit Naa10, and the auxiliary subunit Naa15 (Park and Szostak, 1992). NatA acetylates N-termini starting with Ser-, Ala-, Thr-, Gly-, Val- and Cys- following initiator methionine excision (Perrot et al., 2008). The NatB complex consists of the catalytic subunit Naa20 and the auxiliary subunit Naa25 (Polevoda et al., 2003), and acetylates the N-terminal methionine of substrates with Met-Asp-, Met-Glu-, Met-Asn- or Met-Gln- (Perrot et al., 2008; Van Damme et al., 2012). The NatC complex is composed of the catalytic subunit Naa30 and the auxiliary subunits Naa35 and Naa38 (Polevoda and Sherman, 2001), and acetylates the N-terminal methionine of substrates starting with Met-Leu-, Met-Phe-, Met-Ile and Met-Trp (Perrot et al., 2008). NatD consists of one protein: Naa40. The *in vivo* substrate specificity of NatD lies within the first 30-50 amino-acid residues (Polevoda et al., 2009; Song et al., 2003). The NatE complex consists of Naa50, and the “NatA” subunits Naa10 and Naa15, yet its substrate specificity is not well characterized (Gautschi et al., 2003a). In principle, N-termini that can be N-terminally acetylated by NatA are most prevalent in the proteome, followed by N-termini acetylated by NatB, and N-termini acetylated by NatC. NatD has only two verified substrates: the histones H2A and H4. Taken together, 50-70% of all yeast proteins are N-terminally acetylated, making N-terminal acetylation one of the most abundant protein modifications in the yeast proteome **(**(Aksnes et al., 2016; Perrot et al., 2008; Starheim et al., 2012a; Van Damme et al., 2011).

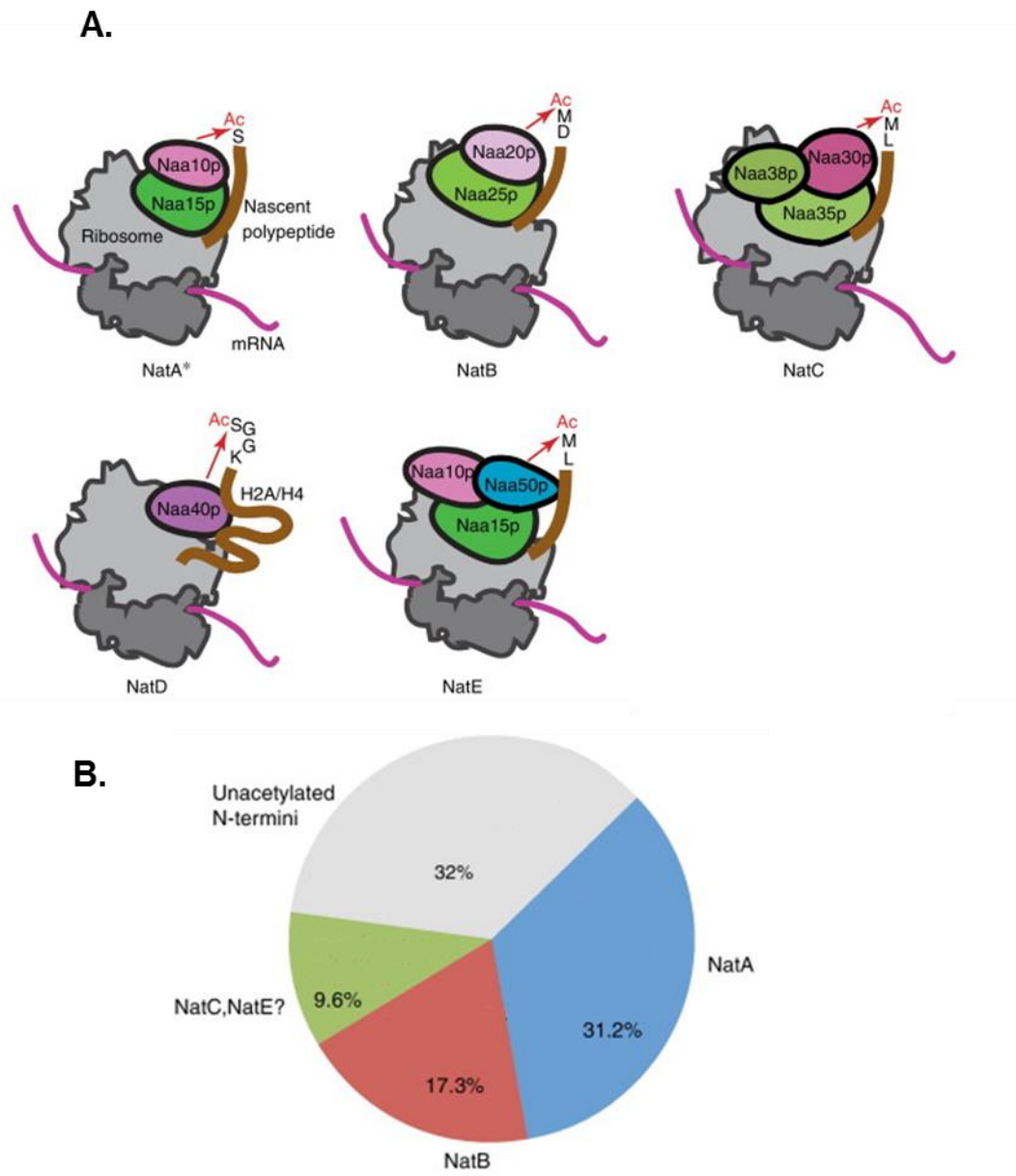

Figure 4: N-terminal acetylation by N-terminal acetyl transferases in yeast.

A. The yeast N-terminal acetyl transferase machinery consists of five distinct NATs (NatA-E) which differ in their protein composition, as well as substrate specificities (Starheim et al., 2012a).
B. The extent of N-terminal acetylation by different NATs (adapted from Starheim et al., 2012a)

N-terminal acetylation is conserved across all kingdoms of life, and it has been linked to diverse biological pathways such as signaling proteins for degradation (Hwang et al., 2010a), establishment of protein localization (Behnia et al., 2004a; Forte et al., 2011), as well as mediating protein-protein interactions (Scott et al., 2011). Despite recent advances in our understanding of the role of N-terminal acetylation, its

exact molecular function is still missing. The proposed roles of N-terminal acetylation are discussed in greater detail in section **1.3**.

1.1.2.2 Protein folding

The yeast protein folding machinery encompasses two spatially and functionally distinct chaperones networks that work together to ensure proper folding of proteins *in vivio* (Albanese et al., 2006) **(Figure 5)**. The first network is formed by "CLIPS": Chaperones Linked to Protein Synthesis, a group of chaperones that are functionally and physically connected to the ribosome. CLIPS bind to nascent chains co-translationally to establish *de novo* folding, and are transcriptionally co-regulated with the translation apparatus **(Figure 5A)**. Another network includes the "HSPs": Heat Shock Proteins, representing chaperones that act post-translationally to establish protein quality control and refolding, and their expression is dramatically increased under stress **(Figure 5B)**.

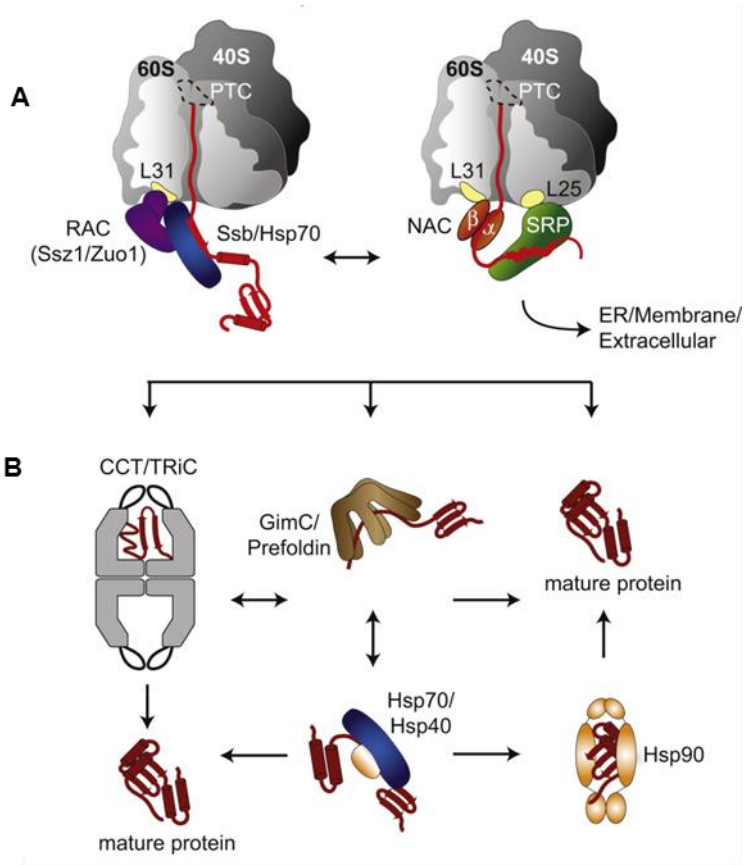

Figure 5: The eukaryotic chaperone network.

Two functionally and spatially distinct chaperone networks that coordinate protein folding

A. Co-translational folding of newly syntheized proteins is mediated by ribosome associated factors (Pechmann et al., 2013).
B. Post-translational folding is mediated by a network of cytosolic chaperones (Pechmann et al., 2013).

1.1.2.3 The co-translational network of chaperones

CLIPS comprise a group of mechanistically diverse chaperones that together coordinate co-translational folding **(Figure 5A**)**:**

The Nascent chain associated complex (NAC): NAC is a complex of two subunits named α and β. The N-terminal part of the β subunit mediates the interaction of the complex with the ribosome, close to L31, near the ribosome exit tunnel (Pech et al., 2010). Global profiling of the NAC-associated nascent chains revealed the broad selectivity of NAC, highlighting the role of NAC as a general chaperone for most of the nascent chains, including nascent chains that are destined for secretion or mitochondrial targeting (Del

Alamo et al., 2011). In addition, NAC was shown to regulate co-translational targeting of proteins by modulating SRP binding (Zhang et al., 2012).

The co-translationally acting Hsp70 (Ssb): The family of Hsp70 chaperones plays central roles in protein quality control (Morano et al., 2012; Verghese et al., 2012). In general, Hsp70s consist a of a C-terminal substrate binding domain whose affinity to the substrate is allosterically regulated by an N-terminal nucleotide binding domain. ADP-bound Hsp70 has high affinity for its substrate, while ATP-bound Hsp70 has low affinity for its substrate. Protein folding is mediated by iterative cycles of substrate binding and release until a protein is properly folded. Two classes of Hsp70 co-chaperones regulate this cycle namely J-proteins which stimulate ATP hydrolysis, and nucleotide exchange factors "NEFs"" which replace ADP by ATP in Hsp70. Hsp70s show broad substrates specificity, and in general bind to hydrophobic segments of a protein. J-proteins are also thought to facilitate substrate recruitment to Hsp70 (Verghese et al., 2012). The yeast co-translationally acting Hsp70 is comprised of two functional isoforms of Ssb: Ssb1 and Ssb2. Ssb is directly associated with the ribosome (Hanebuth et al., 2016). ATP hydrolysis by Ssb is stimulated by the ribosome associated complex (RAC) composed of the non-canonical Hsp70 "Ssz" and the J-protein "Zuotin" (Gautschi et al., 2001; Huang et al., 2005) that associates with the ribosome independent of the nascent chain, close to L31, near the exit tunnel (Leidig et al., 2013), and modulates Ssb interaction with its substrates (Willmund et al., 2013; Döring et al., 2017). The nucleotide exchange factor "Sse1" further regulates Ssb function by facilitating exchanging ADP with ATP (Shaner et al., 2005; Yam et al., 2005). Global profiling of the pool of nascent chains that are engaged with Ssb revealed the broad specificity of Ssb, yet specific enrichment for large proteins, proteins with high aggregation propensity, and intrinsically disordered regions, together suggesting that Ssb plays a role in the folding of nascent chains that are challenging to fold (Willmund et al., 2013). Most recently, profiling of Ssb interaction with translating ribosomes suggested Ssb also engages ER and mitochondrial targeted nascent chains, suggesting a role of Ssb in protein targeting (Döring et al., 2017).

1.1.2.4 The post-translational network of chaperones

HSPs comprise a group of diverse, yet highly interdependent chaperones, and together they mediate both *de novo* folding and refolding of misfolded/aggregated proteins **(Figure 5B)** (Morano et al., 2012; Verghese et al., 2012).

Hsp70 Chaperones: In addition to the co-translationally acting Hsp70s Ssb1 and Ssb2, four cytosolic Hsp70s exist in yeast, with high degree of functional redundancy. Two of them are constitutively expressed (Ssa1 and Ssa2), and two are stress inducible (Ssa3 and Saa4). Hsp70s are also found in the ER (Kar2) and mitochondria (Ssc1 and Ssq1). The family of Hsp70 chaperones plays central roles in posttranslational folding/refolding, protein targeting, as well as protein degradation.

Hsp90 Chaperones: Hsp90 is an ATP dependent chaperone whose function is established by nucleotide cycling, and is regulated by co-chaperones. Both Hsp70 and Hsp90 are interlinked, where substrates are typically first engaged by the Hsp70 then handed over to the Hsp90 for final maturation. In contrast to the Hsp70, Hsp90 are selective in terms of its substrates and it is mainly engaged in the late maturation steps of its client proteins. To date, only specific endogenous proteins are known to require Hsp90 for folding.

Chaperonin TRiC/CCT (TCP1-Ring Complex or Chaperonin Containing TCP1): TriC/CCT is a hetero-oligomeric complex composed of 8 subunits that together form a double ring structure. TriC/CCT folds its substrates in its central cavity, in a nucleotide-dependent manner, and plays a central role under stress. Additional co-factors modulate TriC/CCT activity such as GimC/Prefoldin, which facilities targeting of substrates into TriC.

Disaggregases (Hsp104 and Hsp78): Hsp104 is a member of the AAA+ ATPase family. It forms a hexameric ring with a central channel that has a diameter of roughly 15°A. Hsp104 is capable of extracting proteins from aggregates, and threading them through its central channel. Hsp104 is interlinked to the Hsp70 system, where Hsp70 can facilitate the recruitment of Hsp104 to its substrates, as well as refolding of proteins back to their native conformation. Hsp104 refolding activity is strictly required for thermo-tolerance. In addition to Hsp104, yeast mitochondria comprise Hsp78, which is 65% similar to Hsp104. Hsp78 works together with the mitochondrial Hsp70 Ssc1.

Small heat shock proteins (sHSP): small heat shock proteins are a group of small proteins that tend to form oligomers. sHSP are ATP-independent and they co-aggregate with substrates in order to facilitate subsequent disaggregation by other chaperones such as Hsp70 and Hsp104. Yeast possesses two members of the small heat shock proteins: Hsp42 (constitutively expressed), and Hsp26 (stress-inducible).

1.1.2.5 Targeting of nascent chains

With the exception of mitochondrial encoded proteins, protein biosynthesis is exclusively cytosolic, therefore proteins of others cellular compartments have to be targeted to their corresponding cellular localization. An intricate network of targeting factors ensures proper sorting of proteins into their corresponding cellular compartments either co- or post-translationally.

1.1.2.5.1 Targeting of proteins to the ER

Different pathways exist for targeting proteins to the ER (Barlowe and Miller, 2013). A major pathway is the co-translational targeting of secretory proteins via the signal recognition particle (SRP) **(Figure 6A)**. SRP recognizes N-terminal hydrophobic signal sequences, as well as transmembrane domains. The

complex of SRP engaged with the translating ribosome interacts with the ER membrane through the SRP receptor (SR). Subsequently, SRP-ribosome-nascent chain complex bound to SR transfers the nascent chain to the Sec61 translocon, where co-translational translocation takes place. Unlike the core translocation pore component Sec61, SRP is not essential in yeast, indicating that other SRP-independent pathways exist. In fact, proteins can also be translocated post-translationally via the Hsp70 family, which maintains the targeted proteins in a translocation competent state after complete synthesis. Subsequently, proteins are targeted to the ER membrane via Sec63, followed by translocation through the Sec61 translocon, in coordination with the ER resident Hsp70: Kar2 (**Figure 6B)**. On the other hand, a specific pathway exists for targeting of the tail-anchored (TA) proteins: The Guided Entry of TA proteins (GET) **(Figure 6C)**. First, the Sgt1-Get4-Get5 complex mediates the binding of the C-terminal anchor to the targeting factor: Get3. Get3 delivers the targeted protein to the integral membrane proteins: Get1 and Get2 at the ER membrane, where they facilitate the insertion of the C-terminal tail into the lipid bilayer in an ATP dependent manner.

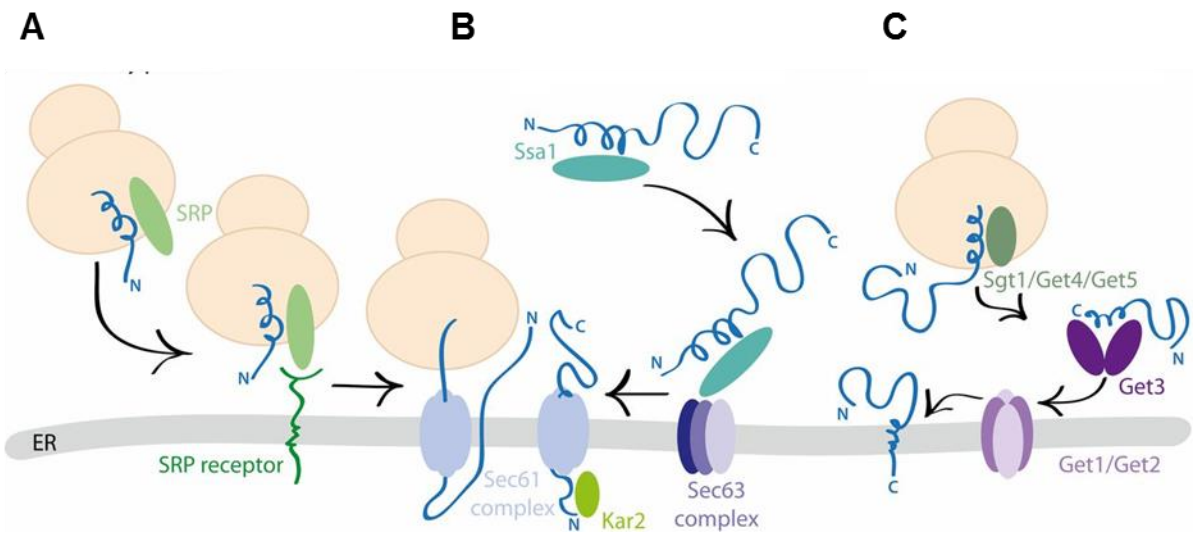

Figure 6: Different pathways for targeting of secretory proteins.

A. Co-translational targeting of proteins into the ER by SRP (Barlowe and Miller, 2013)
B. Post-translational targeting of proteins to the ER (Barlowe and Miller, 2013)
C. Translocation of tail anchored proteins by the GET pathway (Barlowe and Miller, 2013).

1.1.2.5.2 Targeting of mitochondrial proteins

To date, the predominant view is that the targeting of mitochondrial proteins occurs post-translationally, where chaperones play a key role in targeting proteins to the mitochondrial outer membrane proteins for translocation by keeping them in a translocation-competent state and preventing their aggregation (Fox,

2012). However, there is increasing evidence for co-translational targeting of nascent chains to mitochondria, such as localization and translation of mRNA encoding mitochondrial proteins at the mitochondrial outer membrane (Garcia et al., 2007; Marc et al., 2002; Williams et al., 2014), presumably to facilitate the subsequent import of those proteins into the mitochondria.

1.1.2.6 Protein complex assembly

A large number of proteins assemble into complexes which is essential for their molecular function. Until recently the dominant view was that protein complex assembly occurs post-transitionally. However recently accumulating evidence (Duncan and Mata, 2011; Shieh et al., 2015) suggests that protein complex assembly can already occur co-translationally i.e. before full synthesis of at least of one the protein-complex subunits. In principle, co-translational assembly can minimize protein aggregation by decreasing the exposure time of the interaction interface of protein subunits which could be aggregation prone. In addition, co-translational assembly provides a faster and more efficient pathway by localizing protein complex assembly to the sites of protein synthesis (Wells and Bergendahl, 2015). On the contrary, post-translational complex assembly is driven by diffusion which is limited by molecular crowding.

1.1.3 Protein degradation

Protein degradation is an essential process to clear damaged or terminally misfolded proteins, as well as regulating protein concentration in the cell. Protein degradation is mediated by two major pathways: Autophagy and the ubiquitin-proteasome system. Autophagy is the process by which proteins are targeted for intracellular hydrolysis inside the vacuole, and it is responsible for the degradation of whole organelles such as mitochondria and peroxisomes, or large protein assemblies such as ribosomes (Reggiori and Klionsky, 2013). In contrast to autophagy, the ubiquitin proteasome system is a rapid and more selective degradation system for specific proteins in the cytoplasm and the nucleus (Finley et al., 2012).

1.1.3.1 The ubiquitin-proteasome system

Ubiquitin: Ubiquitin is a small protein with β-grasp fold that can modify proteins with its C-terminal Glycine, typically by conjugation to a Lysine residue of the target proteins via an iso-peptide bond. The ubiquitination reaction is catalyzed by a cascade of enzymes: E1-E2-E3. E1 is a ubiquitin activating enzyme that forms a high energy thioester bond with the main chain carboxyl group of the c-terminal Glycine of ubiquitin, in an ATP-dependent manner. Yeast has only one E1, the essential Uba1. The activated ubiquitin is then transferred by one of the 11 yeast Ubiquitin conjugating enzymes (E2s) to E3-ligases. Eventually, E3-ligases catalyze the iso-peptide bond formation between the ε-amino group of the Lysine residue of targeted proteins, and the activated carboxyl group of ubiquitin. E3-Ubiquitin ligases

play a central role in substrates selection, and represent the largest group of proteins involved in ubiquitination, comprising 60-100 putative E3-ligases encoded in the yeast genome. Ubiquitin itself has seven lysine residues; each can be conjugated to another ubiquitin molecule leading to poly-ubiquitination. The poly-ubiquitin chains can have different topologies depending on the position of the Lysine residues that mediate ubiquitin conjugation. Depending on the poly-ubiquitin chain topology, poly-ubiquitination can target proteins for proteasome-mediated degradation. Ubiquitination is a reversible protein modification, and it can undergo de-ubiquitination by a group of enzymes "Deubiquitylases" with diverse functional roles (Finley et al., 2012) **(Figure 7)**.

Proteasome: The main function of the proteasome is to degrade ubiquitin protein conjugates. The proteasome is an ATP dependent protease that is composed of 33 subunits. The proteasome is organized into two major assemblies: the regulatory particle (RP) that mediates recognition of the ubiquitin protein conjugates as well as the unfolding by the hetero-hexameric ATPase assembly, and the core particle (CP) which harbors the proteolytically active center inside its core and mediates protein degradation in a highly regulated fashion. Substrates are transported from the RP to the CP through a translocation channel that opens and closes in a regulated manner. Proteasome assembly is mediated by a set of dedicated chaperones.

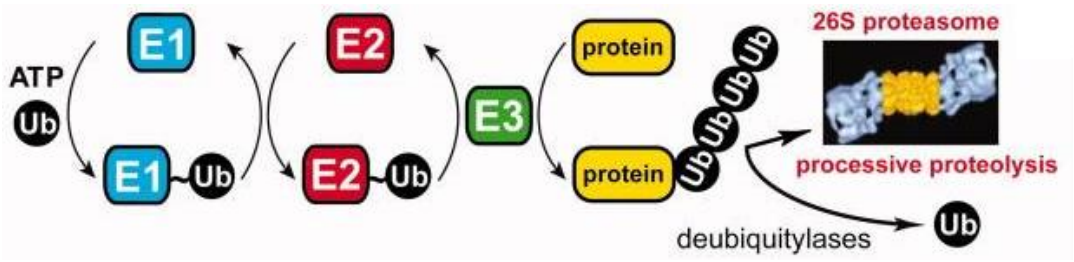

Figure 7: The ubiquitin proteasome system.

Ubiquitination of a target protein is mediated by a cascade of enzymes: E1, E2 and E3. Successive ubiquitination of ubiquitin leads to polyubiquitin chain formation. Polyubiquinated proteins are degradaed by the proteasome. Ubiquitination is a reversible modification that can be removed by deubiquitylases (Varshavsky, 2011).

1.1.3.2 Co-translational ubiquitination of the nascent chains

Recent reports indicate that 10-15% of the nascent chains are co-translationally targeted for degradation (Duttler et al., 2013). At least part of the co-translational ubiquitination is mediated by Ltn1/Rkr1, an E3 ligase that can associate with the ribosome (Bengtson and Joazeiro, 2010). Ribosome stalling during translation triggers the disassembly of the ribosome subunits. The disassembled 60S carrying unreleased

nascent chain is recognized by Ltn1 for ubiquitination (Shao and Hegde, 2014; Shao et al., 2013). Ltn1 acts together with other components such as Cdc48, that ultimately releases the nascent chain from the 60S and targets it for proteasome-mediated degradation (Brandman et al., 2012; Verma et al., 2013).

1.1.3.3 Substrate recognition in the ubiquitin-proteasome system

A fundamental question concerning the ubiquitin-proteasome system is how ubiquitin ligases select target proteins for ubiquitination. Although the mechanisms for substrate selection can be diverse, it is generally classified into two major mechanisms (Finley et al., 2012; Ravid and Hochstrasser, 2008). One mechanism is determined by the folding state of the protein, where E3-ligases recognize its substrates by interaction with hydrophobic patches that are aberrantly exposed by misfolded proteins, typically in coordination with molecular chaperones. The other mechanism is defined by degradation signals that act as recognition elements on the target proteins for E3-ligase recruitment and ubiquitination. Degradation signals can also be diverse and include phosphorylation, ubiquitin like modification such as SUMO, or surface exposed hydrophobic patches. One of the well-studied pathways for targeting proteins for degradation by degradation signals relevant also in the context of N-terminal acetylation is the N-end rule.

The N-end rule links the *in vivo* half-life of a protein to the identity of its N-terminal residues. Based on the N-end rule, specific N-terminal amino acids act as degradation signals (N-degrons) that are recognized by E3-ligases together with its cognate E2 (N-recognins) thereby targeting proteins for ubiquitination and downstream degradation by the proteasome. The N-end rule pathway is composed of two major branches: The Ac/N-end rule, and the Arg/N-end rule (Varshavsky, 2011) **(Figure 8)**.

The Ac/N-end rule pathway is based on the finding that N-terminal acetylation of proteins can act as a N-terminal degradation signal (Ac/N-degron) that is recognized by specific E3-ligases (Ac/N-recognins): Doa10 (Hwang et al., 2010a) and Not4 (Shemorry et al., 2013), thereby targeting proteins for degradation in a regulated manner **(Figure 8A)**. The Ac/N-end rule is discussed in greater detail in section **1.3**.

On the other hand, the Arg/N-end rule pathway targets specific non N-terminally acetylated N-termini for degradation (Varshavsky, 2011) (**Figure 8B)**. N-terminal Arg, Lys, His, Leu, Phe, Tyr, Trp, Ile, Asp, Glu, Asn, Gln, and Cys represent the N-degrons of the Arg/N-end rule pathway that are recognized by the N-recognins: Ubr1-Rad6 and Ufd4-ubc4. N-terminal basic (Arg, Lys, His) and hydrophobic (Leu, Phe, Tyr, Trp, Ile) amino acids can be directly recognized by their cognate N-recognin, therefore they are called “primary destabilizing residues”. In contrast, Asp- and Glu-, and oxidized cysteine cannot be directly recognized by N-recognins unless they undergo an arginylation reaction catalyzed by Arg-tRNA transferase encoded by the Ate1 gene, therefore they are called “secondary destabilizing residues”. N-terminal Asn- and Gln- cannot directly undergo arginylation, yet they are substrates of the N-terminal amidases Nta1 that convert Asn- and Gln- to Asp- and Glu- which can be subsequently arginylated,

therefore they are named “tertiary destabilizing residues”. The specificity of the Arg/N-end rule is complementary to that of MAPs, therefore regular proteins normally do not present N-degrons. However, destabilizing N-degrons can be exposed through post-translational mechanisms such as proteolytic cleavage. In addition to the aforementioned N-degrons, it was recently shown that Ubr1 can target N-terminal methionine, if followed by a hydrophobic amino acid, further expanding the Arg/N-end rule pathway (Kim et al., 2014).

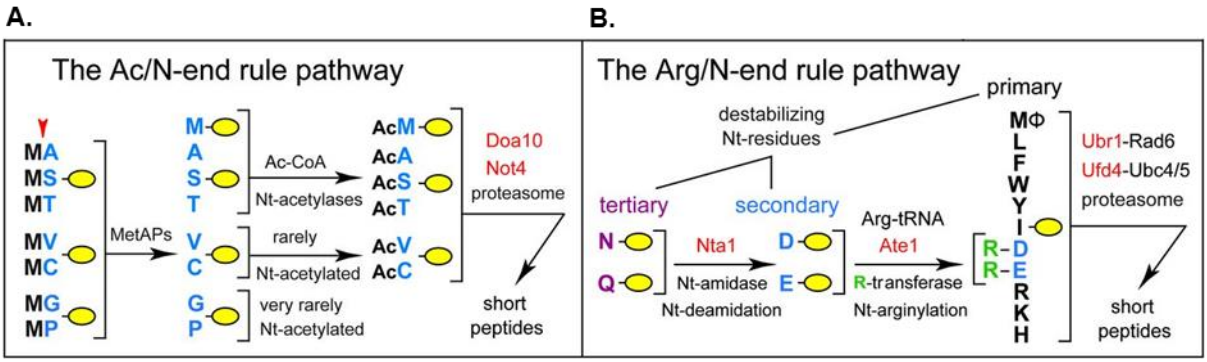

Figure 8: The N-end rule pathway in *S. cerevisiae.*

The N-end rule links the half life of a protein to the identitiy of its N-terminal amino acid. The N-end rule pathway can be divided into two major pathways:

A. The Ac/N-end rule pathway: N-terminal acetylated amino acid acts as a degradation signal that can be recognized by specific E3-ubiquitn ligases for poly-ubiquitination followed by proteasomal degradation (Chen et al., 2017).
B. The Arg/N-end rule pathway: Specific N-terminal amino acids can act as a primary, secondary, or tertiary degradation signal that can be recognized by N-recognins, followed by poly-ubiquitination and proteasome-mediated degradation (Chen et al., 2017).

1.2 Modulation of proteome homeostasis under stress

1.2.1 Transcriptional response upon environmental stress

Perturbation of the yeast proteome homeostasis, for instance due to unfavorable environmental conditions, triggers an integrated transcriptional stress response program that aims to modulate the proteome homeostasis pathways. Although different types of stress can trigger different stress-specific responses, a number of fundamental features are shared by the different stress responses, together representing a general stress response mechanism (Gasch et al., 2000). The common features of the transcriptional response upon environmental stress include induced transcription of genes with cyto-protective functions. A set of molecular chaperones are induced under different environmental stress conditions: Hsp104, Hsp78, small Heat shock proteins (Hsp26 and Hsp42), as well as members of the cytosolic Hsp70s: Ssa4, Sse2. In addition, specific components of the protein degradation machinery are

up-regulated which may indicate elevated levels of protein degradation as consequence of irreversible protein damage upon stress. On the other hand, upregulation of particular metabolic pathways takes place, such as transcription of genes involved in trehalose metabolism, which plays a cyto-protective function, as well as specific components of the glycolysis and respiration machinery, presumably to increase ATP levels. In parallel to the induction of the cyto-protective gene products, repression of genes encoding protein biogenesis factors including ribosomal proteins, translation factors, and aminoacyl-transferases takes place. The transcriptional response upon environmental stress response is mediated by transcription factors that stimulate/repress transcription, in addition to other factors such as chromatin remodeling and regulated mRNA turnover. In general, the changes at the transcriptional level correlate with protein synthesis levels despite the overall translation attenuation upon stress, indicating selective mechanisms for translation under stress.

1.2.2 Translation attenuation

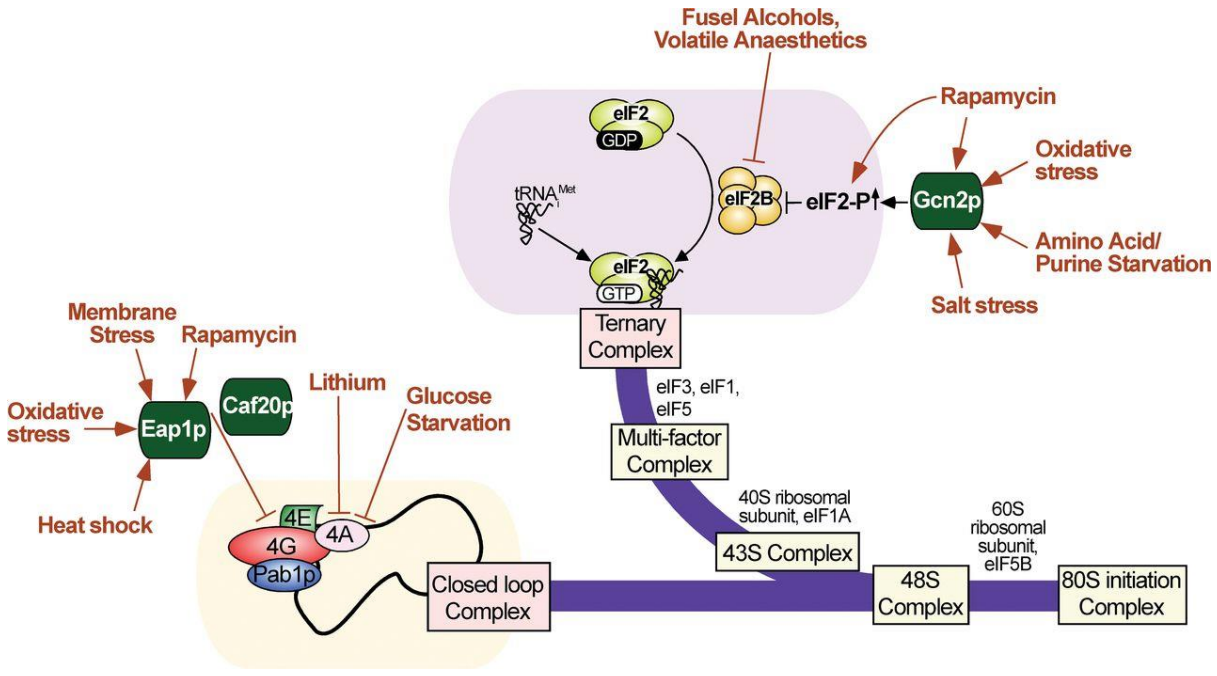

Figure 9: Translation attenuatuin under stress.

Attenuation of translation is one of the common features across the different stress reponses. Translational attenuation can be established by different mechanisms that target different components of the translation initation pathway (Simpson and Ashe, 2012).

One of common features of yeast stress response is translational attenuation. In addition to the repressed transcription of the genes encoding the translation machinery upon stress, different stress conditions can

directly attenuate translation through different mechanisms (Simpson and Ashe, 2012). These include regulation of eIF2B in eIF2α phosphorylation dependent or independent manner. Phosphorylation of eIF2α (by Gcn2 protein kinase) inhibits GTP recycling by eIF2B thereby trapping eIF2 in the GDP bound state, which eventually blocks TC formation. Alternative mechanisms include direct inhibition of eIF2B, independent of eIF2α phosphorylation. In addition, translation attenuation can be established by regulation of the closed loop formation via modulation of eIF4E binding proteins (Eap1 and Caf20) thereby inhibiting eIF4E-eIF4G interaction, or via inhibition of eIF4A. Despite the different mechanisms, the ultimate outcome is down regulation of translation initiation, resulting in global down regulation of translation **(Figure 9)**.

1.2.3 Stress granule formation

The inhibition of translation initiation upon stress leads to the accumulation of mRNA molecules that are stalled in the process of translation initiation, which triggers the assembly of ribonucleoprotein assemblies called “Stress Granules” (Jain et al., 2016; Protter and Parker, 2016). Consistently, stress granules in yeast contain mRNA as well as translation initiation factors such as eIF4E and eIF4G, in addition to the poly-A binding protein Pab1. Stress granules consist of a diverse proteome which reflects the complexity and diversity underlying its assembly. Several factors contribute to the assembly of stress granules including RNA-protein and protein-protein interactions, some of which may involve intrinsically disordered domains. The sequestration of mRNA into stress granules can affect its translation and/or degradation, however the exact mechanism is not yet known.

1.3 The role of N-terminal acetylation in proteome homeostasis

Despite being one of the most common protein modifications, the exact biological significance of N-terminal acetylation remains largely ambiguous. Interestingly, mutations that affect N-terminal acetylation in humans have been linked to specific diseases, underscoring its potential functional implications (Myklebust et al., 2014; Popp et al., 2015). The yeast *natB* deletion mutant shows the most pronounced phenotype compared to deletion mutants lacking other N-terminal acetyl transferases, which includes slow growth under physiological growth conditions, and a more pronounced growth defect under stress conditions especially heat (e.g. 37°C (Caesar et al., 2006a)). The *natA* deletion mutant displays similar yet less severe phenotypes, together suggesting that N-terminal acetylation of proteins has important functional implications in yeast cells (Gautschi et al., 2003b). Recent studies have pointed to diverse molecular functions for N-terminal acetylation of proteins, which further reflects its functional complexity (**Figure 10**).

Interestingly, N-terminal acetylation can act as a signal for targeting proteins to proteasome-mediated degradation through the so-called Ac/N-end rule pathway (Hwang et al., 2010b). According to the Ac/N-end rule, proteins bearing N-terminally acetylated amino acid (Ac/N-degron) are targeted for degradation by specific E3-ubiquitin ligases (Ac/N-recognins). Two of them have been identified so far: The ER-membrane associated E3 ubiquitin ligase Doa10 (Hwang et al., 2010a), and Not4 (Shemorry et al., 2013). The fact that the majority of proteins are N-terminally acetylated during their biogenesis possibly expands the substrate pool of the N-end rule, and raises the question about the regulation of this pathway. The current model is that Ac/N-end rule is a conditional pathway. Presumably, functional proteins do not expose their Ac/N-degrons under normal conditions, as those signals are shielded from the Ac/N-recognins by being buried in the folded structure of the proteins, or within the interface of a protein complex. With this in mind, the Ac/N-end rule can maintain protein quality control by targeting misfolded proteins that aberrantly expose their Ac/N-degrons, or maintain protein-stoichiometry balance by selective targeting of unassembled subunits that have failed to shield its Ac/N-degrons in protein complexes. Indeed, a recent study (Shemorry et al., 2013) has shown that Hcn1 a subunit of the APC/C ubiquitin ligase, contains an Ac/N-degron that is normally repressed by binding of Hcn1 to Cut9. Hcn1 can be targeted for degradation via the Ac/N-end rule only when overexpressed to levels higher than Cut9. Similarly, Cog1 Ac/N-degron is repressed by binding to Cog2 and Cog3, while overexpression of Cog1 over Cog2/Cog3 leads to its Ac/N-end rule mediated degradation. However, to date, only a few endogenous substrates have been shown to undergo N-acetyl mediated degradation, therefore the general functional relevance of this pathway remains poorly understood.

In addition to the role of N-terminal acetylation in controlling protein complex stoichiometry, N-terminal acetylation can increase the affinity of protein complex subunits. Structural analysis of the interaction between the E2 enzyme (Ubc12), and the E3-ligase (Dcn1) revealed a significant role of the N-terminal acetylation of the N-terminal methionine of Ubc12 in mediating its interaction with Dcn1, where the N-terminal acetyl group is completely buried in a hydrophobic pocket in Dcn1 (Scott et al., 2011). Later studies suggested that the N-terminal acetyl mediated recognition of E2 and E3 is structurally conserved and extends to other members of the mammalian E2/E3 family, further highlighting the role of N-terminal acetylation as mediator of protein complexes assembly (Monda et al., 2013). Consistently, several studies have reported that N-terminal acetylation augments protein-protein interactions. These include actin-tropomyosin, which explains the impaired actin filaments in the deletion mutants lacking NatB (Abe et al., 2000; Caesar et al., 2006b; Van Damme et al., 2012), as well as interaction of the silencing factor Sir3 with the nucleosome core particle, which explains the mating deficiency of a NatA deletion mutant (Park and Szostak, 1992; Wang, 2004). In addition, the inhibitory activity of the carboxypeptidase inhibitor Tfs1 was decreased upon lack of its N-terminal acetylation by NatB, presumably by directly inhibiting its physical interaction with CPY (Caesar and Blomberg, 2004).

Furthermore, N-terminal acetylation has been implicated in establishment of protein localization. N-terminal acetylation was suggested to inhibit post-translational targeting of proteins to the ER (Forte et al., 2011). With this in mind, N-terminal acetylation may represent a quality control mechanism that prevents mistargeting of cytosolic proteins into the ER. On the other hand, targeting of the GTPase Arl3 to the Golgi requires its N-terminal acetylation by NatC, which mediates its interaction with the membrane protein Sys1. Thus, N-terminal acetylation may provide an alternative mechanism to N-terminal myristoylation for targeting proteins to the Golgi (Behnia et al., 2004b; Setty et al., 2004).

Interestingly, early studies have linked N-terminal acetylation to protein folding. N-terminal acetylation changes the electrostatic nature of the N-terminus of proteins by transferring an acetyl group to the primary amino-group at the N-terminus, preventing its subsequent protonation. *In vitro* studies showed that N-terminal acetylation increases α-helical stability of peptides and proteins (Chakrabartty et al., 1993; Fairman et al., 1989). Indeed, N-terminal acetylation increases the α-helical stability of several proteins including the N-terminal peptide of the mitochondrial matrix protein chaperonin 10 (Cpn10) (Jarvis et al., 1995), and the N-terminal peptide of tropomyosin (Greenfield et al., 1994). Interestingly, N-terminal acetylation of α-synuclein increases its α-helical propensity, slows down its fibrillation rate, and increases its resistance to aggregation (Bartels et al., 2014). Furthermore, a recent study suggests that lack of N-terminal acetylation by NatA triggers general protein misfolding upon Sup35 amyloid formation (Holmes et al., 2014). Together, these studies suggest a potential function of N-terminal acetylation in protein folding.

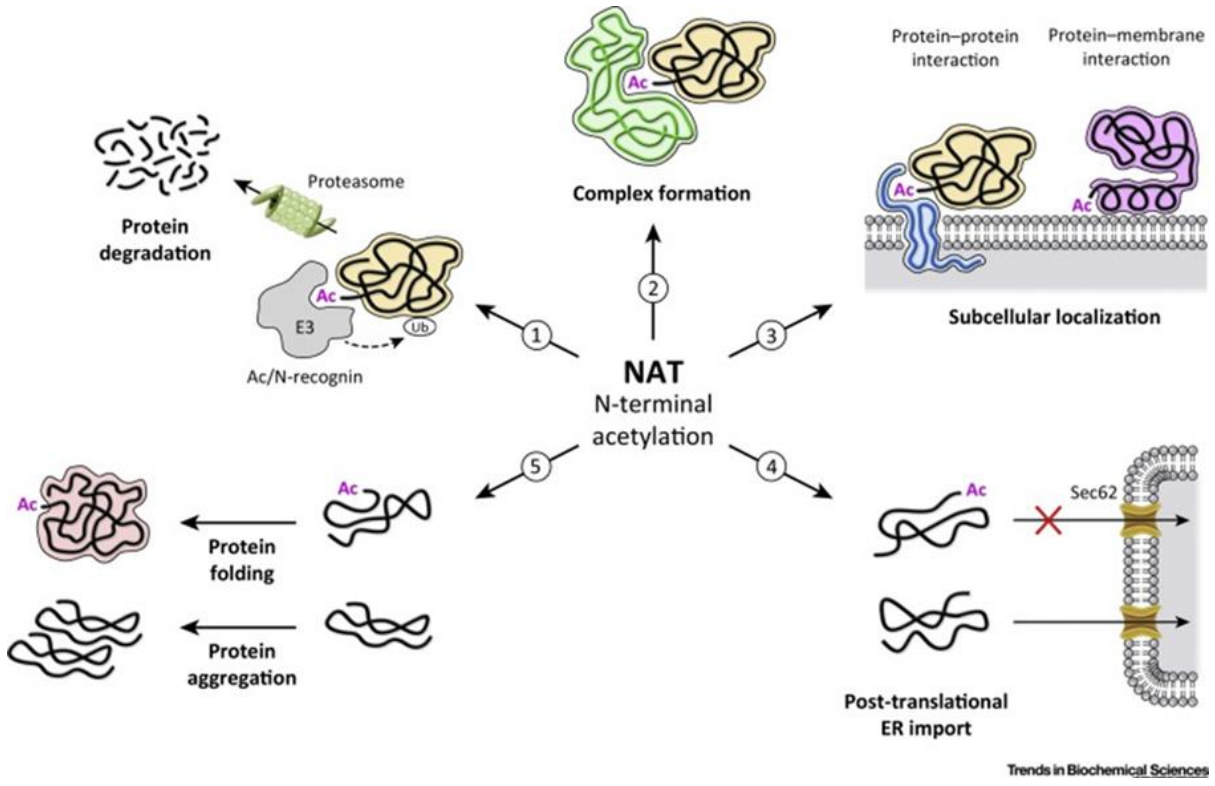

Figure 10: Potential functions of proteins N-terminal acetylation.

N-terminal acetylation can signal proteins for degradation (1) , mediate complex formation (2), establish protein localization (3,4), and prevents protein aggregation (5) (Aksnes et al., 2016).

1.4 Methods for global analysis of proteome dynamics

1.4.1 Ribosome profiling for global analysis of translation

Ribosome profiling is a deep-sequencing based tool that allows global monitoring of translation *in vivo*. The method is based on the fact that ribosomes protect the bound fragment of mRNA from nuclease digestion, allowing selective isolation of ribosome footprints (Ingolia et al., 2009). Subsequently, a deep sequencing library is generated form the extracted ribosomal footprints, followed by deep sequencing and mapping of the reads to the reference genome **(Figure 11)**. Recent advances in high throughput sequencing allow sequencing of millions of reads making ribosome profiling superior in terms of the precision and the sensitivity of quantification. Measuring the density of the ribosome footprints over mRNA allows quantitative measurements of protein synthesis. Furthermore, ribosome profiling allows precise determination of translation start and stop sites which has led to the identification of new coding

regions of the genome, and alternative translation start sites (Brar et al., 2012). In addition, the distribution of ribosome footprints over a given mRNA can provide insights into its translation mechanism, such as revealing stalling events (Guydosh and Green, 2014). Taken together, ribosome profiling is a powerful technique to study translation. Moreover, ribosome profiling is a versatile technique that can be adapted for various purposes. For instance, combining affinity purification of mitochondrial ribosome to ribosome profiling allowed specific analysis of mitochondrial translation (Couvillion et al., 2016).

Interestingly, ribosome profiling can be adapted to study co-translational interactions of any factor selected with nascent chains using “Selective Ribosome Profiling” (Oh et al., 2011, Becker et al 2013). The strategy is centered on purification of translating ribosomes in complex with the factor of interest, followed by ribosome profiling. Based on the identity and the distribution of the isolated ribosome footprints, global and mechanistic analysis of the association of the different factors with nascent chains can be performed.

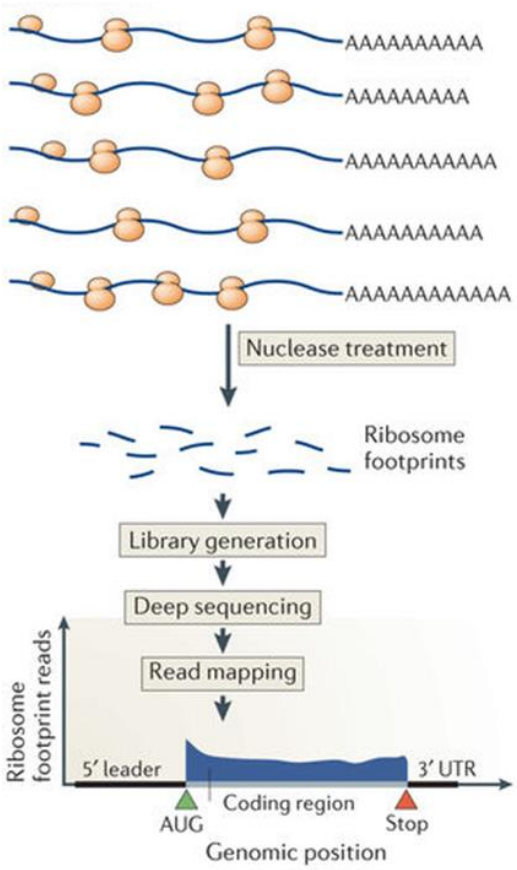

Figure 11: Ribosome profiling outline.

Ribosome profiling is centered around sequencing of ribosome footprints following degradation of the mRNA that is not protected by the ribosome (Brar and Weissman, 2015).

1.4.2 Tandem fluorescent timer for the analysis of proteome turnover

A fluorescent timer is a protein that changes its color by time thereby allowing relative estimation of protein age. The technique exploits the different maturation kinetics of fluorescent proteins: Super folder green fluorescent protein (sfGFP) and mCherry. While sfGFP becomes fluorescent within minutes after its synthesis, mCherry matures with a half-life of 40 min (Khmelinskii et al., 2012). The ratio of mCherry to GFP fluorescence intensity reflects protein age, where the ratio of mCherry to GFP fluorescence increases by increasing protein age. The kinetics of the maturation of the timer allows analysis of protein turnover in the range from 10 min to several hours **(Figure 12)**.

A genome wide library composed of 4044 tagged genes with the tandem fluorescent timer (tFT) allows global systematic protein turnover analysis upon environmental and/or genetic perturbations (Khmelinskii et al., 2014). High throughput double mutant strain construction using a synthetic genetic array (SGA) (Baryshnikova et al., 2010) enables studying the effects of specific gene deletions on proteome turnover measured by tFT fluorescence.

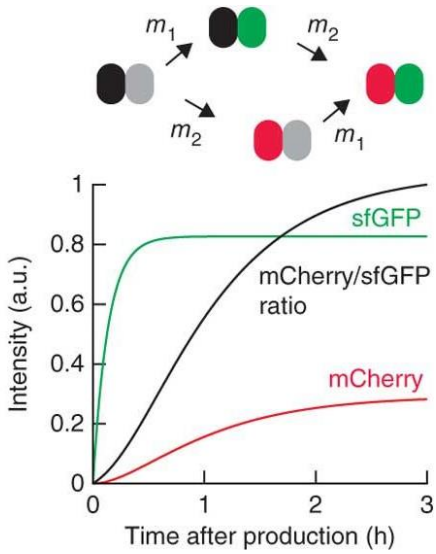

Figure 12: Tandem fluroescent timer as a tool for monitoring proteins turnover.

sfGFP becomes fluroesecnt within minutes of its synthesis, while mCherry matures with a half-time of 40 min, thereby mCherry/GFP ratio can be used as a proxy for protein half life (Khmelinskii et al., 2012).

1.4.3 Quantitative proteomics

Quantitative proteomics has become a pivotal tool applied to the investigation of many different biological processes. Stable isotope labeling techniques have facilitated the quantitation of changes in protein abundance by mass spectrometry, between different genetic and environmental conditions. Stable isotope labeling by amino acids in cell culture (SILAC) is an easy and reliable method for *in vivo* incorporation of a label into proteins for mass spectrometry (MS)-based quantitative proteomics (Mann, 2006). SILAC relies on metabolic incorporation of amino-acids with substituted stable isotopic nuclei (e.g. ^{13}C ^{15}N). Thus in such an experiment, two cell populations (e.g. wild type and gene deletion mutant) are grown in culture media that are identical except that one contains a 'light' and the other a 'heavy' form of a particular amino acid (e.g. ^{13}C ^{15}N labeled L-Lysine and L-Arginine). The heavy amino acid that is supplied to cells in culture gets incorporated into all proteins after a number of cell divisions. There is

hardly any chemical difference between the heavy and light amino acid. Both the unlabeled and labeled samples can be combined prior to cell harvest, and then be treated as a single sample in all subsequent steps, which include preparation of cell lysate, as well as preparation of the sample for mass spectrometry analysis. The intensity differences of the MS signal between heavy and light peptides reveals the relative abundance of any protein in both cells populations. Recent developments in the field of quantitative proteomics led to the development of new techniques that allow more consistent and reproducible label-free quantifications such as “SWATH” (Selevsek et al., 2015).

2 Aims of the study

Despite recent advances in our understanding of the role of N-terminal acetylation of proteins in eukaryotes, its precise molecular functions remain obscure. The general aim of the study is to understand the physiological function of N-terminal acetylation in yeast as a simple model of eukaryotic cells. Since N-terminal acetylation is a highly prevalent protein modification, I aimed to understand the global effects of the lack of N-terminal acetylation on the yeast proteome dynamics. Toward this aim, I employed unbiased high throughput approaches that together allow multi-dimensional proteome-wide analysis of the functional consequences of lacking N-terminal acetylation. Using this approach, I aimed to dissect the key steps of proteome homeostasis: protein synthesis analysis using ribosome profiling, protein steady-state levels analysis using quantitative proteomics, as well as protein turnover analysis using the tandem fluorescent timer. Furthermore, I complemented our approach with quantitative proteomics of isolated protein aggregates to investigate the effect of N-terminal acetylation on protein solubility. In addition, I aimed to analyze the genetic interaction network of the N-terminal acetyl transferase genes by performing an unbiased genetic screening for synthetic growth defects using the yeast deletion library. The combination of the different methods provided an integrated approach for a systematic and global analysis of the functional relevance of N-terminal acetylation. The project was performed in collaboration with Ulrike Friedrich, a PhD student in Bukau lab. All experiments presented here were performed by me unless mentioned otherwise.

3 Results

3.1 Translatome/proteome analysis under lack of N-terminal acetylation by NatB

Understanding global proteome dynamics upon loss of N-terminal acetylation can provide insights into its functional implications. With this in mind, we performed a combined translatome/proteome analysis of the consequences of loss of N-terminal acetylation by employing ribosome profiling, as well as quantitative proteomics in deletion mutants of specific NATs, in comparison to the wild type. Since deletion of *natB* leads to the most pronounced phenotype when compared to deletion of other N-terminal acetyl transferases (Caesar et al., 2006a; Gautschi et al., 2003c), we aimed to first analyze the consequences of loss of N-terminal acetylation by NatB in strains where the gene encoding the catalytic subunit of NatB is deleted (hereafter *natB*Δ).

3.1.1 Verification of *natB*Δ phenotypes

Consistent with earlier reports (Caesar et al., 2006a; Gautschi et al., 2003c), *natB*Δ cells showed slow growth at physiological growth conditions (30°C). In addition, *natB*Δ confers higher sensitivity to different stress conditions such as heat stress (37°C), DNA damage induced by Methyl Methanesulfonate (MMS) (alkylating agent), as well as osmotic stress induced by high concentration of NaCl. Deletion of the gene encoding the catalytic subunit of NatA (hereafter *natA*Δ) showed more subtle effects compared to *natB*Δ (**Figure 13)**.

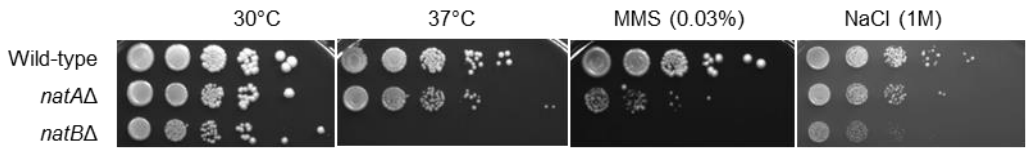

Figure 13: *natA* and *natB* deletion mutant growth phenotypes.

Spot test showing the growth behavior of wild type, *natA*Δ and *natB*Δ at 30°C, or under stress conditions such as heat (37°C), DNA-damage (MMS: alkylating agent), and osmotic stress (1 M NaCl).

3.1.2 Establishment of the labeling conditions for SILAC-based proteomics

A prerequisite for SILAC-based quantitative proteomics analysis is near to complete labeling of proteins with heavy amino-acids during cell culture. To maximize the labeling efficiency, we constructed a strain

auxotrophic for Arginine and Lysine (*ARG4*Δ *LYS1*Δ*)* where two genes encoding proteins that are critical for Arginine and the Lysine biosynthesis are deleted. Furthermore, the labeling rate of proteins by incorporation of heavy amino acids was determined by growing the auxotrophic strain in Lysine and Arginine synthetic dropout medium supplied with ^{13}C ^{15}N labeled Lysine, and ^{13}C ^{15}N labeled Arginine for three different doubling times (6, 7, and 8 doublings) followed by protein extraction and mass spectrometry analysis. The labeling efficiency was calculated based on the identified peptides at each of the tested doubling time. The incorporation efficiency of Arginine and Lysine was over 95% in all tested conditions **(Table 1)**. Based on the incorporation rate test, we have verified that 6 doublings in the labeling media is sufficient for both heavy Arginine and Lysine to get incorporated with an efficiency that exceeds 95%.

Table 1: Incorporation efficiency of ^{13}C ^{15}N labeled Arginine and Lysine.

Yeast cells deficient in Lysine and Arginine biosynthesis were grown in the presence of heavy Arginine and Lysine in the absence of its light counterpart. Protein extracts prepared from cells grown for 6, 7, and 8 doubling times were analyzed by MS and the incorporation efficiency of the heavy amino acids were calculated.

Doubling times	6	7	8
Incorporation efficiency of Arginine (%)	0.97	0.99	0.97
Incorporation efficiency of Lysine (%)	0.98	0.98	0.97

3.1.3 Correlation between replicates

In summary, steady state levels of 2909 proteins were reproducibly quantified in *natBΔ* relative to the wild type using SILAC-based quantitative proteomics in two label-swap replicates (Pearson correlation coefficient (r) = 0.74) **(Figure 14B)**. This compares to 4030 genes that were consistently quantified in *natBΔ* relative to the wild type at the translation level, in two replicates (r = 0.91) using ribosome profiling **(Figure 14A)**. Furthermore, in complementation to the SILAC-based proteomics, we employed SWATH-based quantitative proteomics which allows reproducible and consistent label-free quantification (in collaboration with Prof. Dr. Ruedi Aebersold lab at ETH-Zurich) where 1483 proteins were reproducibly quantified in *natBΔ* relative to wild type consistently across three replicates, at FDR<0.05.

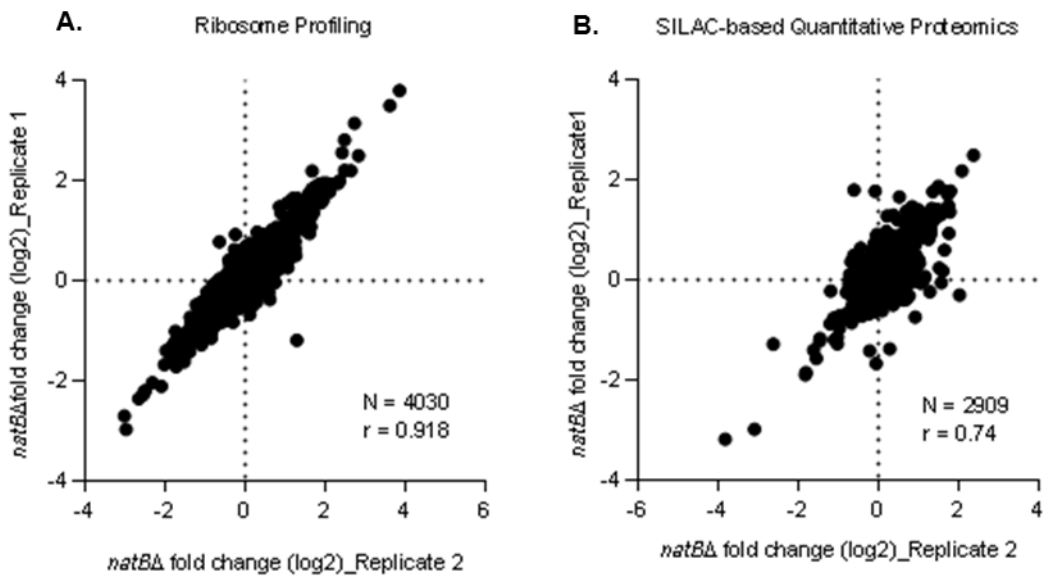

Figure 14: Correlation between replicates.

A. Correlation of fold-change (log2) of protein synthesis levels between *natB*Δ and wild type measured by ribosome profiling from two replicates. Pearson correlation coefficient equals 0.918 based on the analysis of 4030 genes.
B. Correlation of fold change (log2) of protein steady state levels in *natB*Δ versus wild type measured by SILAC-based quantitative proteomics from two label-swap replicates. Pearson correlation coefficient equals 0.74 based on 2909 proteins.

3.1.4 Quantification of N-terminally acetylated peptides

To verify that *natB*Δ indeed causes the loss of N-terminal acetylation of predicted NatB substrates, we analyzed N-terminal acetylation by SILAC-based quantitative proteomics of N-terminally acetylated peptides in *natB*Δ relative to the wild type. Interestingly, 198 unique N-terminally acetylated peptides were consistently quantified in wild type relative to *natB*Δ in two label swapped replicates. Confirmatory to the predicted NatB substrate specificity, N-terminally acetylated peptides starting with MD-, ME-, MQ-, MN- showed consistently higher abundance in the wild type compared to *natB*Δ indicating deficient N-terminal acetylation of those proteins in the absence of NatB **(Figure 15A)**. This is not due to decreased steady state level of those proteins in *natB*Δ compared to wild type (**Figure 15B**).

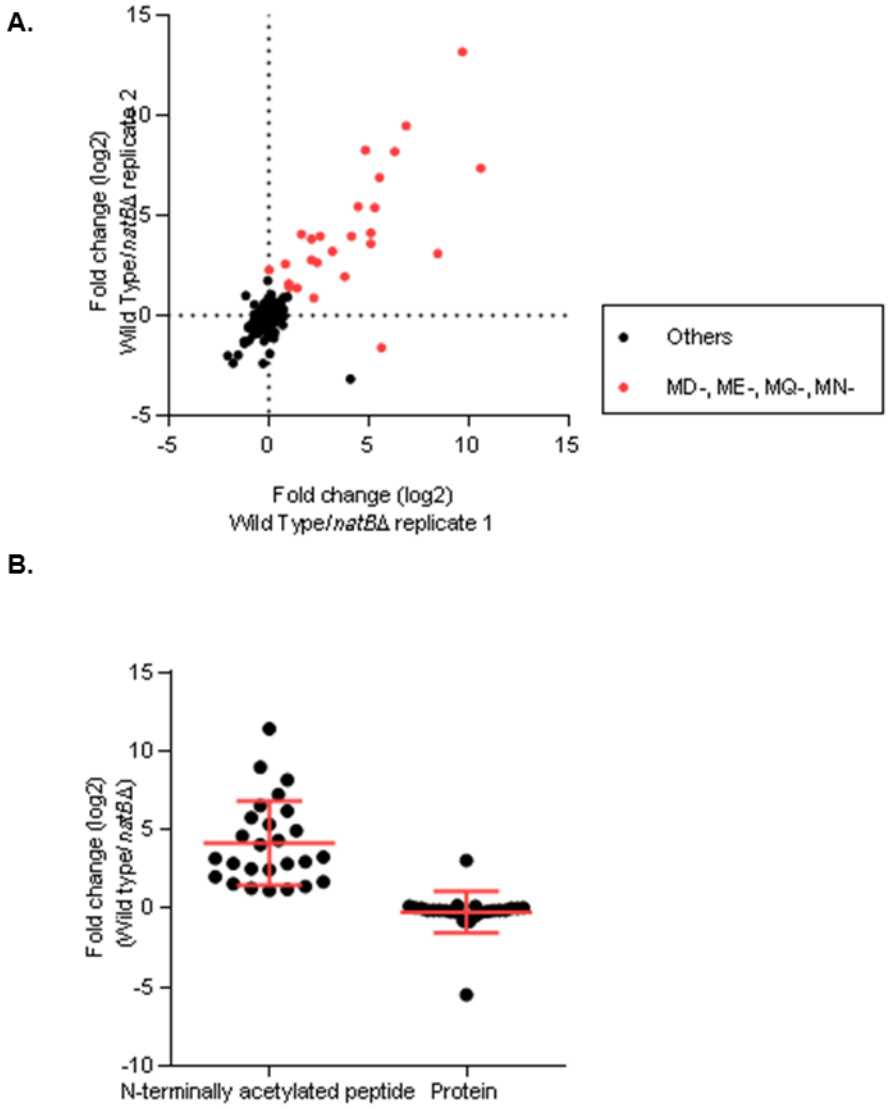

Figure 15: SILAC-based quantification of N-terminal acetylation in *natB*Δ relative to the wild type.

A. Correlation of fold change (log2) between wild type and *natB*Δ for N-terminally acetylated peptides from two label-swap replicates. Peptides starting with MD-, ME-, MQ-, and MN- are highlighted.
B. Steady state levels fold change (log2) between wild type and *natB*Δ for proteins starting with MD-, ME-, MQ-, and MN-, and their corresponding N-terminally acetylated peptide.

When both the N-terminally acetylated and non-acetylated forms of the same peptide were quantified, the percentage of N-terminal acetylation for the corresponding protein was calculated for wild type as well as in *natB*Δ. Consistently, proteins starting with MD-, ME-, and MN- showed close to full N-terminal acetylation in wild type (in contrast to MQ-), versus minimal N-terminal acetylation levels in *natB*Δ. On the

contrary, proteins starting with N-termini other than MD-, ME- , MQ-, and MN- (including MS-, MA-, MT-) are acetylated to comparable levels in wild type and *natB*Δ confirming the highly distinct substrate specificities of NatB under the tested experimental conditions (**Figure 16**).

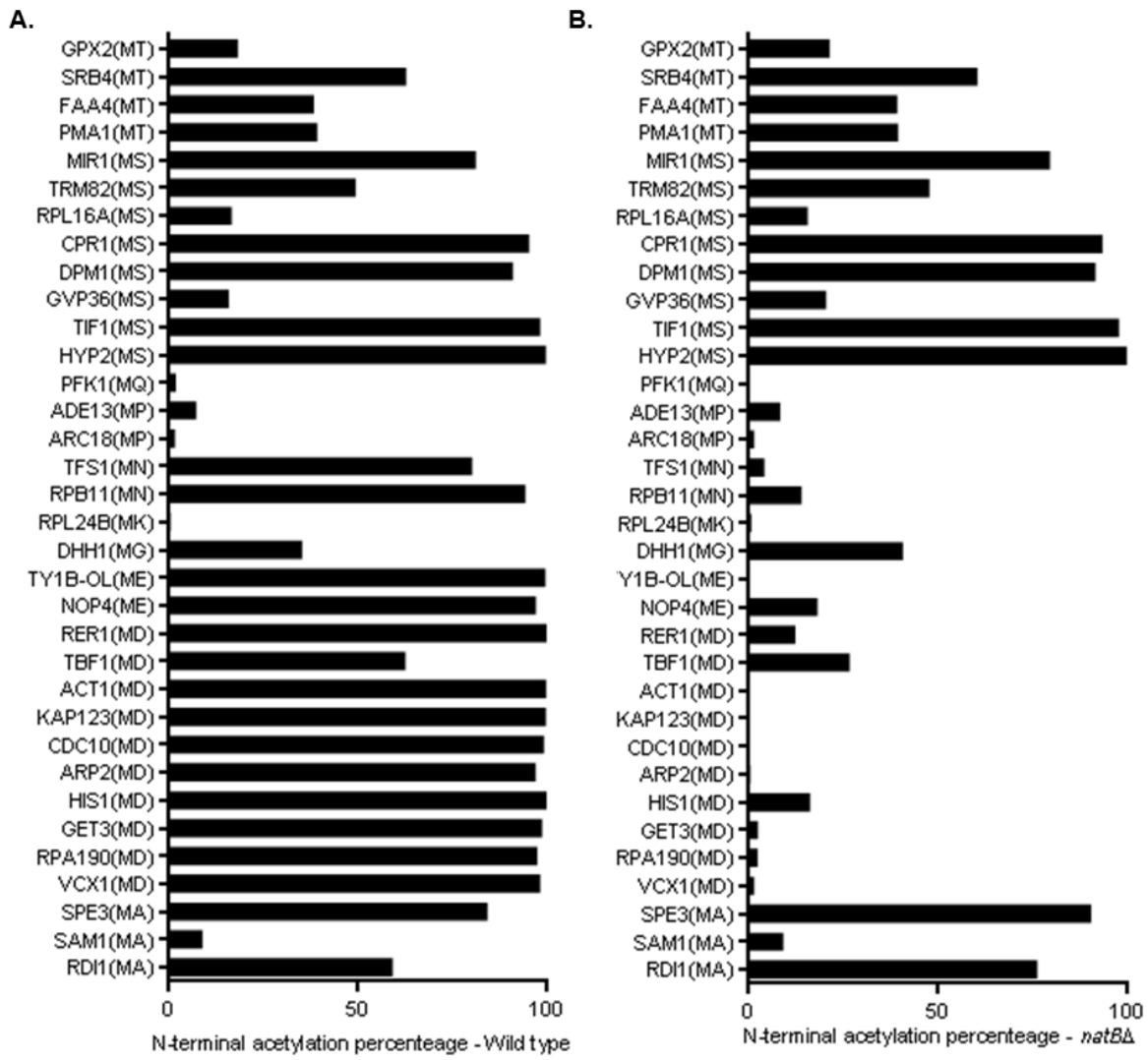

Figure 16: SILAC-based quantification of the degree of N-terminal acetylation in *natB*Δ relative to the wild type.

A. The percentage of N-terminal acetylation in wild type for proteins where both N-terminally acetylated and non N-terminally acetylated forms of the same peptides were quantified. The sequence of the first two N-terminal amino-acids is listed in brackets.
B. The percentage of N-terminal acetylation in *natB*Δ for proteins where both N-terminally acetylated and non N-terminally acetylated forms of the same peptides were quantified. The sequence of the first two N-terminal amino acids is listed in brackets.

3.1.5 Gene ontology (GO) enrichment analysis of the changes at the translatome and proteome level in *natBΔ*

To further elucidate the biological significance of the proteome dynamics in *natBΔ*, we performed gene ontology (GO) enrichment analysis of the changes at the translatome (based on ribosome profiling) and proteome level (based on quantitative proteomics) in *natBΔ* relative to the wild type. We employed two-dimensional statistical analysis that systematically tests whether changes in *natBΔ*, both at the translatome or proteome level, for proteins annotated to every GO term, significantly deviates from the overall distribution of all proteins (Cox and Mann, 2012). A major advantage of this analysis is that it is not restricted to predefined proteins based on arbitrary thresholds. Statistically significant GO terms are assigned a directional score, where a score>0 means the particular GO term is elevated in *natB*Δ relative to the wild type (1 is the maximum score), while a score<0 means the particular GO term is reduced in *natB*Δ relative to the wild type (-1 is the minimum score). Interestingly, the 2D-GO enrichment analysis revealed modulation of specific biological processes in *natBΔ* **(Figure 17)**.

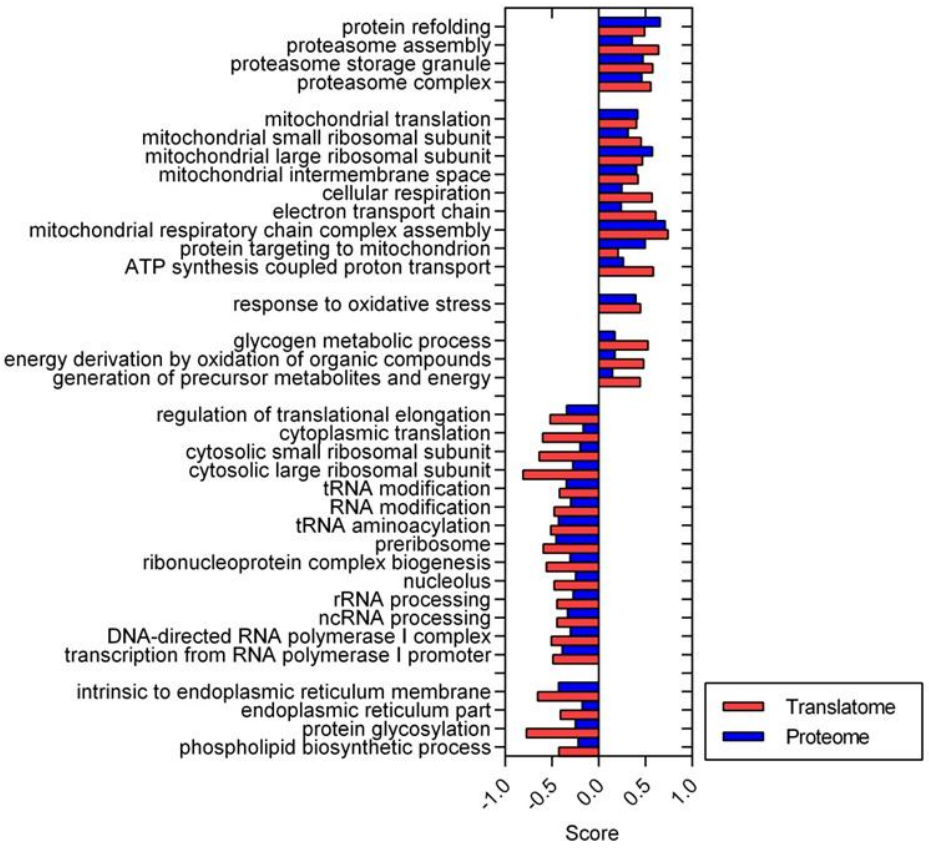

Figure 17: Gene ontology (GO) enrichment analysis of the changes at the translatome and proteome level for *natBΔ* versus wild type.

Two-dimensional annotation analysis of all quantified genes at the translation level (analyzed by ribosome profiling) or protein level (quantitative proteomics) in *natB*Δ relative to wild type. Analysis was done at threshold FDR = 0.05. Only significant GO terms with a score>0.4 or <-0.4 at the translation or protein level are shown. GO terms that have less than 10 genes are not shown.

3.1.6 Elevated protein refolding capacity in *natB*Δ

Remarkably, both translatome and proteome analyses indicated that the protein refolding machinery is significantly elevated in *natBΔ* cells **(Figure 17)**. Specifically, the stress inducible small heat shock protein (Hsp26), the stress inducible Hsp70 (Ssa4), as well as the cytosolic and mitochondrial disaggregase (Hsp104, Hsp78) are >2 fold elevated in *natB*Δ at the translation and steady state protein level **(Figure 18A)**. Consistent with this finding, the capacity to refold plasmid-encoded firefly luciferase after heat denaturation (Gupta et al., 2011) is higher in *natB*Δ cells compared to the wild type, suggesting higher chaperone content in *natB*Δ cells **(Figure 18B)**.

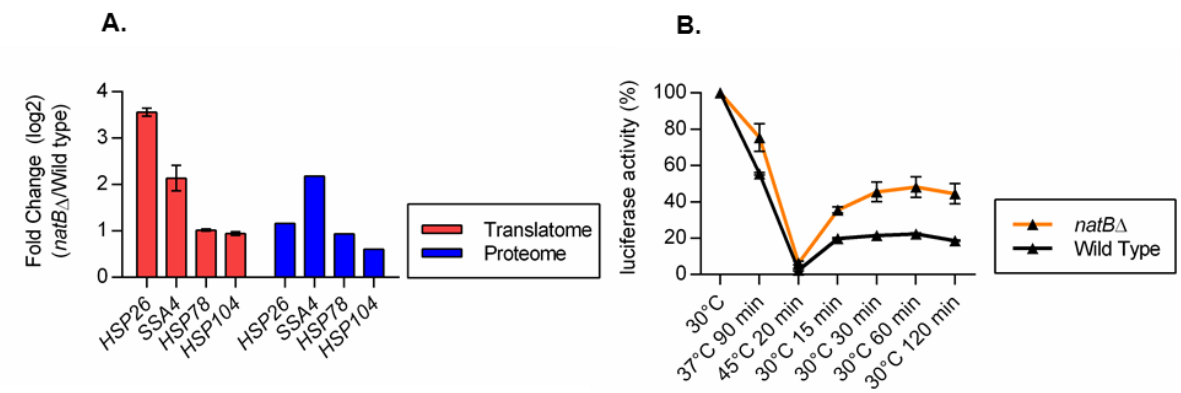

Figure 18: Elevated protein refolding capacity in *natB*Δ.

A. Comparison of the levels of molecular chaperones that are involved in protein refolding between *natB*Δ and wild type at the translation level (ribosome profiling) and protein level (quantitative proteomics).
B. Comparison of the refolding kintetics of heat denatured luciferase refolding between *natB*Δ and wild type.

3.1.7 Compartment-specific translation modulation in *natB*Δ cells

Interestingly, proteins annotated to mitochondrial translation and electron transport chain are elevated in *natBΔ* suggesting elevated mitochondrial respiration in *natBΔ* **(Figure 17)**. In contrast to the mitochondrial ribosomal proteins elevation, cytoplasmic ribosomal proteins are significantly repressed in *natBΔ* at both translation/steady-state levels, together indicating a compartment specific translation modulation in *natBΔ*

(Figure 19A). Cytoplasmic translation repression in *natBΔ* is not limited to repressed levels of ribosomal proteins but also comprises proteins annotated to ribosome biogenesis, tRNA aminoacylation, as well as translation factors, suggesting an orchestrated mechanism for translation repression **(Figure 17)**, analogous to the stress response mediated transcriptional repression of the protein biosynthesis machinery (Gasch et al., 2000). In line with the reduced levels of the cytoplasmic translation proteins, *natB*Δ cells showed ~2-fold less incorporation of radiolabeled ^{35}S Methionine compared to the wild type, indicating reduced translation efficiency in *natB*Δ cells **(Figure 19B)**. In addition, polysome profiling shows higher monosome to polysome ratio in *natB*Δ cells, indicating less active global translation **(Figure 19C)**.

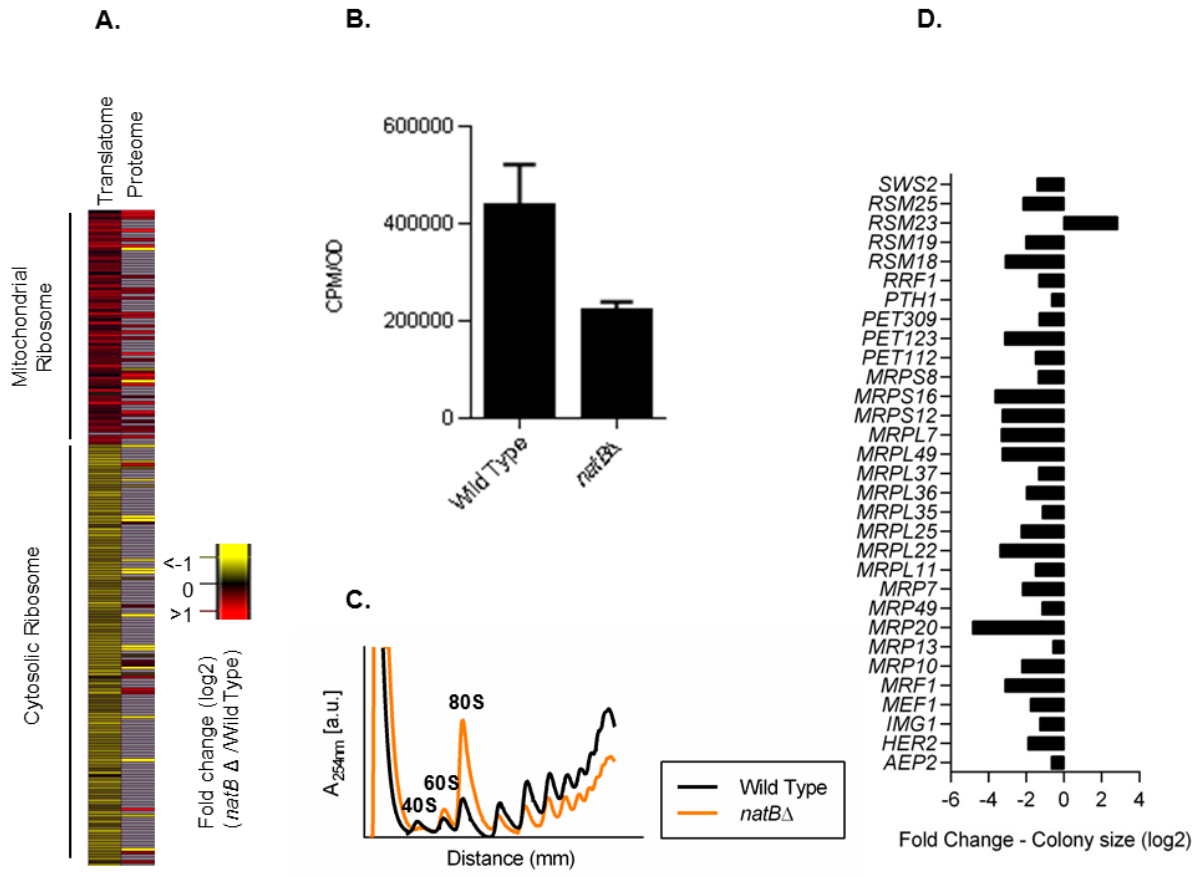

Figure 19: Compartment-specific translation modulation in *natB*Δ.

A. Comparison of the levels of cytosolic and mitochondrial ribosomal proteins between *natB*Δ and wild type at the translation level (ribosome profiling) and protein level (quantitative proteomics).
B. ^{35}S Methionine incorporation in wild-type and *natB*Δ (measured in counts per million (CPM) normalized to cell density (OD_{600}))
C. Polysome profile of *natB*Δ and wild type performed by fractionation of cell lysate in 10-50% sucrose gradient (polysome profiling was performed by Ulrike Friedrich).
D. Comparison of colony size fold change (log2) for deletion mutants for genes encoding components of the mitochondrial translation machinery in the presence/absence of *natB.*

In complementation to the high-throughput analysis of proteome dynamic in *natB*Δ, we performed an unbiased genetic screen that aims to dissect the effect of single gene perturbation on the fitness of *natB*Δ cells, thereby highlighting biological processes that are critical for *natB*Δ viability. In summary, *natB*Δ was introduced into a library of non-essential yeast gene deletions using SGA (Baryshnikova et al., 2010), and the fitness of double mutants was compared to the single mutants based on average colony size measurements. Interestingly, genes involved in mitochondrial translation showed the strongest effect among genes whose deletion lead to significant synthetic growth defect in *natB*Δ based on enrichment analysis (score = -0.76, p-value= 4E-12) **(Figure 19D)**. This observation underscores the critical role of mitochondrial translation for maintaining cellular fitness in *natB*Δ, in line with the elevated levels of mitochondrial translation proteins in *natB*Δ**.**

3.1.8 Constitutive stress response in *natB*Δ

In line with the aforementioned indications of stress response activation in *natBΔ*, we found that the heat shock transcription factor (Hsf1) is elevated in *natBΔ* cells at both translation and protein steady state level **(Figure 20A)**, which is reminiscent to the increase of Hsf1 expression under heat stress (Gasch et al., 2000). We further asked whether the increased expression of genes in *natBΔ* is mediated by Hsf1, by analyzing the genes with >2-fold increase in *natBΔ* at the translation level or protein steady state levels using Yeastract database (Teixeira et al., 2006). We found that approximately 50% of the elevated genes in *natBΔ* at the translation or protein level are experimentally verified inducible targets of Hsf1. This is significantly higher than the percentage of genes that are targets of Hsf1 in a list of all genes quantified at the protein synthesis or protein steady state level (background) **(Figure 20B)**.

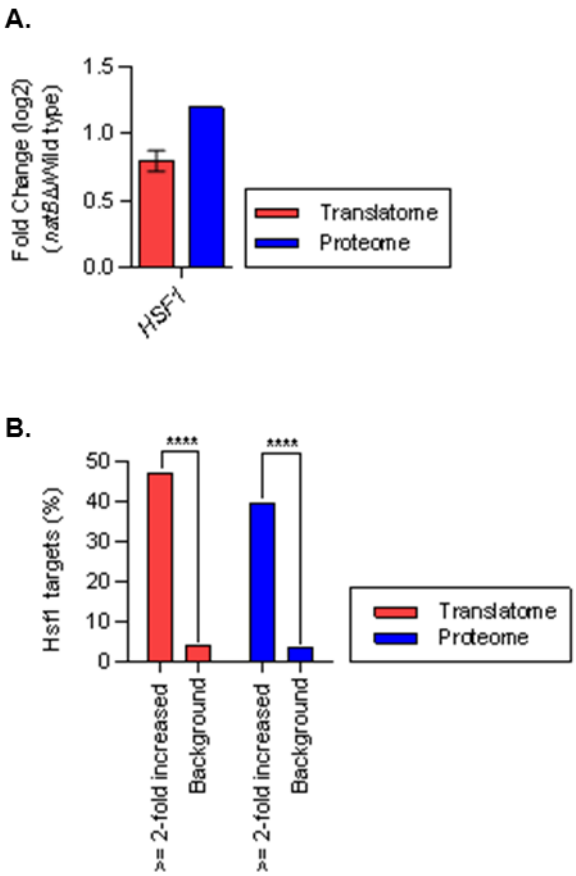

Figure 20: Constitutive stress response in *natB*Δ.

A. Hsf1 synthesis and abundance in wild-type and *natB*Δ cells determined by ribosome profiling and quantitative proteomics.
B. The percentage of Hsf1 targets among genes that are more than two fold increased at the translation level or protein level in *natB*Δ, compared to the background of all quantified proteins at the translation or protein levels. Only experimentally verified targets are included in the analysis. *** p-value ≤ 0.001. Statistical significance was calculated based on Fisher exact test.

3.2 Proteome turnover analysis in *natB*Δ

N-terminal acetylation was recently described as a signal for protein degradation. With this in mind, we asked whether the constitutive stress response observed in *natB*Δ is triggered by perturbation of protein degradation of NatB substrates that have failed to be N-terminally acetylated. If the model were true, the lack of N-terminal acetylation of NatB substrates in *natB*Δ would prevent their N-acetyl mediated degradation resulting in elevated steady-state levels of those proteins.

To address this possibility, we tested whether experimentally identified NatB substrates tend to be elevated in terms of steady state levels in *natB*Δ relative to the wild type, as measured by quantitative proteomics. Interestingly, the distribution of the protein steady state levels fold change between *natB*Δ and wild type for the verified NatB substrates showed no significant difference when compared to the distribution of all quantified proteins (background) **(Figure 21A).**

Protein steady state levels measured by quantitative proteomics are the net outcome of both protein stability (degradation) and protein biogenesis (translation). Therefore, we normalized the relative protein levels to their corresponding relative translation levels, to specifically analyze the effects on proteins turnover. The distribution of the normalized protein steady state levels fold change between *natB*Δ and wild type for the verified NatB substrates showed no significant differences when compared to the distribution of all proteins **(Figure 21B).**

Next, we aimed to directly measure protein stability in *natB*Δ relative to the wild type, by employing the newly developed tandem fluorescent timer analysis that allows relative estimation of protein stability, independent of protein abundance. We introduced *natB*Δ to the tFT library consisting of strains expressing 4,044 genome encoded tFT-tagged proteins using SGA, followed by high throughput fluorescence measurement of colonies. This allows for relative systematic stability profiling of proteins between wild type and *natB*Δ. Similarly, we asked whether experimentally verified NatB substrates tend to have different mCherry/GFP ratios in *natB*Δ cells relative to wild type. Confirming our previous analysis, the distribution of the mCherry/GFP fold change between *natB*Δ and wild type of the verified NatB substrates was not significantly different to the distribution of all measured proteins. Taken together, our data suggests no general effect of the loss of N-terminal acetylation on protein levels or protein stability under physiological conditions **(Figure 21C).**

Since N-acetyl mediated degradation may represent a quality control mechanism that gets manifested only upon specific perturbations including stress conditions, we asked whether lack of N-terminal acetylation by NatB would lead to global stabilization of NatB substrates under stress that compromises proteome integrity and triggers protein quality control pathways. Since *natB*Δ cells have a strong growth defect at 37°C **(Figure 13)**, we repeated the experiments under prolonged upshift to this elevated temperature. Therefore wild type and *natB*Δ cells were grown at 30°C, and then shifted to 37°C for two doubling time (for tFT analysis: plates were incubated at 30°C for 1 day then shifted to 37°C for 1 day) to allow enough time for re-establishing protein levels under stress. In line with the analysis at 30°C, our results suggest no general effect of loss of N-terminal acetylation on protein levels or protein stability under heat stress **(Figure 21D-F)**. Our analysis does not exclude that N-acetyl mediated degradation can take place for specific substrates.

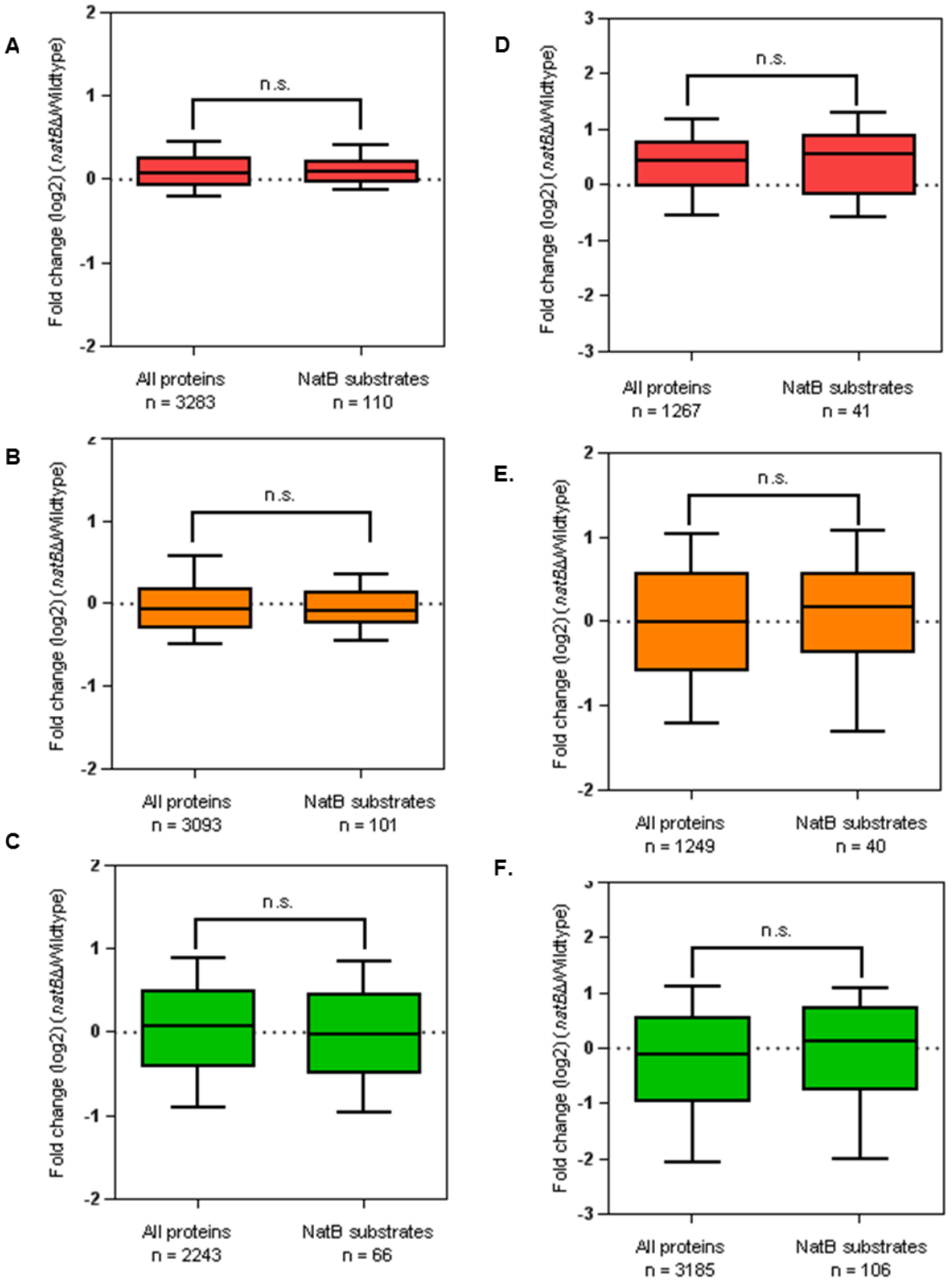
A
Fold change (log2) (natBΔ/Wildtype)
n.s.
All proteins
n = 3283
NatB substrates
n = 110
B
Fold change (log2) (natBΔ/Wildtype)
n.s.
All proteins
n = 3093
NatB substrates
n = 101
C
Fold change (log2) (natBΔ/Wildtype)
n.s.
All proteins
n = 2243
NatB substrates
n = 66
D
Fold change (log2) (natBΔ/Wildtype)
n.s.
All proteins
n = 1267
NatB substrates
n = 41
E.
Fold change (log2) (natBΔ/Wildtype)
n.s.
All proteins
n = 1249
NatB substrates
n = 40
F.
Fold change (log2) (natBΔ/Wildtype)
n.s.
All proteins
n = 3185
NatB substrates
n = 106

Figure 21: Loss of N-terminal acetylation by NatB has no global impact on substrate stability.

A. Comparison of the distribution of protein levels fold change (log2) between *natB*Δ and wild type at 30° (quantitative proteomics) for verified NatB substrates (n =110) and a background consisting of all proteins quantified at the protein level.
B. Comparison of the distribution of protein levels (normalized to the translation levels) fold change (log2) between *natB*Δ and wild type at 30° (quantitative proteomics and ribosome profiling), for the verified NatB substrates (n =101) and a background consisting of all proteins quantified at both translation (ribosome profiling) and protein level (quantitative proteomics).
C. Comparison of the distribution of the mCherry/GFP fold change (log2) between *natB*Δ and wild type at 30°, for verified NatB substrates (n =66) and a background consisting of all measured tFT protein fusions.
D. Comparison of the distribution of protein levels fold change (log2) between *natB*Δ and wild type (quantitative proteomics) upon shift from 30°C to 37°C for 2 doubling times for verified NatB substrates (n =41) and a background consisting of all proteins quantified at the protein level.
E. Comparison of the distribution of protein levels (normalized to the translation levels) fold change (log2) between *natB*Δ and wild type (quantitative proteomics and ribosome profiling) upon shift from 30°C to 37°C for 2 doubling times for the verified NatB substrates (n =40) and a background consisting of all proteins quantified at both translation (ribosome profiling) and protein level (quantitative proteomics).
F. Comparison of the distribution of mCherry/GFP fold change (log2) between *natB*Δ and wild type upon shift from 30°C to 37°C for verified NatB substrates (n =106) and a background consisting of all measured tFT protein fusions.

Statistical significance in (a-f) was calculated based on unpaired t-test. Whiskers in box plots in (a-f) represent 10%-90% interval. Verified NatB substrates were selected based on a manually curated list of all experimentally identified N-terminally acetylated proteins from literature, prepared by Ulrike Friedrich.

3.3 Global aggregation of endogenous proteins in *natB*Δ

The elevated levels of protein refolding machinery in *natB*Δ suggest that loss of N-terminal acetylation by NatB compromises protein integrity. To address this possibility, we isolated protein aggregates from *natB*Δ and wild type cells. Interestingly, *natB*Δ showed elevated protein aggregation as compared to the wild type **(Figure 22A)**. To identify and quantify aggregated proteins enriched in *natB*Δ cells we employed SILAC-based quantitative proteomics analysis of the aggregate fraction. In summary, we quantified 849 aggregated proteins that are more than 2-fold enriched in *natB*Δ relative to the wild type cells in each of two label-swap replicates. Increased aggregation of those proteins is not because of their increased protein steady state levels in *natB*Δ cells, when comparing protein level fold changes (*natB*Δ/Wild type) measured by quantitate proteomics of the aggregates fraction versus total lysate **(Figure 22B)**. In line with the quantitative proteomics analysis of protein aggregates, the GFP tagged variant of Gsy2, the most enriched protein in the aggregate fractions of *natB*Δ compared to wild type, forms foci in *natB*Δ cells but a diffuse distribution in the wild type **(Figure 22C)**.

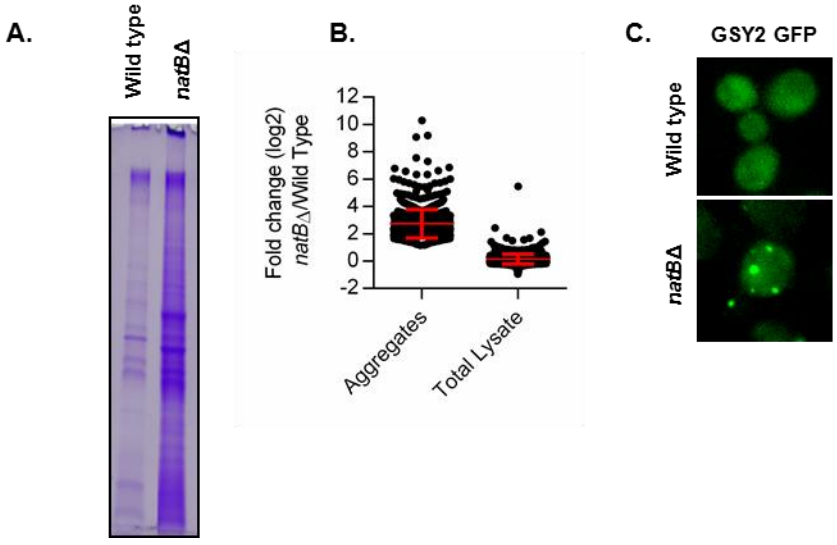

Figure 22: Global endogenous proteins aggregation in *natB*Δ.

A. Isolated protein aggregates from wild type and *natB*Δ followed by SDS-PAGE and coomassie-staining.
B. Comparison of the distribution of the protein level fold change (log2) between *natB*Δ and wild type, for aggregating proteins versus their corresponding levels in the total lysate (only proteins of >2-fold increase in *natB*Δ relative to the wild type, in the aggregates fraction, in each of the two replicates were included in the analysis).
C. Live cell microscopy of GFP tagged Gsy2 in *natB*Δ compared the wild type.

3.3.1 Protein aggregation in *natB*Δ cannot be solely explained as a direct consequence of the loss of N-terminal acetylation

We next asked whether protein aggregates in *natB*Δ is enriched with proteins that have failed to be N-terminally acetylated by NatB. Analysis of protein aggregates in *natB*Δ showed no significant enrichment of verified NatB substrates when compared to a background consisting of all the proteins quantified from the total lysate **(Figure 23A)**. Moreover, verified NatB substrates among *natB*Δ aggregates show no significant difference in their protein level fold change (*natB*Δ/wild type) in the aggregates fraction, when compared to all aggregated proteins in *natB*Δ **(Figure 23B)**. Taken together, protein aggregation in *natB*Δ cannot be explained only on the basis of aggregation of proteins that fail to be N-terminally acetylated in *natB*Δ, suggesting contribution of additional factors.

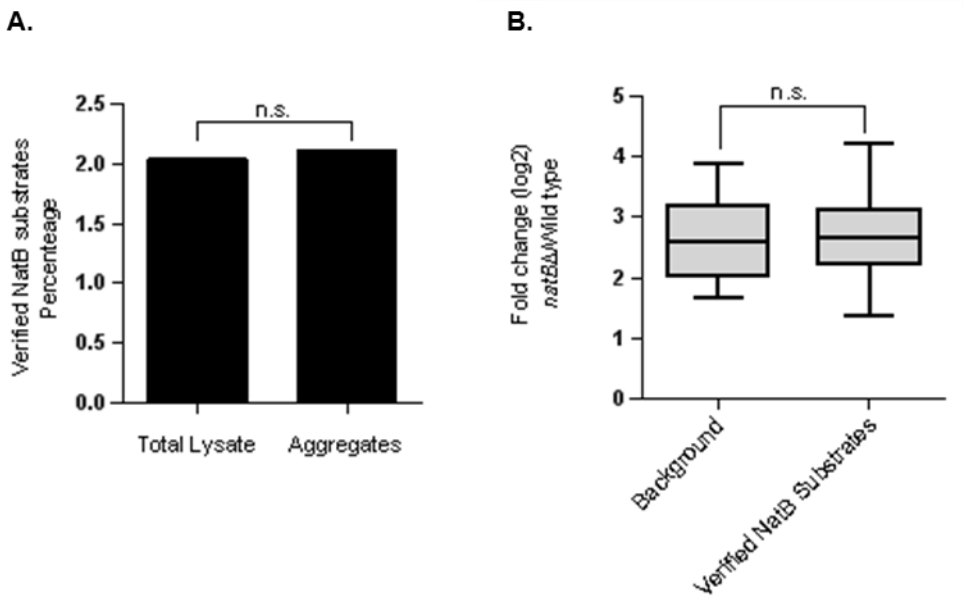

Figure 23: Protein aggregation in *natB*Δ cannot be solely explained as direct consequence of the loss of N-terminal acetylation.

A. The percentage of verified NatB substrates among quantified proteins in the total lysate, or aggregated proteins. Statistical significance was calculated based on Fisher exact test.
B. Comparison of the distribution of protein level (log2) fold change between *natB*Δ and wild type in the aggregates fraction for verified NatB substrates versus all aggregated proteins in *natB*Δ. Statistical significance was calculated based on unpaired two samples t-test.

3.3.2 Analysis of protein aggregates in *natB*Δ suggests an underlying selective sequestration mechanism

We next asked whether protein aggregates in *natB*Δ are enriched for specific pathways or cellular compartments. To address this question, we performed functional annotation clustering of protein aggregates in *natB*Δ using DAVID (Dennis et al., 2003). Interestingly, the most enriched group of proteins among the protein aggregates in *natB*Δ is the cytoplasmic translation machinery including cytosolic small and large ribosomal subunits, translation factors, ribosome biogenesis factors, as well as tRNA-aminoacylation machinery, together representing more than 15% of all proteins aggregating in *natB*Δ **(Figure 24A)**. Moreover, 65-85% of the proteins annotated to cytoplasmic translation that were quantified in the total lysate, were enriched in *natB*Δ aggregates, suggesting a global sequestration of the translation machinery into protein aggregates **(Figure 24A)**. In addition, *natB*Δ protein aggregates show significant enrichment of mitochondrial and ER proteins **(Figure 24B).** Furthermore, *natB*Δ aggregates sequester chaperones including those known to associate with protein aggregates (Hsp26 and Hsp104),

as well as Hsp70, Hsp40s, and Hsp90, TriC/CCT, and ribosome associated chaperones **(Figure 24C)**. In addition, ER and mitochondrial chaperones are also sequestered into aggregates in *natB*Δ aggregates **(Figure 24C)**. Interestingly, proteins aggregating in *natB*Δ showed significantly higher interactions between each other compared to a randomized list with equal number of proteins (STRING database (Szklarczyk et al., 2010)) **(Figure 24D)**, underscoring the role of protein-protein interactions in sequestration of proteins to aggregates in *natB*Δ.

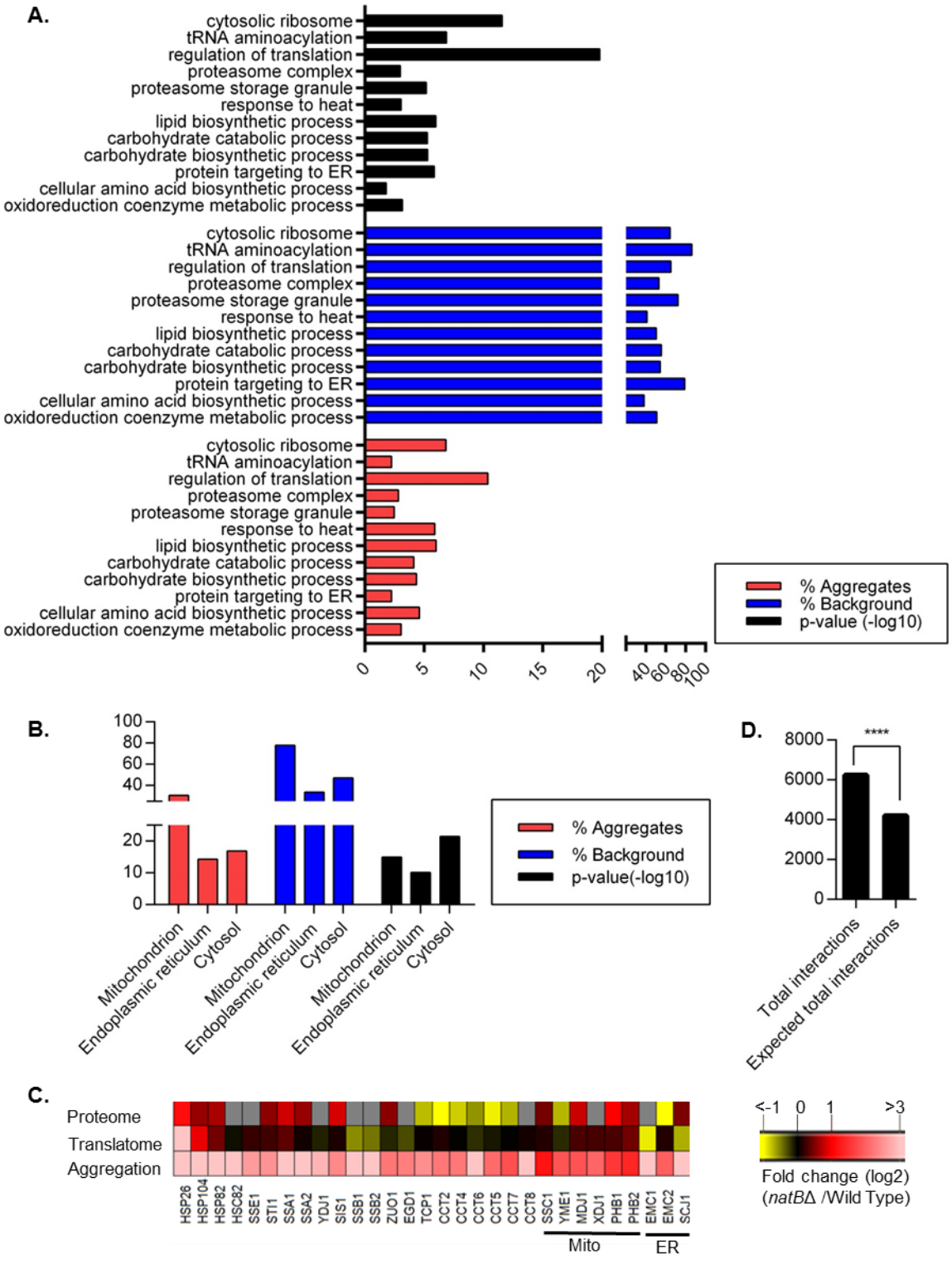
A.
cytosolic ribosome
tRNA aminoacylation
regulation of translation
proteasome complex
proteasome storage granule
response to heat
lipid biosynthetic process
carbohydrate catabolic process
carbohydrate biosynthetic process
protein targeting to ER
cellular amino acid biosynthetic process
oxidoreduction coenzyme metabolic process
0 5 10 15 20 40 60 80 100
% Aggregates
% Background
p-value (-log10)
B.
100 80 60 40 20 10 0
Mitochondrion
Endoplasmic reticulum
Cytosol
% Aggregates
% Background
p-value(-log10)
D.
8000 6000 4000 2000 0
****
Total interactions
Expected total interactions
C.
Proteome
Translatome
Aggregation
HSP26 HSP104 HSP82 HSC82 SSE1 STI1 SSA1 SSA2 YDJ1 SIS1 SSB1 SSB2 ZUO1 EGD1 TCP1 CCT2 CCT4 CCT6 CCT5 CCT7 CCT8 SSC1 YME1 MDJ1 XDJ1 PHB1 PHB2 EMC1 EMC2 SCJ1
Mito
ER
<-1 0 1 >3
Fold change (log2)
(natBΔ /Wild Type)

Figure 24: Analysis of protein aggregates in *natB*Δ suggests an underlying coordinated sequestration mechanism for specific groups of proteins.

A. Functional annotation clustering (DAVID) for biological processes of proteins aggregating in *natB*Δ. Clusters with enrichment score <2 are not shown. Background consists of all proteins quantified in the total lysate. %Aggregates: The percentage of all aggregated proteins that are annotated to a particular GO term. % Background: The percentages of proteins which are quantified in the total lysate that are also enriched in the aggregates, for a particular GO term.
B. Functional annotation clustering (DAVID) for cellular compartments of proteins aggregating in *natB*Δ. Clusters with enrichment score <2 are not shown. %Aggregates: The percentage of aggregated proteins that are annotated to a particular GO term. % Background: The percentages of proteins which are quantified in the total lysate, that are also enriched in the aggregates, for a particular GO term.
C. Protein level fold change (log2) between *natB*Δ and wild type of all quantified molecular chaperones in *natBΔ* protein aggregates, and their corresponding steady state levels (quantitative proteomics), and translation levels (ribosome profiling).
D. Comparison of total protein-protein interactions between proteins aggregating in *natB*Δ and a randomized list of proteins with equal number (analysis was performed by STRING database). *** P ≤ 0.001

3.3.3 The pattern of protein aggregation in *natB*Δ and *ssb1,2*Δ cells is highly similar

To further understand the reasons for sequestration of protein aggregates in *natB*Δ, we asked whether proteins that aggregate in *natB*Δ, tend to aggregate under other conditions. Indeed, protein aggregates in *natB*Δ showed a substantial overlap with stress induced protein aggregation (De Laureto et al., 2014; Stoecklin et al., 2015; Wallace et al., 2015), suggesting that protein aggregates in *natB*Δ may comprise aggregation-prone proteins that are sensitive to changes in the cellular protein folding environment **(Figure 25A)**. Interestingly, *natB*Δ aggregates show the largest overlap with protein aggregates present in cells lacking both isoforms of the ribosome associated Hsp70 Ssb (Koplin et al., 2010; Willmund et al., 2013) **(Figure 25A)**. Furthermore, deletion of *SSB* in *natB*Δ cells leads to a synthetic growth defect, suggesting that Ssb and NatB work in parallel pathways **(Figure 25B)**.

Given that N-terminal acetylation takes place co-translationally, it is likely that the loss of N-terminal acetylation can impact the integrity of nascent proteins. To address this possibility, we isolated radiolabeled protein aggregates after a short pulse with ^{35}S Methionine. Indeed, *natB*Δ showed elevated ^{35}S Methionine labeled aggregates compared to wild type indicating that a fraction of newly translated is readily sequestered into aggregates **(Figure 25C)**.

Specific components of the translation apparatus are known to aggregate under different stress condition thereby mediating translation repression (Stoecklin et al., 2015). On the contrary, ribosomal proteins do not globally aggregate under stress conditions, yet they aggregate in *natB*Δ and in *SSB*Δ **(Figure 25D)**, which further underscores the overlap between NatB and Ssb functions. Interestingly, cytoplasmic

translation components that are enriched in protein aggregates in *natB*Δ also tend to be reduced at the translation/protein level underscoring a multilayered modulation of cytoplasmic translation in *natB*Δ **(Figure 25D)**.

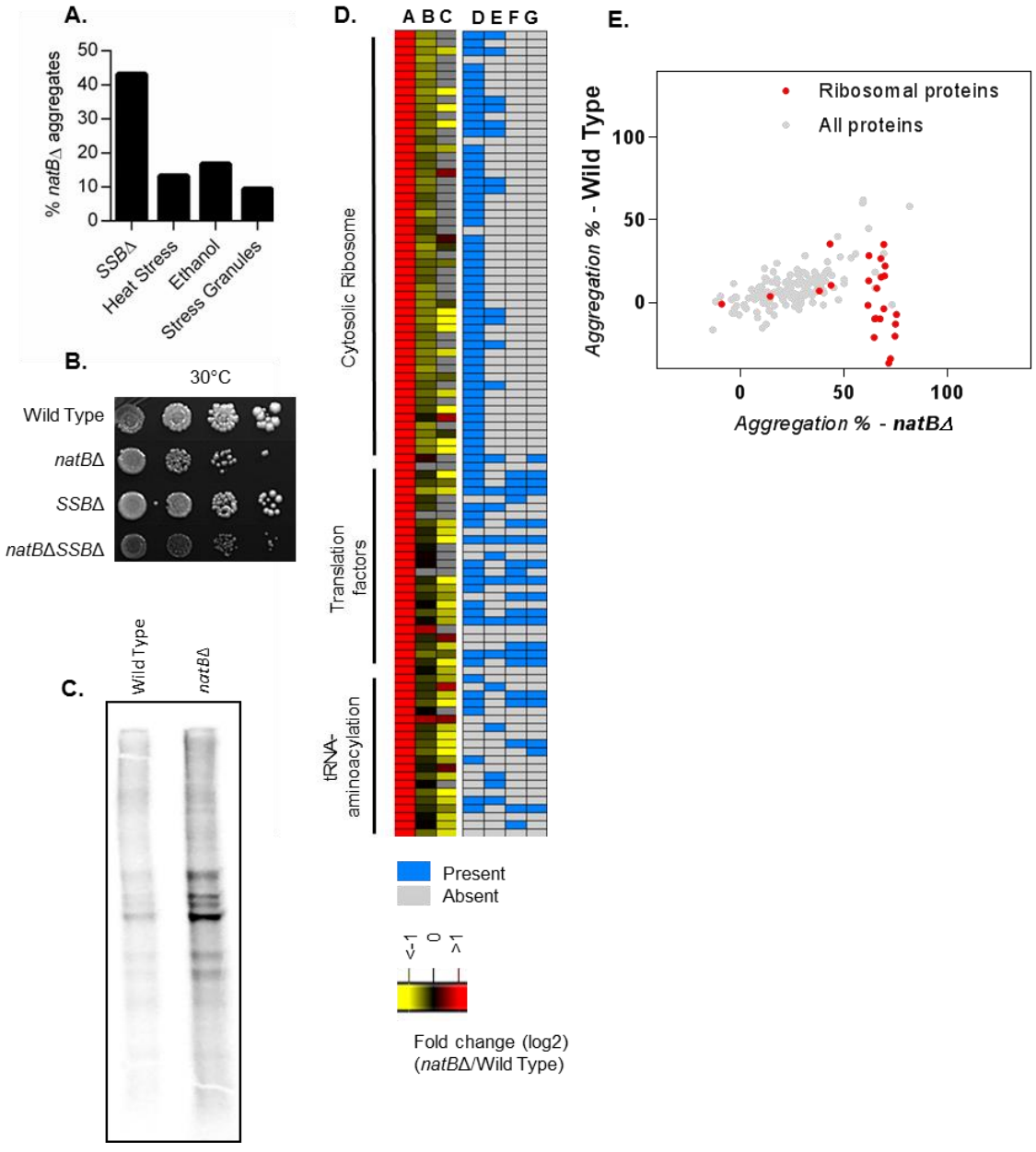

Figure 25: Protein aggregation in *natB*Δ overlap with aggregation upon deletion of *SSB*.

A. The overlap between protein aggregates in *natB*Δ and protein aggregates in *SSB*Δ or under different stress conditions calculated as percentage of *natB*Δ protein aggregates.

B. Growth behavior of *SSB* and *natB* double deletion mutant in comparison to single deletion mutants, and wild type.
C. ^{35}S labeled protein aggregates isolated from wild type and *natB*Δ, after 5 min incorporation.
D. The fold change (log2) of translation components between wild type and *natB*Δ in the protein aggregates (A), at the translation levels (B) and the protein steady state levels (C), and its aggregation behavior under other conditions (D: protein aggregation upon *SSB* deletion, E: Protein aggregation upon heat stress, F: Protein aggregation upon ethanol treatment. G: Stress granules).
E. Comparison of the percentage of a given protein that undergo aggregation in wild type versus *natB*Δ, using dimethyl labeling based quantitative proteomics of supernatant versus total lysate.

We further aimed to quantify the proportion of a given protein that aggregates upon loss of N-terminal acetylation. Towards this aim, I quantified protein abundances in the soluble fraction versus the total lysate after dimethyl labeling (Wallace et al., 2015). The relative protein levels before and after aggregate isolation reflects the percentage of a given protein that gets sequestered into protein aggregates. Ribosomal proteins showed the strongest depletion from the soluble fraction in *natB*Δ. On average, approximately ~ 40% of each of the quantified ribosomal proteins is sequestered into protein aggregates upon loss of N-terminal acetylation by NatB **(Figure 25E).**

3.4 Proteome-wide analysis of the effects of loss of N-terminal acetylation by NatA

3.4.1 Analogous protein aggregation in *nat*AΔ to *natB*Δ protein aggregation:

Protein aggregation in *natB*Δ can be explained as a primary effect of the loss of N-terminal acetylation where lack of N-terminal acetylation of a specific set of proteins directly triggers protein aggregation. Alternatively, it can be explained by secondary effects where lack of N-terminal acetylation of one or more NatB substrates that are important to prevent protein aggregation, compromise its functionality thereby leading to protein aggregation. To distinguish between the two possibilities, we asked whether loss of N-terminal acetylation of a distinct set of proteins (i.e. NatA substrates) may also lead to global protein aggregation. Towards this end, we isolated protein aggregates from *natA*Δ cells, and compared these to aggregates isolated from wild type and *natB*Δ cells. Interestingly, *natA*Δ caused elevated aggregation of proteins to a comparable level to the aggregated proteins in *natB*Δ **(Figure 26A).** To further characterize protein aggregation in *natA*Δ, we performed quantitative proteomic analysis of *natA*Δ protein aggregates. In summary, we quantified 707 proteins that are >2-fold elevated in the aggregate fraction in *natA*Δ relative to the wild type in each of the two replicates. Interestingly, protein aggregates in *natA*Δ and *natB*Δ strongly overlap **(Figure 26B)**, and enriched for similar biological processes and compartments **(Figure 26C)**, further highlighting a unifying mechanism for organized protein sequestration into aggregates, in

response to the loss of N-terminal acetylation of yet completely distinct sets of proteins. Notably, comparison of the protein aggregates in *natA*Δ and *natB*Δ based on the quantitative proteomics analysis showed a higher fold change in *natB*Δ compared to *natA*Δ cells **(Figure 26D).**

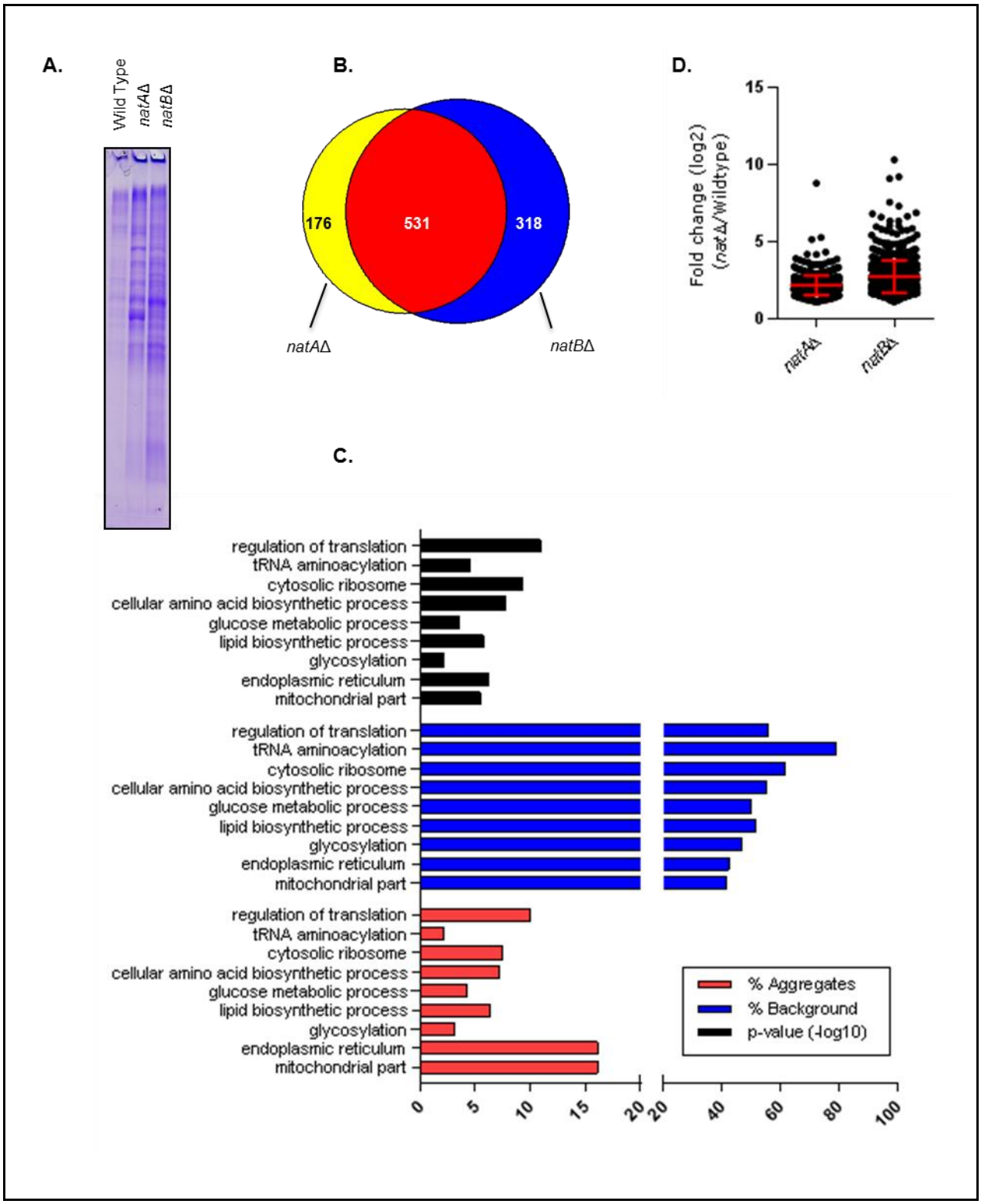

Figure 26: Analogous protein aggregation in *natA*Δ to *natB*Δ protein aggregation.

A. Comparison of protein aggregates between wild type, *natA*Δ and *natB*Δ by isolation of protein aggregates followed by SDS-PAGE and coomassie staining.
B. The overlap between protein aggregates in *natA*Δ and *natB*Δ cells quantified by SILAC-based mass spectrometry.
E. Functional annotation clustering (DAVID) of proteins aggregating in *natA*Δ (clusters with enrichment score <2 are not shown). Background consists of all proteins quantified in the total lysate. %Aggregates: The percentage of all aggregated proteins that are annotated to a particular GO term. % Background: The percentages of proteins which are quantified in the total lysate, that are also enriched in the aggregates, for a particular GO term.
C. Comparison of the fold change (log2) of protein aggregates between *natA*Δ, *natB*Δ and wild type.

(only proteins of >2-fold increase in *natA*Δ relative to the wild type, in the aggregates fraction, in each of the two replicates were included in the analysis).

3.4.2 Protein aggregation in *natA*Δ is due to the lack of NatA catalytic activity

Similar to co-translationally acting chaperones, N-terminal acetyl transferase complexes are ribosome associated and interact with the nascent chains co-translationally. With this in mind, we asked whether NATs - like chaperones - may mediate co-translational folding by directly interacting with the nascent chains independent of their enzymatic activity, which may then cause aggregation in NAT deletion mutants. To address this possibility, we complemented the *natA*Δ cells by either a plasmid-encoded wild type NatA catalytic subunit, or a catalytically dead mutant (Liszczak et al., 2013), followed by isolation of aggregates, as well as characterization of *natA*Δ growth phenotypes. Expression of wild type NatA catalytic subunit fully complemented *natA*Δ growth phenotypes **(Figure 27A)**, and suppressed aggregates formation **(Figure 27B).** In contrast, the catalytic dead mutant neither suppressed the aggregation **(Figure 27B)** nor the growth phenotype **(Figure 27A)** indicating that the loss of the N-terminal acetylation is the cause of protein aggregation.

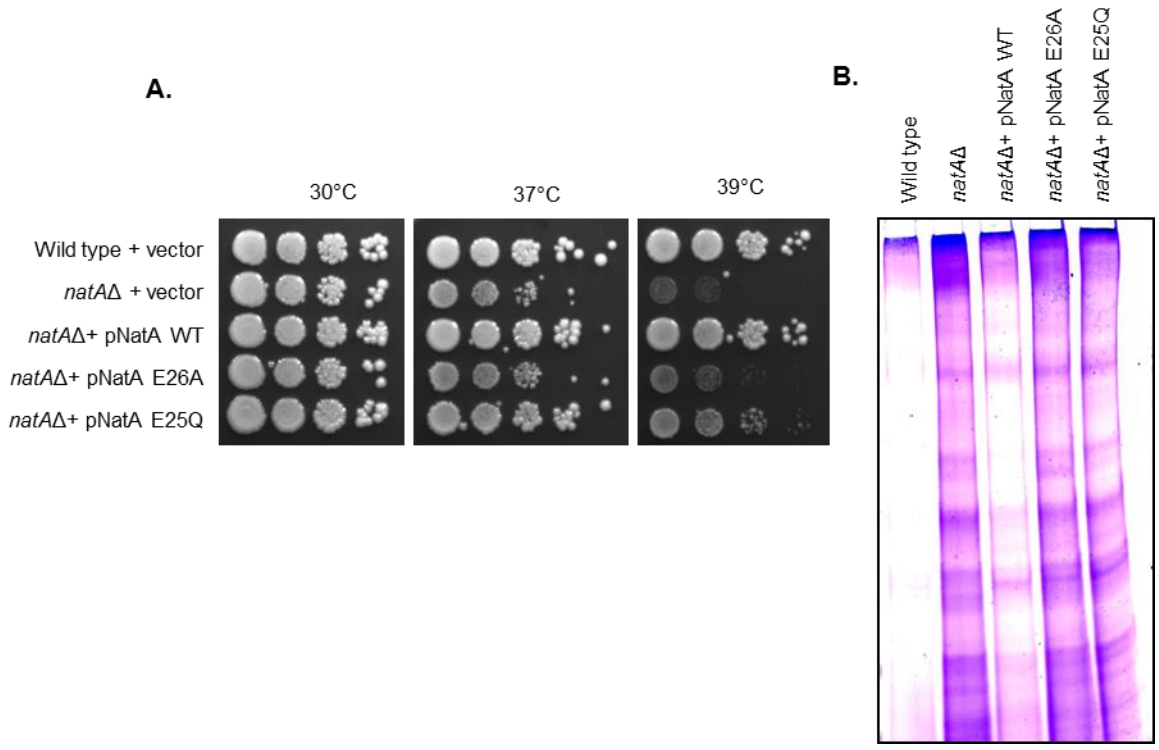

Figure 27: Protein aggregation in *natA*Δ is due to the lack of NatA catalytic activity.
A. Growth behavior of wild type, *natA*Δ, and *natA*Δ expressing plasmid encoded wild type NatA catalytic subunit, or the catalytically dead mutant of the NatA catalytic subunit.
B. Comparison of the levels of isolated protein aggregates from wild type, *natA*Δ, and *natA*Δ expressing plasmid encoded wild type NatA catalytic subunit, or the catalytically dead mutant of the NatA catalytic subunit.

3.4.3 Translatome/proteome analysis of *natA*Δ

To further understand the underlying mechanism/consequences of protein aggregation in *natA*Δ, we aimed to analyze changes at the protein synthesis (ribosome profiling), or protein levels (quantitative proteomics) in *natA*Δ cells in comparison to wild type, similar to the *natB*Δ translatome/proteome analyses described before (see section **3.1**).

3.4.3.1 Correlation between replicates

In summary, expression of 3989 genes were consistently quantified in *natA*Δ relative to the wild type (r = 0.88) based on ribosome profiling **(Figure 28A)**, while the steady state levels of 2402 proteins were

reproducibly quantified in *natA*Δ relative to wild type cells (r = 0.77) based on quantitative proteomics **(Figure 28B)**.

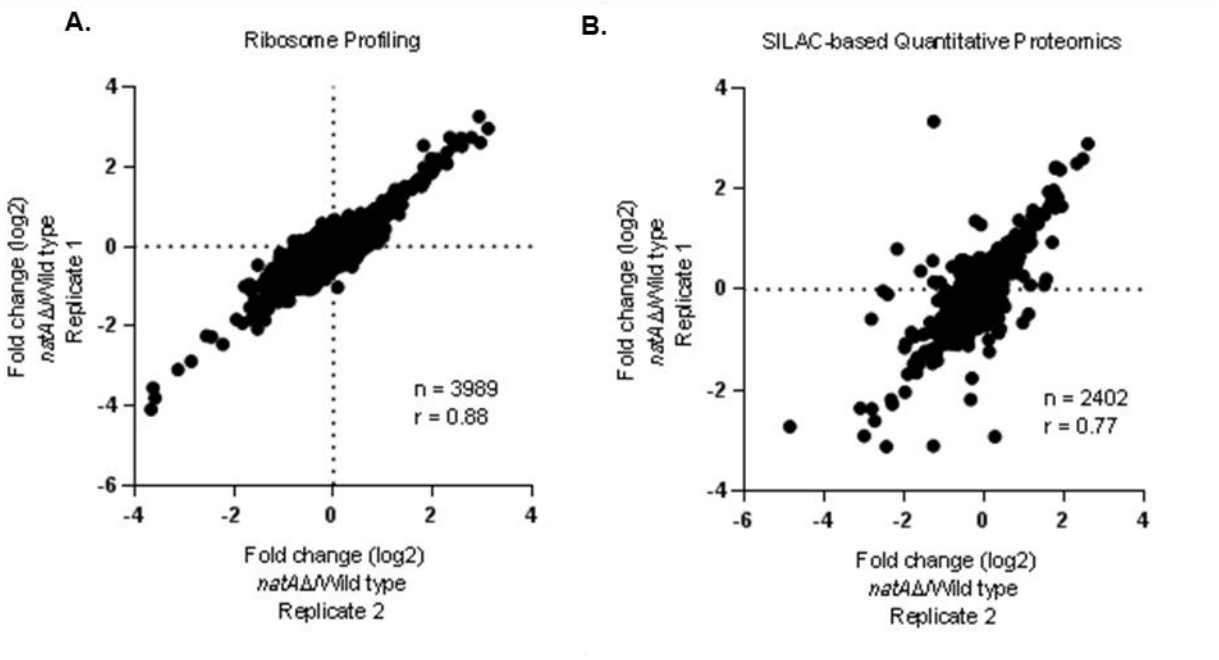

Figure 28: Translatome/proteome analysis of *natA*Δ.

A. Correlation between fold change (log2) of protein synthesis between *natA*Δ and wild type measured by ribosome profiling from two replicates. Pearson correlation coefficient (r) equals 0.88 based on 3989 genes.
B. Correlation between fold change (log2) of protein steady state levels between *natA*Δ and wild type measured by SILAC-based quantitative proteomics from two label-swap replicates. Pearson correlation coefficient (r) equals 0.77 for 2402 proteins.

3.4.3.2 Quantification of N-terminally acetylated peptides

To verify that NatA shows distinct substrate specificity under our experimental conditions, we analyzed N-terminal acetylation by SILAC-based quantitative proteomic analysis of the total lysate in *natA*Δ and wild type cells. Interestingly, 123 unique N-terminally acetylated peptides were consistently quantified in *natA*Δ relative to wild type, in two label swapped replicates. Confirmatory to the predicted NatA substrate specificity, N-terminally acetylated peptides starting with MS-, MT-, MS-, MV- showed consistently higher abundance in the wild type compared to *natA*Δ indicating deficient N-terminal acetylation of those proteins in *natA*Δ **(Figure 29A)**. This is not due to decreased steady state levels of those proteins in *natA*Δ compared to wild type **(Figure 29B)**.

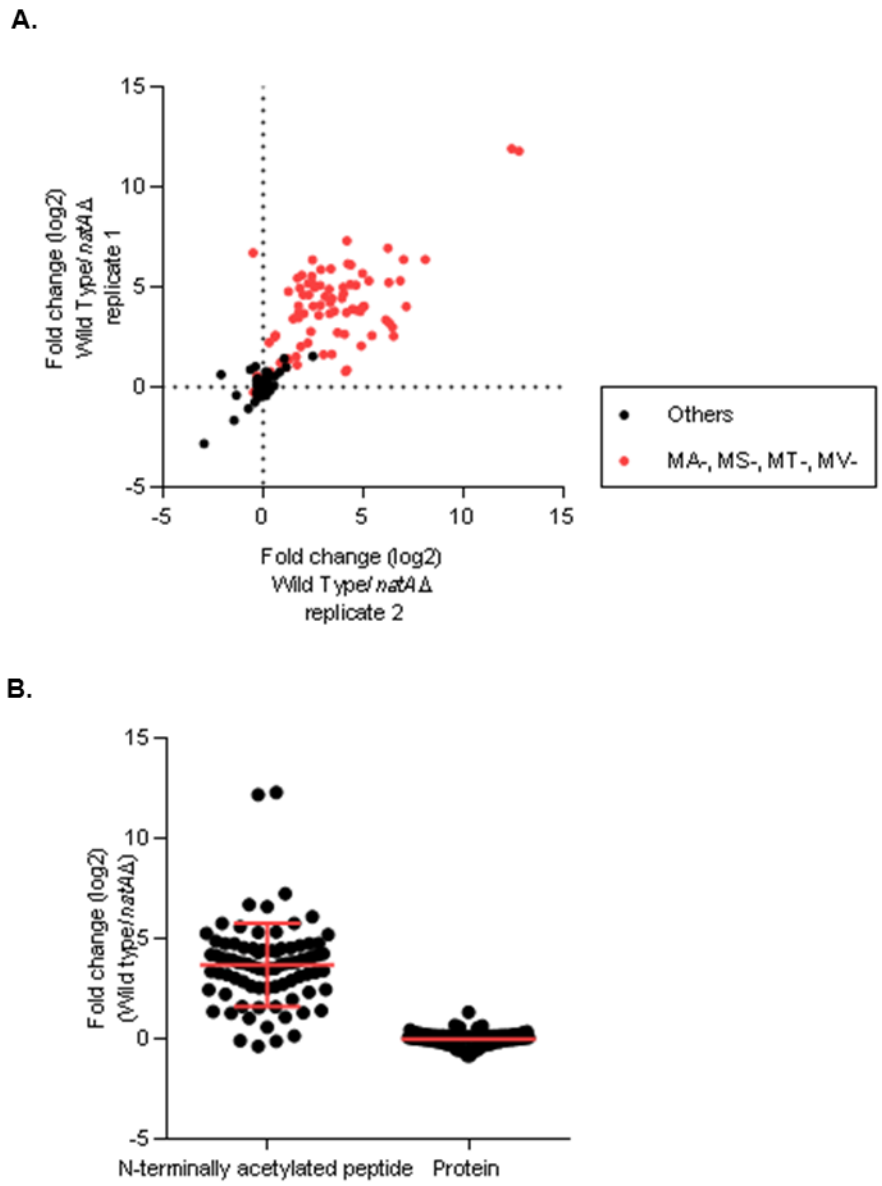

Figure 29: Quantification of N-terminal acetylation in *natA*Δ relative to the wild type.

A. Correlation of fold change (log2) between wild type and *natA*Δ for N-terminally acetylated peptides from two label-swap replicates. Peptides starting with MA-, MS-, MT-, and MV- are highlighted.
B. Steady state levels fold change (log2) between wild type and *natA*Δ for proteins starting with MA-, MS-, MT-, MV- and their corresponding N-terminally acetylated peptides.

When both the N-terminally acetylated and non N-terminally acetylated forms of the same peptide were quantified, the percentage of N-terminal acetylation for the corresponding proteins was calculated for wild type as well as *natA*Δ.

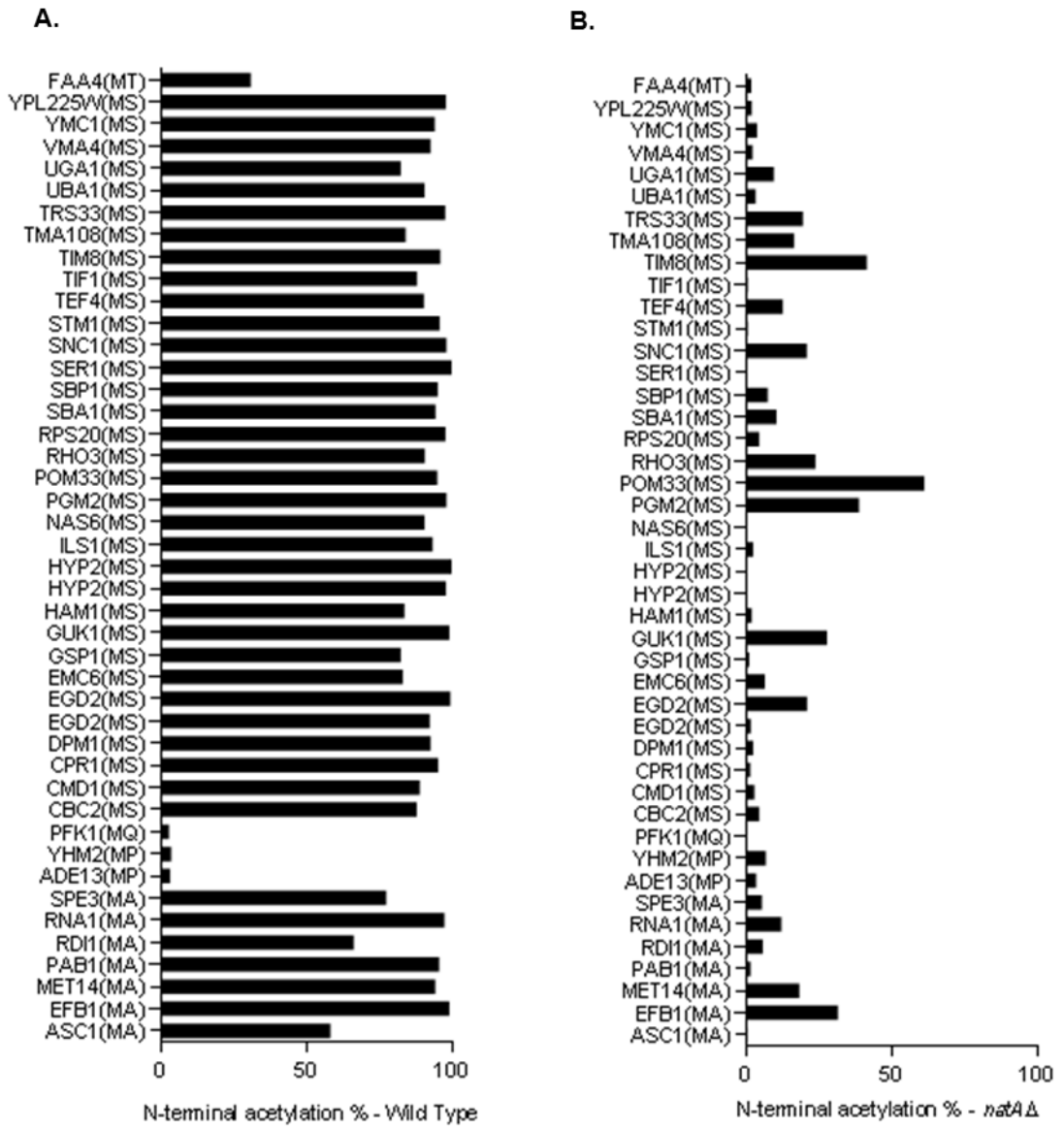

Figure 30: Quantification of the degree of N-terminal acetylation in *natA*Δ relative to the wild type.

A. The percentage of N-terminal acetylation in wild type for proteins where both N-terminally acetylated and non N-terminally acetylated forms of the same peptides were quantified. The sequence of the first two N-terminal amino-acids is listed between brackets.
B. The percentage of N-terminal acetylation in *natA*Δ for proteins where both N-terminally acetylated and non N-terminally acetylated forms of the same peptides were quantified. The sequence of the first two N-terminal amino-acids is listed between brackets.

Consistently, proteins starting with MS-, MA-, MT- and MV- were efficiently N-terminally acetylated in wild type, but not in *natA*Δ cells **(Figure 30)**. On the contrary, proteins starting with N-termini other than MS-,

MT-, MV-, and MA- (including MD-, ME-, or MQ-) show comparable levels of N-terminal acetylation between wild type and *nat*AΔ cells **(Figure 30)**. Taken together, NatA and NatB have highly distinct substrate specificities under the tested experimental conditions.

3.4.3.3 *natA*Δ cells display a more subtle stress response when compared to *natB*Δ cells

Given the elevated protein aggregation in *natA*Δ, we asked whether *natA*Δ cells show a constitutive stress response, similar to *natB*Δ **(Figure 20)**. We analyzed the genes with >2-fold increase in *natA*Δ at the translation level or protein steady state levels using Yeastract database. We found that approximately 10% of the elevated genes in *natA*Δ at the translation or protein level are experimentally verified inducible targets by Hsf1 **(Figure 31)**. This is only slightly higher than the percentage of genes that are targets of Hsf1 among all quantified proteins (background). Similar analysis of *natB*Δ showed that 50% of the elevated genes in *natB*Δ at the translation or protein level are experimentally verified inducible targets by Hsf1 **(Figure 20B, Figure 31)**. In summary, translatome/proteome analysis of *natA*Δ, suggests only a subtle stress response, when compared to *natB*Δ.

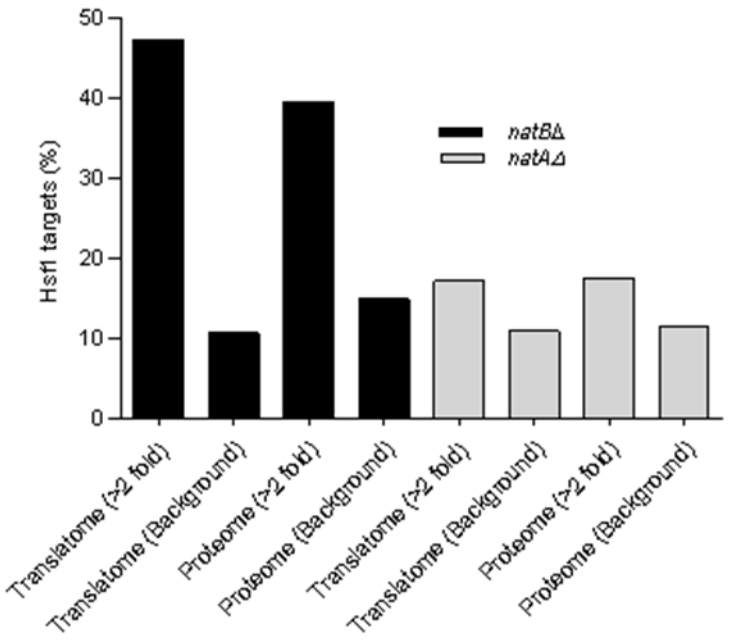

Figure 31: Subtle stress response in *natA*Δ.

The percentage of Hsf1 targets among genes that are more than two fold increased at the translation level or protein level between *natA*Δ, or *natB*Δ and wild type, versus background of all quantified protein at the translation or protein steady state levels. Only experimentally verified targets are included in the analysis.

3.5 Co-translational assembly of the NatB complex

Recent studies have indicated that protein complexes can assemble co-translationally, and suggested that co-translational protein complex assembly may represent an effective strategy to minimize protein aggregation (see section **1.1.2.6**). The crystal structure of the NatB complex was recently solved (Hong et al., 2017), and showed that the auxiliary subunit (Naa25) wraps around the catalytic subunit (Naa20) to form a stable dimeric complex **(Figure 32A).** Expression of the catalytic subunit in the absence of the auxiliary subunit leads to its aggregation, while no aggregation is observed when the auxiliary subunit was expressed in the absence of the catalytic subunit (Hong et al., 2017), suggesting that the catalytic subunit requires the auxiliary subunit for stable folding. With this in mind, we aimed to analyze whether NatB complex assembly takes place co-translationally.

Towards this aim, we employed a selective ribosome profiling approach where one subunit of the NatB complex is C-terminally tagged with GFP, followed by GFP immunoprecipitation “IP” and sequencing of the ribosome footprints. If the NatB complex assembles co-translationally, the IP of one subunit should lead to the co-IP of the nascent chains of the interacting subunit, which can be identified by analysis of the corresponding ribosome footprints. Indeed IP of Naa25 leads to co-IP of nascent chains of Naa20 **(Figure 32B)** indicating co-translational complex assembly, where Naa25 interacts with the nascent chains of Naa20. This correlates with the aggregation propensity of Naa20 in the absence of Naa25 (Hong et al., 2017). Interestingly, fully synthesized auxiliary subunit can interact with nascent chains of the catalytic subunit only after exposure of approximately 100 amino acids outside the peptide exit tunnel **(Figure 32B**). Consistently, the crystal structure of the NatB complex shows that the interaction interface of the catalytic subunit is primarily located in the first 100 amino acids (Hong et al., 2017). Taken together, our data suggests that the NatB complex assemble co-translationally by co-translational interaction of the NatB auxiliary subunit with the nascent NatB auxiliary subunit, as soon as the interaction interface emerges from the ribosome.

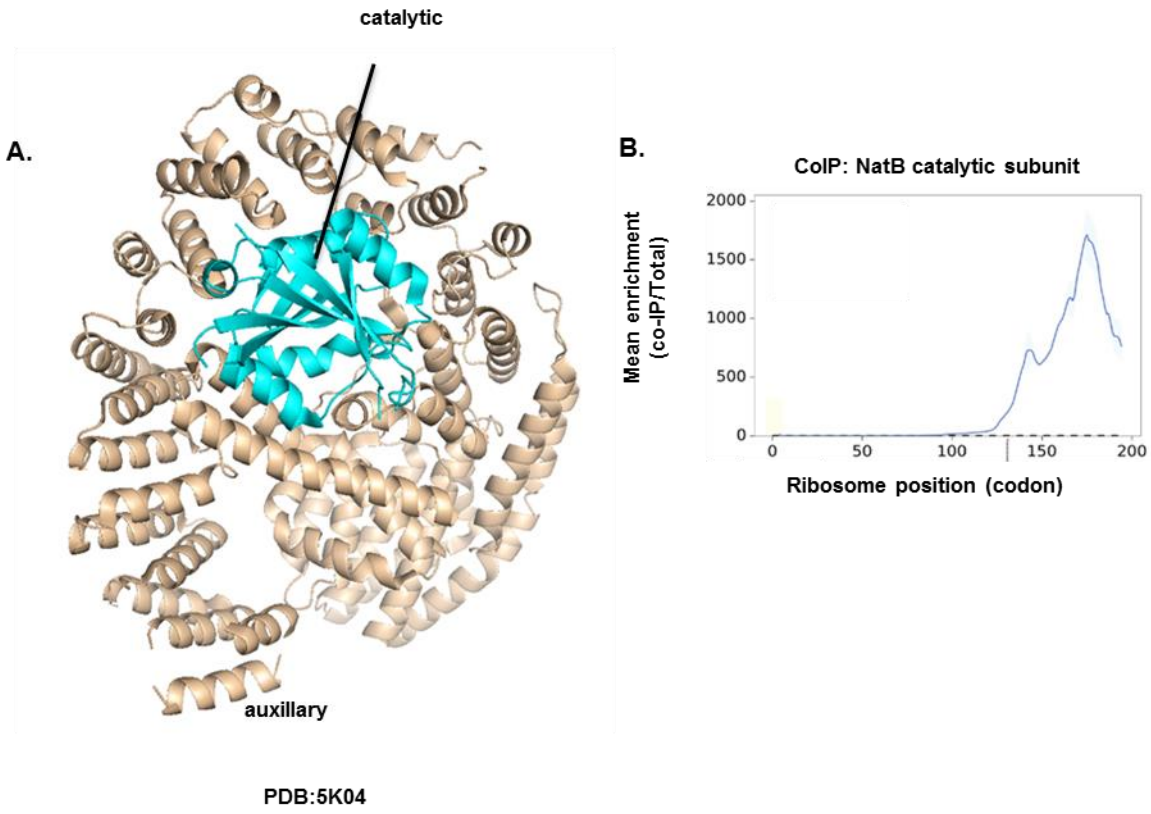

Figure 32: Cotranslational assembly of the NatB complex.

A. The crystal structure of the NatB complex showing the catalytic (light blue) and the auxiliary subunit (wheat).
B. Mean enrichment of co-IP over total for nascent NatB catalytic subunit upon NatB auxiliary subunit IP.

4 Discussion

Despite recent developments in our understanding of the biological significance of N-terminal acetylation, its function remains largely ambiguous. In this study, we employed unbiased high throughput approaches for multi-dimensional proteome-wide analysis of the functional consequences of lacking N-terminal acetylation. We analyzed key steps of proteome homeostasis: protein synthesis using ribosome profiling, steady-state protein levels using quantitative-proteomics, as well as protein turnover using the tandem fluorescent timer. Our results revealed an integrative constitutive stress response in *natB*Δ that induces protein quality control pathways, while repressing protein biogenesis pathways. Systematic analysis of proteome stability in *natB*Δ suggests no global effect of the loss of N-terminal acetylation of NatB substrates on their stability. Further analysis revealed global endogenous protein aggregation upon loss of N-terminal acetylation that includes aggregation prone proteins, as well as networks of interacting proteins. In addition, our results suggest a so far unknown link between N-terminal acetylation and co-translational protein folding by Ssb.

4.1 Constitutive stress response upon lack of N-terminal acetylation

Translatome/proteome analysis of *natB*Δ revealed elevated levels of specific molecular chaperones that are active in protein refolding such as Hsp78 and Hsp014 disaggregases, stress inducible Hsp70, and small heat shock proteins **(Figure 18A)**, which can explain the more efficient refolding of heat denatured luciferase expressed in *natB*Δ **(Figure 18B)**. In addition, multiple components of the cytoplasmic translation machinery were repressed in *natB*Δ including tRNA-aminoacylation enzymes, translation factors, as well as ribosomal proteins **(Figure 17)**. The translation repression is further manifested by decreased incorporation of radiolabeled methionine **(Figure 19B)** and high monosome/polysome ratio **(Figure 19C)**, together indicating decreased protein biogenesis. The coordinated elevation of protein quality control pathways and repression of the protein biogenesis capacity is reminiscent of the response of yeast cells to stress (Gasch et al., 2000), and consistent with elevated Hsf1 levels **(Figure 20A)** as well as enrichment of Hsf1 targets in the elevated genes in *natB*Δ **(Figure 20B)**.

Interestingly, metabolic pathways that are involved in energy regeneration are also elevated in *natB*Δ, in particular mitochondrial translation as well as components of the electron transport chain **(Figure 17)**. This may reflect impaired energy generation by glycolysis, or impaired mitochondrial respiration in *natB*Δ. In both cases, inducing the levels of mitochondrial respiration machinery can provide a compensatory effect. Alternatively, elevated mitochondrial respiration can compensate for stress induced ATP depletion (Gasch et al., 2000), consistent with the aforementioned indications of stress response activation in *natB*Δ. Remarkably, deletion of the mitochondrial translation components dramatically reduced *natB*Δ fitness, further highlighting that mitochondrial respiration is critical for the cell viability in *natB*Δ **(Figure 19D)**.

Interestingly, parallel analysis of *natA*Δ indicated only a subtle activation of the stress response **(Figure 31)**. This might be explained by substrate-specific effects of loss of N-terminal acetylation by either NatA or NatB, where loss of N-terminal acetylation of one or more specific substrates may lead to deleterious loss or gain of function effects. Remarkably, the magnitude of the stress response activation in *natA*Δ and *natB*Δ correlates with the severity of their growth phenotypes **(Figure 13, Figure 31)**.

4.2 N-terminal acetylation is not a general major determinant of protein stability

The stress response activation upon lack of N-terminal acetylation underscores its role in the maintenance of protein homeostasis. Interestingly, N-terminal acetylation was suggested to act as a degradation signal (Hwang et al., 2010a), that may mediate protein quality control and control protein stoichiometry (Shemorry et al., 2013). However, only a few endogenous substrates are known to date to undergo N-acetyl mediated degradation. Our systematic analysis of the effect of N-terminal acetylation on protein stability using quantitative proteomics combined with ribosome profiling, and tandem fluorescent timer analysis, showed that the experimentally identified substrates do not show a significant tendency to increase in steady state levels or half-lives upon loss of N-terminal acetylation **(Figure 21A-C)**, as it would be expected if protein degradation of those substrates is blocked by failure of recognition into the Ac/N-end rule pathway. N-acetyl mediated degradation was not more pronounced under heat stress, since similar analysis in cells grown at elevated temperatures showed again no significant global change of the substrates turnover **(Figure 21D-F)**.

The fact that substrates do not show global change in protein turnover upon loss of N-terminal acetylation argues against Ac/N-end rule as a general mechanism for substrates degradation. However, our results do not exclude that N-acetyl mediated degradation may take place for specific proteins that have additional features, or under specific perturbation conditions that can trigger their N-acetyl mediated degradation such as imbalanced protein complex stoichiometry. It is also likely that upon perturbation of the Ac/N-end rule pathway by preventing N-terminal acetylation, other degradation pathways can take over to target the non N-terminally acetylated proteins for degradation. In fact, N-terminally acetylated methionine was shown to act as a degradation signal for the Ac/N-end rule, while the non-acetylated methionine can still act as a degradation signal for the Arg/N-end rule if followed by hydrophobic amino-acids (Kim et al., 2014). With this in mind, it is likely that the robustness of the protein degradation signaling pathways may mask the contribution of the individual pathways. In addition, the employed methods show only the average change in a population of proteins, therefore if N-acetyl mediated degradation only affects a minor fraction of the protein species, those changes will not be observable since they will be averaged by the major population that is probably not sensitive to the absence of N-terminal acetylation. Further analysis of the role of Ac-N/end rule pathway under more specific perturbation conditions that systematically alter protein complex subunits stoichiometry may reveal more

profound role of the Ac/N-end rule pathway. In addition, analysis of the Ac/N-end rule upon perturbation of parallel degradation pathways may reveal its uncompensated contribution to protein degradation. Furthermore, new approaches need to be adopted to carefully analyze the fraction of a given protein that is susceptible to degradation.

4.3 Protein aggregation upon lack of N-terminal acetylation

The elevated levels of protein refolding machinery in *natB*Δ suggested compromised proteins integrity **(Figure 18A)**. Consistently, isolation of protein aggregates revealed substantial protein aggregation upon loss of N-terminal acetylation **(Figure 22A, Figure 26A)**, which we were able to identify and quantify by quantitative proteomics (**Figure 26D)**.

The observed protein aggregation can be explained by a primary effect of loss of N-terminal acetylation leading to aggregation of the non-acetylated proteins. Alternatively, it can also be explained on the basis of secondary substrate-specific effects where lack of N-terminal acetylation impairs the functions of specific proteins that are normally acetylated and important for the prevention of protein aggregation e.g. chaperones. Two lines of evidence suggest a direct effect of N-terminal acetylation on protein stability and folding. First, earlier studies suggest that N-terminal acetylation is important for maintaining structural integrity for at least a number of endogenous proteins (Bartels et al., 2014; Greenfield et al., 1994; Jarvis et al., 1995), while N-terminal acetylation of α-synuclein increases its resistance to aggregation (Bartels et al., 2014). Second, the accumulation of protein aggregates upon loss of N-terminal acetylation in *natA/natB* deletion mutants, despite their highly distinct substrate specificities, makes secondary substrate-specific effects less likely **(Figure 26A)**.

Interestingly, the lack of one specific NAT does not cause a significant enrichment of the specific substrates in the protein aggregates, indicating that protein aggregation upon loss of N-terminal acetylation is not necessarily only a result of an impairment of folding of the non-acetylated substrate **(Figure 23)**. A potential explanation could be that failure of N-terminal acetylation for specific proteins may directly trigger their aggregation, while indirectly leading to co-aggregation of other proteins by other downstream effects. This “down-spiral” effect can eventually mask substrate-specific enrichment of proteins in the isolated aggregates. Consistently, the aggregated proteins have a substantial overlap with aggregates that form upon other stresses, e.g. heat stress (De Laureto et al., 2014; Stoecklin et al., 2015; Wallace et al., 2015). This may indicate that proteins that are sensitive to changes in the protein folding environment, for instance due to chaperones sequestration into aggregates, would also tend to aggregate upon loss of N-terminal acetylation **(Figure 25A)**. Consistently, protein aggregation upon loss of N-terminal acetylation sequesters molecular chaperones that are involved protein disaggregation such as Hsp26 and Hsp104, in addition to Hsp70/40/90 (**Figure 24C)**. On the other hand, proteins found in aggregates of NAT mutants showed significantly higher interaction between each other **(Figure 24D)**

underscoring that protein interactions can drive co-aggregation of proteins regardless of its N-terminal acetylation status.

N-terminal acetylation is a co-translational modification catalyzed by ribosome associated NATs (Polevoda et al., 2008b). If N-terminal acetylation plays a role in optimizing protein folding, it is likely that N-terminal acetylation exerts its effect co-translationally during the maturation of the nascent chains. Consistently, isolation of radiolabeled protein aggregates with ^{35}S Methionine after a short labeling of 5 min, showed accumulation of radiolabeled aggregated proteins in *natB*Δ **(Figure 25C)**, indicating that a fraction of newly translated proteins gets sequestered into protein aggregates upon lack of N-terminal acetylation. Interestingly, protein aggregates in *natB*Δ revealed a strong overlap with protein aggregation upon deletion of the genes encoding the co-translational Hsp70 chaperones (Ssb1 and Ssb2) (Koplin et al., 2010; Willmund et al., 2013) **(Figure 25A)**, while deletion of the genes encoding both Ssb1 and Ssb2 in *natB*Δ led to synthetic growth defect **(Figure 25B)**, together suggesting a functional overlap between co-translational N-terminal acetylation by NatB and co-translational folding by Ssb.

Remarkably, the most enriched group of proteins among the protein aggregates in *natB*Δ is the cytoplasmic translation machinery, including most of the ribosomal proteins **(Figure 24A)**. Furthermore, quantification of the total lysate versus the soluble protein revealed that a substantial fraction of each of the quantified ribosomal proteins gets sequestrated into protein aggregates upon loss of N-terminal acetylation **(Figure 25E)**. While the sequestration of specific components of the translation machinery into protein aggregates is one of the common features of stress that may underlie stress granule formation (Stoecklin et al., 2015), stress granules do not contain ribosomes nor ribosomal proteins, except under very specific conditions (Jain et al., 2016). The observed ribosomal proteins aggregation upon loss of N-terminal acetylation could be explained by a consequence of secondary substrate-specific effects that affect ribosome biogenesis or assembly for instance, or as a result of co-sequestration of ribosomes together with misfolded nascent chains upon loss of co-translational N-terminal acetylation. Several observations suggest the second possibility. First, the sequestration of the vast majority of the ribosomal proteins into the aggregates **(Figure 24A)** suggests sequestration of intact ribosomes. Second, similar patterns of aggregation of ribosomal proteins are observed upon deletion of the co-translational chaperone Hsp70 (Koplin et al., 2010; Willmund et al., 2013), which is directly implicated in the maturation of nascent chains **(Figure 24D).** Finally, ribosomal proteins aggregate both in the deletion mutant of *natA* or *natB* despite their highly distinct substrate specificities, which makes secondary substrate-specific effects less likely **(Figure 26A)**. Interestingly, protein aggregates formed upon loss of N-terminal acetylation include several ER and mitochondrial chaperones **(Figure 24C)**, and they are significantly enriched for mitochondrial and ER proteins **(Figure 24B)**. These results may suggest protein misfolding in the mitochondria and ER, or protein import defects that hinder targeting of ER/mitochondrial proteins rendering them insoluble in the cytosol.

4.4 Working Model

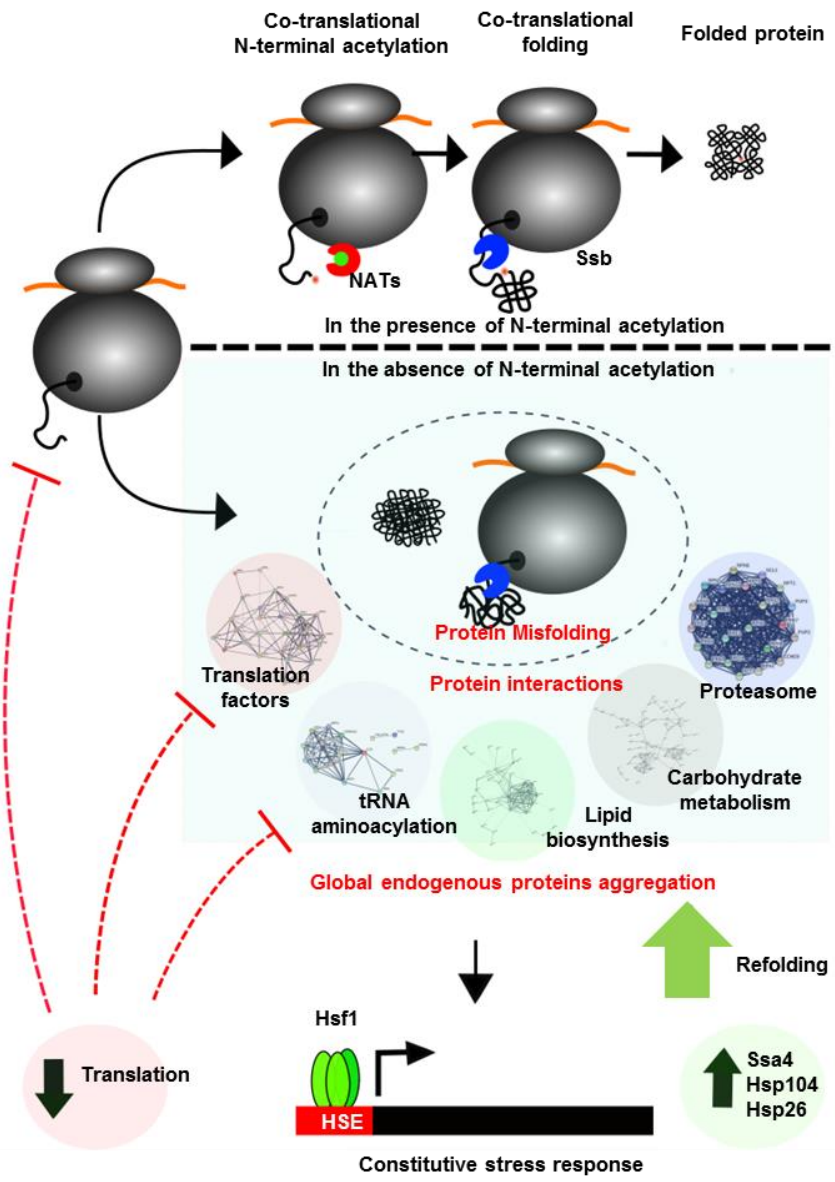

Figure 33: Working model for the function of proteins N-terminal acetylation.

Our working model **(Figure 33)** is that N-terminal acetylation, in line with the aforementioned reports, may facilitate protein folding and prevent certain protein species from aggregation. Given that N-terminal acetylation takes place co-translationally (Gautschi et al., 2003a), lack of N-terminal acetylation may

impose particular challenges for the co-translational folding of those proteins. Compromised folding of nascent chains that fail to be N-terminally acetylated may explain the sensitivity of *natB*Δ for the absence of the co-translational Hsp70 chaperone Ssb. In line with this view, misfolding of nascent chains may drive co-aggregation of the associated translational machinery, leading to the observed strong enrichment of translation components into the aggregates. The aggregation of misfolded nascent chains, together with the associated translation machinery, may trigger co-aggregation of other proteins through specific or unspecific protein-protein interactions. In addition, the disturbance of protein folding environment upon chaperones sequestration can eventually lead to the collapse of aggregation-prone proteins. The cellular response to protein aggregation is basal activation of stress response that induces protein refolding machinery to allow disaggregation, while decreasing protein influx by repressing protein biogenesis pathways.

4.5 Assembly of the NatB complex co-translationally

Selective ribosome profiling of NatB revealed that the NatB complex consisting of the catalytic subunit and the auxiliary subunit assemble co-translationally **(Figure 32)**. IP of the auxiliary subunit followed by ribosome profiling analysis revealed co-IP of the nascent chains of the catalytic subunit **(Figure 32B)**. Ribosome occupancy on the catalytic subunit after IP of the auxiliary subunit revealed the onset of co-translational assembly. Exposure of the interaction interface residues (Hong et al., 2017) of the nascent chains of the catalytic subunit is required before co-translational assembly with the auxiliary subunit **(Figure 32B)**. Co-translational assembly may represent a faster and more efficient assembly pathway for protein complexes by concentrating assembly to the synthesis sites. In addition, co-translational assembly may prevent protein aggregation by minimizing exposure of the interaction surface that may otherwise interact non-specifically with other proteins, or aggregate. Consistently, the catalytic subunit of the NatB complex was shown to be aggregation prone when expressed in the absence of the auxiliary subunit (Hong et al., 2017). Key questions regarding the mechanism of co-translational assembly of NatB remains to be addressed. Since co-translational assembly of luciferase was shown to be facilitated by the operon structure (Shieh et al., 2015), it is therefore intriguing to analyze the contribution of the mRNA localization to the co-translational complex assembly process. Furthermore, it is still not known whether complex assembly is predominately co-translational or post-translational, or whether the two pathways are mutually exclusive, and whether additional factors play a role to favor one pathway over the other.

5 Materials

5.1 Computer software

- Adobe Acrobat Reader (Adobe Systems Inc.)
- Bowtie2 ver. 2.2.5.0 (OSI Certified)
- GIMP2 (Free and Open Source Software)
- ImageJ (National Institutes of Health)
- ImageReader LAS-4000 (FUJIFILM Co.)
- Inkscape 0.91 (Free and Open Source Software)
- Microsoft Office 2011 (Microsoft Corp.)
- Perseus (Max Planck Institute of Biochemistry)
- Prism 6 (GraphPad Software, Inc.)
- PyMOL (Schrödinger)
- Python ver. 2.7 (Python Software Foundation)
- R ver. 3.1.1. (R Foundation for Statistical Computing)
- RStudio ver. 0.98.1102 (RStudio, Inc.)
- Samtools ver. 0.1.19 (GitHub Inc.)
- Serial Cloner ver. 2.6 (Franck Perez [SerialBasics])
- Spyder ver. 2.3.8 (The Spyder Development Team)
- Tophat2 ver. 2.0.13 (OSI Certified)

5.2 Consumables

- 10% TBE-Urea polyacrylamid gel, 12 wells (Noves, Invitrogen)
- 15% TBE-Urea polyacrylamid gel, 10 wells (Noves, Invitrogen)
- 8% TB polyacrylamid gel, 10 wells (Noves, Invitrogen)
- 96/384/1536 Pins and Plates for SGA (Singer Instruments)
- BD Falcon Round bottom polystyrene tube, 5 mL (BD)
- Cellulose acetate filters, 0.2 µm (Sartorius AG)
- Cover slides (Carl Roth GmbH + Co. KG)
- Criterion™ TGX™ Precast Gels (Bio-Rad Laboratories, Inc.)
- Cuvettes (Sarstedt AG & Co.)
- Entsorgungsbeutel, 200mm*300mm (Roth)
- Filter tips P10, P20, P200 and P1000 (Steinbrenner)
- Gel breaker tubes (IST Engineering Inc.)

- Glass beads (500 µm diameter)
- Lumat PP tubes, 5 ml (Greiner Bio-One International AG)
- Microcentrifuge tubes, 1.5 ml, 2 ml (Sarstedt AG & Co.)
- Nitrocellulose membrane, 0.2 µm (Roth)
- Non-stick RNase free tubes, 1.5ml (Ambion)
- Open-Top_polyclear centrifuge tubes 14x95 mm (Seton)
- PCR tubes, 200 µl (Sarstedt AG & Co.)
- Petri dishes (Greiner)
- Polycarbonate centrifuge tubes 11x34 mm (Beckman Coulter)
- Polypropylene conical centrifuge tubes, 15 ml, 50 ml (Sarstedt AG & Co.)
- PVDF membrane, Roti-PVDF (Carl Roth GmbH + Co. KG)
- Roti-NC membrane 0.45µm (Roth)
- RunBlue SDS-PAGE Precast Gels 8x10 cm (Expedeon Ltd.)
- Scalpel, 5518016 (Braun)
- Scintillation vials (Fisher Scientific)
- Spin-X-cellulose acetate columns, 2ml, 0.45µm (Sigma-Aldrich Co.)
- Sterile bottle filters (Sarstedt AG & Co.)
- Sterile filters Filtropur, 0.2 µM (Sarstedt AG & Co.)
- Syringe filters, 0.22 µm (Sarstedt)
- Syringe, 50 ml (BD, 300865)
- UV-Star Microplate µClear (Greiner Bio-One)
- Whatman Paper, 3 mm (Schleicher & Schuell BioScience GmbH)

5.3 Equipment

- 2100 Bioanalyzer Instruments (Agilent Technologies, Inc)
- Agarose gel chamber and trays (ZMBH workshop)
- ÄKTA purifier system (Amersham Pharmacia Biotech/GE Healthcare)
- Balances PG603-S and PB1502-S (Mettler-Toledo International, Inc.)
- Centrifuge (Sorval RC6 Thermo Scientific Inc.)
- Centrifuges 5424 and 5424R (Eppendorf AG)
- Centrifuges Biofuge pico/ Multifuge 3SR (Heraeus Instruments GmbH)
- Criterion™ Cell, electrophoresis chamber (Bio-Rad Laboratories, Inc.)
- EM900 microscope (Zeiss)
- FastPrep 24 (MP Biomedical).

- Filtering equipment: glass filter holder with glass funnel 1L (Millipore), ground joint flask 1L (Millipore), stainless steel screen, gasket and spring, clamp, vacuum base and cap (ZMBH workshop).
- FLA-3000 Fluorescent Image Analyzer (FUJIFILM Co.)
- French Pressure Cell (SLM/Aminco)
- Gel chamber, XCell SureLock Mini-Cell, EI0001 (Invitrogen)
- GenoSmart gel documentation system (VWR)
- Gradient station, 153 (BIO-COMP)
- High-Throughput Screening: ROTOR HDA (Singer Instruments)
- HiSeq 2000 (Illumina)
- ImageQuant LAS-4000, biomolecular imager (FUJIFILM Co.)
- Incubator MIR-254 SANYO Electric Biomedical Co. Ltd.
- Infinite M1000 or Infinite M1000 Pro plate reader (TECAN)
- Intelli-Mixer (Neolab)
- ISF1-X/Climo-Shaker (Kuhner)
- LS 55 Fluorescence Spectrometer (PerkinElmer)
- Lumat LB 9507 (Berthold Technologies Gmbh & Co. KG)
- Magnetic stir bar (Roth)
- Magnetic stirrer MR 3001 K (Heidolph)
- Microwave KOR 6D07 (Daewoo)
- Mini Trans-Blot® Cell (Bio-Rad Laboratories, Inc.)
- Mini-PROTEAN Cell, electrophoresis cell (Bio-Rad Laboratories, Inc.)
- Mixer mill, MM400 (Retsch)
- Multi-channel pipette, 20-200 µl (Gilson)
- Nanodrop spectrophotometer, ND2000 (Thermo Scientific)
- Novaspec Plus (GE Healthcare)
- Overhead roller (Neolab)
- Packard 1900 TR β Scintillation Counter
- pH-Meter FE20 and pH-electrode LE438 (Metter-Toledo International, Inc.)
- Power supply ST 606 T (Gibco BRL Life technologies, Inc.)
- Radaiation imager
- Rotor Type S120AT2 (Beckman)
- Rotor Type SW 40 Ti (Beckman)
- Scoopula, 14-357Q (Fisher Scientific)
- Shaker 3018 (GFL)
- Sonifier S-450 (BRANSON)

- Spectrophotometer SPECORD 205 (Analytik Jena AG)
- Stainless steel grinding balls, 12 mm and 25 mm (Retsch)
- Stainless steel jars, 10 ml and 50 ml (Retsch)
- T-Gradient Thermocycler (Biometra GmbH)
- Thermomixer comfort (Eppendorf AG)
- Trans-Blot® Turbo™ (Bio-Rad Laboratories, Inc.)
- Ultracentrifuge, Discovery 90SE (Sorvall)
- Ultracentrifuge, Discovery M120SE (Sorvall)
- Vortex-Genie 2 (NeoLab)

5.4 Growth Media

All media were sterilized by autoclaving prior to usage. To prepare agar plates, 2% (w/v) agar was added to the medium prior to autoclaving. 2% (w/v) glucose from a sterile-filtered glucose stock solution was added to the media after sterilization, except when alternative carbon sources were used. Antibiotics and/or additional reagents were added at the given concentrations, after allowing the media to cool down to approximately 55°C. Stock solutions were sterilized by filtration (0.2µm filter).

- LB medium (1L): 10 g tryptone, 5 g yeast extract, 5 g NaCl
- YP medium (1L): 20 g yeast extract, 10 g peptone
- SD (Synthetic Dropout) medium (1L): 6.7 g Yeast Nitrogen Base without amino acids, x g CSM mix (according to desired dropout))
- Specific media used in the synthetic genetic array procedure:
  - Amino-acids mixture: Thoroughly mixed 10 g of each of: Alanine, Asparagine, Aspartic acid, Cysteine, Glutamine, Monosodium Glutamic Acid (MSG), Glycine, Inositol, Isoleucine, Methionine, Phenylalanine, Proline, Serine, Threonine, Tryptophan, Tyrosine, Uracil, Valine, with 2.5g of Adenine, and 1g of 4-Aminobenzoic acid to get a mixture that has a total of 183.5 g. To prepare a Histidine/Lysine/Arginine dropout mixture of amino-acids, 36.7 g of the mixture were mixed with 4g of Leucine. Alternatively, to prepare a Leucine/Lysine/Arginine dropout mixture of amino-acids, 36.7 g of the mixture were mixed with 2g of Histidine. 2 g/l of the final amino-acids mixture was used for media preparation.
  - 1000x Stocks solutions: Canavanine (50 mg/ml), Thialysine (50 mg/ml), Nourseothricin (clonNAT) (100 mg/ml,), and Geneticin (G418) (200 mg/ml) are all filtered-sterilized and stored in aliquots at 4ºC, then added to the autoclaved medium at 55°C, at 1000x dilution of the indicated stock concentration.
  - Sporulation media: 2% agar, 2% potassium acetate.

- SD media, with Monosodium Glutamate (MSG): 1.7 g/l yeast nitrogen base without amino acids and ammonium sulfate, 1 g/l MSG, 2 g/l amino acid mixture, 20 g/l glucose. To prepare solid media 20 g/l agar was added.
- SD His/Arg/Lys media (with MSG) with Canavanine and Thialysine: 1.7 g/l yeast nitrogen base without amino acids and ammonium sulfate, 1 g/l MSG, 2 g/l (amino-acids mixture minus His/Arg/Lys), 20 g/l glucose, plus standard concentrations of Canavanine and Thialysine (added at 55°C), and 20 g/l agar.
- SD His/Arg/Lys media (with MSG) with Canavanine, Thialysine, CloNAT and G418: 1.7 g/l yeast nitrogen base without amino acids and ammonium sulfate, 1 g/l MSG, 2 g/l (minus His/Arg/Lys) amino acid mixture, 20 g/l glucose, plus standard concentrations of Canavanine, Thialysine, and antibiotics (added at 55°C), and 20 g/l agar.
- SD His with galactose and raffinose as an alternative carbon sources for glucose: 6.7 g/l yeast nitrogen base without amino acids, 2 g/l (minus His) amino acid mixture, 10 g/l galactose, 10 g/l raffinose, and 20 g/l agar to prepare solid media.
- SD His with 5-FOA: 6.7 g/l yeast nitrogen base without amino acids, 2 g/l amino acid mix-His, 20 g/l glucose, 1g/l 5-Fluoroorotic acid hydrate (5-FOA) (added as powder at 55°C), and 20 g/l agar.
- Imaging media: 6.7 g/l yeast nitrogen base without amino acids, 2 g/l complete amino acid mixture, 20 g/l glucose, 300 mg/l Adenine, and 20 g/l agar.

5.5 Kits

- Agilent High Sensitivity DNA kit (Agilent)
- Agilent RNA 600 NANO kit (Agilent)
- Agilent Small RNA kit (Agilent)
- GenElute™ Gel Extraction Kit (Sigma-Aldrich Co.)
- GenElute™ Miniprep Kit (Sigma-Aldrich Co.)
- GenElute™ PCR purification Kit (Sigma-Aldrich Co.)
- KAPA2G™ Robust und Robust 'Hot Start' PCR Kit (Peqlab)
- QIAprep Spin Miniprep Kit (QIAGEN GmbH)
- QIAquick Gel Extraction Kit (QIAGEN GmbH)
- QIAquick PCR Purification Kit (QIAGEN GmbH)
- Z-Competent E. coli Transformation Kit (Zymo Research Europe GmbH)

5.6 Reagents

- 10bp DNA ladder, 10821-015 (Invitrogen)
- 13C6,15N2-L-Lysine HCl (Silantes)
- 13C6,15N4-L-Arginine HCl (Silantes)
- 20% SDS (Ambion)
- 2x sample loading buffer for TBE-Urea gels (Invitrogen)
- 5-Fluoroorotic acid hydrate (Sigma-Aldrich Co.)
- Acid-Phenol-Chloroform (Ambion)
- Amino acids (Sigma-Aldrich Co.)
- Ampicillin (Amp) 100 µg/ml Carl (Roth GmbH)
- Aprotinin (AppliChem)
- Bacto™Agar Becton (Dickinson and Company)
- Bacto™Peptone Becton (Dickinson and Company)
- Bacto™Yeast extract Becton (Dickinson and Company)
- Bestatin hydrochlorid (Roth)
- Bio-Rad Protein Assay Dye Reagent Concentrate (5 x Bradford reagent) (Bio-Rad Laboratories, Inc.)
- Bromphenol Blue (Bio-Rad Laboratories, Inc.)
- Canavanine (Sigma-Aldrich Co.)
- Chloramphenicol (Cm) 25 µg/ml (Sigma-Aldrich Co.)
- CircLigase, CL9025K (Epicentre)
- Complete Supplement Mixture (CSM) (- amino acids for drop out media) (MP Biomedicals, LLC)
- cOmplete, EDTA free protease inhibitor tablets (Roche Diagnostics GmbH)
- Cycloheximide (CHX) 100 µg/ml in (Sigma-Aldrich Co.)
- DEPC (Roth)
- Difco™Yeast Nitrogen Base w/o amino acids Becton (Dickinson and Company)
- DNase I (Sigma-Aldrich Co.)
- dNTP set (Bioline)
- E-64 (Roth)
- ECF Substrate (GE Healthcare Life Sciences)
- EDTA (Roth)
- GeneRuler 1 kb DNA Ladder (#SM0312) (Thermo Scientific Inc.)
- Geneticin (G418) 200 µg/ml (Sigma-Aldrich Co.)
- Glycoblue (Ambion)
- Hoechst 33442 Life Technologies Life Technologies

- Hygromycin B (Hyg) 250 µg/ml (InvivoGen)
- Immersion Oil Immersol™ 518F (Carl Zeiss Microscopy GmbH)
- Isopropyl β-D-1-thiogalactopyranoside (Sigma-Aldrich Co.)
- Kanamycin (Kan) 50 µg/ml in (Carl Roth GmbH)
- Leupeptin (AppliChem)
- Luciferin (Synchem UG & Co. KG)
- Methyl methanesulfonate “MMS” (Sigma-Aldrich Co.)
- Nourseothricin (clonNAT) 100 µg/ml (Werner BioAgents)
- PageRuler Prestained Protein Ladder (#26616) (Thermo Scientific Inc.)
- Pepstatin A (AppliChem)
- Phenylmethylsulfonyl Fluoride “PMSF” (Thermo Scientific Inc.)
- Phusion®High-Fidelity DNA polymerase (New England Biolabs GmbH)
- Restriction enzymes (New England Biolabs, Thermo Scientific Inc.)
- RNase away (Roth)
- RNase-free Dnase I, 4716728001 (Roche)
- Superase-In (Ambion)
- Superscript III, 18080-044 (Invitrogen)
- SYBR gold (Invitrogen)
- T4 DNA Ligase (Thermo Scientific Inc.)
- T4 polynucleotide kinase, M0201L (NEB)
- T4 RNA ligase 2, truncated, M0242L (NEB)
- Taq DNA polymerase (Lab collection)
- Thialysine/S-Aminoethyl-L-cysteine (Sigma-Aldrich Co.)
- Trans-Blot® Turbo™ 5x Transfer Buffer (Bio-Rad Laboratories, Inc.)
- Ulp1 Sumo-protease (Lab collection)
- UltraPure 10x TBE buffer (Invitrogen)
- Yeastmaker™ Carrier DNA ‘(Clonetech Laboratories, Inc)
- Zymolyase 20T (United States Biological)

5.7 Strains

Yeast strains: Gene deletions or tagging were performed by PCR targeting as described (Janke et al., 2004). The genotypes of all strains used in this study are listed below. All strains are derivatives of BY4741 (MATa *his3Δ1 leu2Δ0 met15Δ0 ura3Δ0*) or BY4742 (MATα *ura3Δ0 leu2Δ0 his3Δ1 lys2Δ0*)

Genotype	Background	Experiment	Source
BY4741 ARG4Δ::hphMX LYS1Δ::kanMX	BY4741	Quantitative proteomics and ribosome profiling	This Study
BY4741 ARG4Δ::hphMX LYS1Δ::kanMX NAA10Δ::URA3	BY4741	Quantitative proteomics and ribosome profiling	This Study
BY4741 ARG4Δ::hphMX LYS1Δ::kanMX NAA20Δ::URA3	BY4741	Quantitative proteomics and ribosome profiling	This Study
BY4741 SSB1Δ::LEU2 SSB2Δ::natMX	BY4741	Spot test	Bukau lab
BY4741 SSB1Δ::LEU2 SSB2Δ::natMX NAA20Δ::URA3	BY4741	Spot test	This Study
BY4741 HIS3Δ::kanMX	BY4741	Tandem fluorescent timer analysis	Knop lab
BY4741 NAA20Δ::kanMX	BY4741	Tandem fluorescent timer analysis	Ulrike Friedrich
BY4741 pRS306-ADH-GFPLuciDM	BY4741	Luciferase activity test	This Study
BY4741 pRS306-ADH-GFPLuciDM NAA20Δ::URA3	BY4741	Luciferase activity test	This Study
MATα CAN1Δ::STE2pr-HIS5 LYP1Δ::STE3pr-LEU2 LEU2Δ0 HIS3Δ1 MET15Δ0 ΔHML:hphMX NAA20Δ::URA3	BY4742	Synthetic growth defects screen	This Study
MATα CAN1Δ::STE2pr-HIS5 LYP1Δ::STE3pr-LEU2 LEU2Δ0 HIS3Δ1 MET15Δ0 ΔHML::hphMX GSY2::GFP::HIS3	BY4742	Fluorescence microscopy	Bukau lab
MATα CAN1Δ::STE2pr-HIS5 LYP1Δ::STE3pr-LEU2 LEU2Δ0 HIS3Δ1 MET15Δ0 ΔHML:hphMX GSY2::GFP::his3 NAA20Δ::URA3	BY4742	Fluorescence microscopy	This Study
BY4741 NAA25::GFP::kanMX	BY4741	Selective ribosome profiling	Ulrike Friedrich

E.coli Strains

XL1-blue: *rec*A1 *end*A1 *gyr*A96 *thi*-1 *hsd*R17 *sup*E44 *rel*A1 *lac* (Stratagene)

BL21 DE3 Rosetta: F^- *ompT* *hsdS*$_B$(r_B^- m_B^-) *gal* *dcm* (DE3) pRARE (Cam^R) (Novagen)

5.8 Primers

Target Gene	Purpose	Sequence	Source
ARG4	deletion	gtaccagacctgatgaaattcttgcgcataacgtcgccatctgct acggccgccagctgaagcttcg	This study
ARG4	deletion	gagctcaaaagcaggtaactatataacaagactaaggcaaa catgaaccgtattaccgcctttgagtgagc	This study
ARG4	verification	cttatattcaaccatcacacacgtctttcc	This study
ARG4	verification	tttgttcgttcttgtggtggttactcattgg	This study
HML	deletion	ttttcttattttcattttatttttttcgccttttatacagacttcaacacaat cacggccgccagctgaagcttcg	This study
HML	deletion	gaaagaaagctcccgcttaattatatatatgcagctgttacgga gatgcaaagctaaccgtattaccgcctttgagtgagc	This study
HML	verification	agctttcaatacattcatgaagtcattaggtac	This study
HML	verification	gatttataagaatgtgttccgtaataatcttccc	This study
LYS1	deletion	gtaaatgtcagcgtaacgataatgtatatactttaaatgtaaact aaagcttcgtacgctgcaggtc	This study
LYS1	deletion	Cataagataacaacgaaaacgctttatttttcacacaaccgca aaaatgcgcccaatacgcaaaccgcctctcc	This study
LYS1	verification	gcaaagttcttgctgggaaatgaaagg	This study
LYS1	verification	ttcagcgacaaagagtcataaagtcatcc	This study
NAA10	cloning in p413	Ggatcgcccgggatgcctattaatattcgcagagcg	This study

NAA10	cloning in p413	Gactgggtcgacttatacaatgatatcatttacgccttgc	This study
NAA10	Sequencing	ttatacaatgatatcatttacgccttgc	This study
NAA10	Sequencing	atgcctattaatattcgcagagcgac	This study
NAA10	E25Q mutagenesis	caaaatgccaaccttcataacctaccccagaattatatgatgaaatattatatgtatc	This study
NAA10	E25Q mutagenesis	gatacatataatatttcatcatataattctggggtaggttatgaaggttggcattttg	This study
NAA10	E26A mutagenesis	catataatatttcatcatataatttgcgggtaggttatgaaggttggcat	This study
NAA10	E26A mutagenesis	atgccaaccttcataacctacccgcaaattatatgatgaaatattatatg	This study
NAA10	verification	gggtctaattcaccaagtttctgcc	This study
NAA10	verification	Atcaagaagcttgaatattatactgtagtcaaaaattag	This study
NAA10	deletion	taaatacatacgatcaagctccaaaataaaacttcgtcaaccatgcagctgaagcttcgtacgc	Ulrike Friedrich
NAA10	deletion	agcctggatgaaaatatactacgtttatataggttgatttaattacataggccactagtggatctg	Ulrike Friedrich
NAA20	verification	ctttggacaagcttctgccag	This study
NAA20	verification	aaccttaccatcactaatagtatctcgatc	This study
NAA20	deletion	acattgagaatattcaaggaaagagacaggaggattcgagaaatgcagctgaagcttcgtacgc	Ulrike Friedrich
NAA20	deletion	tcattattatgttctgagtatgaggacgaggtaatacataccttacataggccactagtggatctg	Ulrike Friedrich

6 Methods

6.1 SILAC-based quantitative proteomics

First, we aimed to construct strains where Arginine and Lysine biosynthesis is abolished by deletion of the genes encoding specific biosynthetic enzymes to ensure efficient incorporation of heavy Arginine and Lysine. Deletion mutants were generated as described (Janke et al., 2004). To generate a deletion of *ARG4* gene in the wild type *Saccharomyces cerevisiae* BY4741 (MATa; *his3Δ1; leu2Δ0; met15Δ0; ura3Δ0*), the hphMX cassette was amplified from pUG75 (which has the hphMX cassette that confers resistance to Hygromycin) using the respective primer pair that targets the *ARG4* gene. The purified disruption gene cassette was transformed into yeast cells by a heat shock procedure for *in vivo* homologous recombination. In brief, yeast cells were grown at 30°C in 45 ml YPD inoculated with 5 ml overnight culture so that the OD_{600} roughly equals (0.1). The cells were harvested at OD_{600} of (0.4-0.8) by centrifugation at 3000g for 5 min at room temperature, suspended in 5 ml of Li-Ac mix (10mM Lithium Acetate, 10 mM Tris HCl pH 7.5, 1mM EDTA), and centrifuged at 3000g for 5 min at room temperature. The cells were re-suspended in 250 µl of Li-Ac mix. 100 µl aliquots were then used for each transformation, followed by the addition of 10-20 µl of the PCR reaction of the relevant gene cassette, 2 mg/ml of salmon sperm DNA, and 700 µl of PEG-mix (40% PEG 4000, 10 mM Lithium Acetate, 10 mM Tris HCl pH 7.5, 1 mM EDTA), then incubated on a rotating wheel for 30 min at room temperature. The cells were heat shocked at 42°C for 15 min, centrifuged at 3000 rpm for 1 min at room temperature, and re-suspended in 300 µL of YPD. The cells were incubated for 2 hours at 30°C, then spread on YPD plus Hygromycin (250 µg/ml) agar plates, and incubated for 2-4 days at 30°C. Colonies were re-streaked on YPD plus Hygromycin agar plates, and incubated for 2-4 days at 30°C. Single colonies were randomly picked for verification by colony PCR using the respective primers and phenol-chloroform extracted genomic DNA. The colony PCR reaction was performed by a primer pair where the forward primer anneals upstream of the gene in the non-coding region, and the reverse primer anneals downstream of the gene in the non-coding region. Gene deletion was confirmed based on the size of the PCR product. Once the correct recombination was verified, the colonies were grown to stationary phase in YPD plus Hygromycin, and stocked in YPD plus Hygromycin with 15% Glycerol at 80°C. To introduce the second deletion of *LYS1* gene, the same transformation protocol was implemented; where the kanMX cassette was amplified from pUG6 (which have the kanMX cassette that confers resistance to Geneticin (G418)) using the respective primer pair which targets the *LYS1* gene, then transformed into *ARG4*Δ strain. The transformed cells were plated on YPD agar plates plus G418 (200 µg/ml) and Hygromycin (250 µg/ml), followed by verification by colony PCR reactions using the respective primers. Finally, NATs deletions were introduced using the same transformation protocol described earlier. The KIURA3 cassette which confers Uracil auxotrophy was amplified from pUG72 using the respective primer pairs which target the

NATs genes: *NAA10*, *NAA20* individually, then transformed into *ARG4ΔLYS1Δ* cells. The transformed cells were plated on Uracil synthetic dropout media, in addition to G418 (200 µg/ml) and Hygromycin (250 µg/ml). Colonies were re-streaked on the same media followed by verification using colony PCR with the respective primers.

For the incorporation efficiency test, *ARG4ΔLYS1Δ* yeast cells were grown in 200 ml Lysine/Arginine synthetic dropout media adjusted to 20 mg/l ($^{13}C^{15}N$) Arginine, and 30 mg/l ($^{13}C^{15}N$) Lysine. Cells were grown for six, seven or eight doubling times at 30 °C to an OD_{600} of (0.8). Cells were harvested by centrifugation at 3000g for 5 min, then suspended in 1ml lysis buffer composed of (20mM Tris-HCL pH 8.0, 500 mM NaCl, 10 mM $MgCl_2$, 5 mM $MnCl_2$, 5 mM $CaCl_2$, 0.5% NP-40, 2x complete EDTA-free protease inhibitor tablets, 1 mM PMSF, 20 µg/ml Leupeptin, 20 µg/ml Aprotinin, 40 µg/ml Bestatin, 1 µg/ml E-64, 20 U/ml DNase). Frozen cells were mechanically lysed for 2 min at 30 Hz (Mixer mill, MM400 (Retsch)). Cell lysates were thawed and centrifuged at 4 °C and 20,000g for 5 min, and the supernatant was transferred to a new tube. Protein concentration was quantified using Bradford (Biorad), followed by SDS-PAGE and mass spectrometry analysis.

For SILAC-based quantitative proteomics of the total lysate, yeast cells were grown in synthetic media adjusted to 20 mg/l light ($^{12}C^{14}N$) or heavy ($^{13}C^{15}N$) Arginine, and 30 mg/l light ($^{12}C^{14}N$) or heavy ($^{13}C^{15}N$) Lysine. Cells were grown for six doubling times to an $OD6_{00}$ of (0.8). Wild type control and mutant cells were mixed 1:1 based on OD_{600}. 200 OD_{600} (mixed cells) were suspended in 1ml lysis buffer composed of (20mM Tris-HCl pH 8.0, 500 mM NaCl, 10 mM $MgCl_2$, 5 mM $MnCl_2$, 5 mM $CaCl_2$, 0.5% NP-40, 2x complete EDTA-free protease inhibitor tablets, 1 mM PMSF, 20 µg/ml Leupeptin, 20 µg/ml Aprotinin, 40 µg/ml Bestatin, 1 µg/ml E-64, 20 U/ml DNase). Frozen cells were mechanically lysed for 2 min at 30 Hz (Mixer mill, MM400 (Retsch)). Cell lysates were thawed, followed by centrifugation at 4 °C and 20,000g for 5 min, and the supernatant was transferred to a new tube followed by protein concentration quantification using Bradford (Biorad). The experiment was repeated twice with a swap of heavy and light Arginine and Lysine between wild type and mutant. Protein extracts were analyzed by mass spectrometry.

The following downstream procedure was performed by the ZMBH proteomics facility: 50 µg of proteins were loaded into SDS-PAGE. Each sample was fractionated into eight fractions by cutting the protein-loaded gel into eight parts. Gel pieces were reduced with DTT, alkylated with iodoacetamid and digested with trypsin using the DigestPro MS platform (Intavis AG) following the protocol described by (Shevchenko et al., 2007). Peptides have then been analyzed by Liquid chromatography–mass spectrometry (LCMS) using an UltiMate 3000 LC (Thermo Scientific) coupled to either an Orbitrap Elite or a Q-Exactive mass spectrometer (Thermo Scientific). Peptides analyzed by the Orbitrap Elite have been loaded on a C18 Acclaim PepMap100 trap-column (Thermo Fisher Scientific) with a flow rate of 30µl/min 0.1% TFA. Peptides were eluted and separated on an C18 Acclaim PepMap RSLC analytical column (75

µM x 250 mm) with a flow rate of 300 nl/min in a 2 h gradient of 3% buffer A (0.1% formic acid, 1 % acetonitril) to 40% buffer B (0.1% formic acid, 90 % acetonitrile). MS data were acquired with an automatic switch between a full scan and up to 30 data-dependent MS/MS scans. Peptides analyzed on the Q-Exactive have been directly injected to an analytical column (75µm x 300 mm), which was self-packed with 3µm Reprosil Pur-AQ C18 material (Dr. Maisch HPLC GmbH) and separated using the same gradient as described before. MS data were acquired with an automatic switch between a full scan and up to 15 data-dependent MS/MS scans. Data analysis was carried out with MaxQuant version 1.5.3.30 (Cox and Mann, 2008) using standard settings for each instrument type and searched against a yeast specific database extracted from UniProt (UniProt Consortium). Carbamidomethylation of cysteine was specified as fixed modification; Oxidation of methionine and acetylation of protein N-termini was set as variable modification. 'Requantify' as well as 'Match Between Runs' options were both enabled. Results for filtered for an 1% false discovery rate (FDR) on peptide spectrum match (PSM) and protein level. MaxQuant output files have been further processed and filtered using Perseus (Tyanova et al., 2016)and self-compiled R-scripts.

For SILAC-based quantitative proteomics of protein aggregates: Yeast cells were grown as described earlier, followed by isolation of protein aggregates from mutant and wild type control (see section **6.6**). Re-suspended protein aggregates in SDS-sample buffer from wild type and mutant were mixed in 1:1 ratio based on volume, followed by similar mass-spectrometry analysis.

6.2 SWATH–based quantitative proteomics

Yeast cells were grown in synthetic media adjusted to 20 mg/l Arginine and 30 mg/l Lysine for six doubling times at 30 °C to OD_{600} of (0.8). For quantitative proteomics under heat stress, cells were shifted from 30°C to 37°C for 2 doubling times, and harvested at OD_{600} of (0.8). Before harvesting, cells were quenched by addition of Trichloroacetic Acid (TCA) to the culture to a final concentration of 6.25%, followed by incubation on ice for 10 min. The culture was centrifuged at 4°C, 1500g for 5 min. The pellet was washed twice with 10 ml ice-cold acetone. For cell lysis, 1 volume of lysis buffer (8M Urea, 100 mM Ammonium Bicarbonate, 5 mM EDTA, adjusted to pH 8.0) was added to 1 volume of cell pellet, followed by vortexing to re-suspend the cell pellet. 1 volume of ice cold glass beads (500 µm diameter) was added to 1 volume of re-suspended pellet, followed by vortexing for 40 seconds at 6.0 m/s (FastPrep 24 (MP Biomedical)). The cell lysate was centrifuged at maximum speed for 5 min (4°C) and the supernatant was transferred to a new tube. The cell pellet was re-suspended in equal volume of fresh lysis buffer, followed by vortexing for 40 seconds at 6.0 m/s (FastPrep 24 (MP Biomedical)). The last step was repeated for five times to ensure efficient protein extraction, and the supernatant from each grinding cycle was pooled together, followed by Bradford quantification (Biorad) of protein concentration. Quantitative proteomics analysis was performed using SWATH-mass spectrometry as described earlier (Selevsek et al., 2015). The experiment was repeated three times for each of the mutant and wild type control.

6.3 Ribosome Profiling

Yeast cells were grown in synthetic media adjusted to 20 mg/l Arginine and 30 mg/l Lysine for six doubling times at 30 °C to an optical density (OD_{600}) of (0.8). For ribosome profiling under heat stress, cells were shifted from 30°C to 37°C for 2 doubling times, and harvested at OD_{600} of (0.8). Cells were collected by fast filtration and immediately flash-frozen in liquid nitrogen. Frozen cells were mechanically lysed for 2 min at 30 Hz (Mixer mill, MM400 (Retsch)) in a lysis buffer composed of (20 mM Tris-HCl pH 8.0, 140 mM KCl, 6 mM $MgCl_2$, 0.1 mg/ml Cycloheximide, 0.1% NP-40, 2x complete EDTA-free protease inhibitor, 1 mM PMSF, 20 µg/ml Leupeptin, 20 µg/ml Aprotinin, 40 µg/ml Bestatin, 1 µg/ml E-64, 20 U/ml DNase). Lysates were thawed, followed by centrifugation at 30,000g for 5 min at 4 °C, and the supernatant was transferred to a new tube followed by RNA quantification (Nanodrop spectrophotometer, ND2000 (Thermo Scientific)). 1mg of RNA was digested using 125 U of RNAse I at 25 °C, 650 rpm, for 1 h. Digestion was stopped by adding 200 U SUPERase·In. The digested RNA was overlaid on 10–50% sucrose gradient (20 mM Tris pH 8.0, 140 mM KCl, 6 mM $MgCl_2$, 0.1 mg/ml Cycloheximide, 1x complete EDTA-free protease inhibitor tablets) followed by ultracentrifugation at 35,000 rpm for 2.5h at 4°C (Rotor Type SW 40 Ti (Beckman)). The sucrose gradient was fractionated (Gradient station, 153 (BIO-COMP)) and the monosome fractions were pooled. RNA was isolated from monosomes by hot-phenol extraction followed by deep sequencing library preparation (Becker et al., 2013). Analysis of the deep sequencing data was performed as described (Döring et al., 2017). In summary, adaptor sequence was first trimmed from the reads using Cutadapt, and reads that were mapped to the ribosomal RNA were filtered out (Bowtie2). Reads were mapped to the yeast genome (*S. cerevisiae* strain S288C) using Tophat2. Reads were processed according to center-weighing approach. In summary, for footprints between 22-42 nucleotide long, 11 nucleotides were trimmed from each end and the remaining positons were given a score of 1/N in which N equals the length of the footprint after trimming. To quantify the expression for each gene in RPM (Reads Per Million base), the total reads aligned to each open reading frame (ORF) was normalized to the total number of reads aligned to all ORFs per sample after center-weighting, and multiplied by 1 million. Genes with less than 64 reads were excluded from the analysis. Experiment was done in 2 replicates.

6.4 Polysome Profiling

Yeast cells were grown in synthetic media at 30 °C to an optical density OD_{600} of (0.8). Cells were collected by fast filtration and immediately flash-frozen in liquid nitrogen. Frozen cells were mechanically lysed for 2 min at 30 Hz in a lysis buffer composed of (20 mM Tris-HCl pH 8.0, 140 mM KCl, 6 mM $MgCl_2$, 0.1 mg/ml Cycloheximide, 0.1% NP-40, 2x complete EDTA-free protease inhibitor tablets, 1 mM PMSF, 20 µg/ml Leupeptin, 20 µg/ml Aprotinin, 40 µg/ml Bestatin, 1 µg/ml E-64, 20 U/ml DNase). Lysates were thawed, followed by centrifugation at 4 °C and 30,000g for 5 min, and the supernatant was transferred to a new tube followed by RNA quantification (Nanodrop spectrophotometer, ND2000 (Thermo Scientific)).

1mg of RNA was overlaid on 10–50% sucrose gradient (20 mM Tris pH 8.0, 140 mM KCl, 6 mM $MgCl_2$, 0.1 mg/ml Cyclohexamide, 1x complete EDTA-free protease inhibitor tablets, followed by ultracentrifugation at 4°C and 35,000rpm for 2.5h (Rotor Type SW 40 Ti (Beckman)), and fractionation (Gradient station, 153 (BIO-COMP)).

6.5 Selective ribosome profiling of the NatB complex

Yeast cells expressing C-terminally GFP tagged NatB auxiliary subunit were grown in 1L YPD for six doubling times at 30 °C to an OD_{600} of (0.8). Cells were collected by fast filtration and immediately flash-frozen in liquid nitrogen. Frozen cells were mechanically lysed for 2 min at 30 Hz (Mixer mill, MM400 (Retsch)) in a lysis buffer composed of (20mM Tris-HCl pH 8.0, 140 mM KCl, 6 mM $MgCl_2$, 0.1 mg/ml Cycloheximide, 0.1% NP-40, 2x complete EDTA-free protease inhibitor tablets, 1 mM PMSF, 20 µg/ml Leupeptin, 20 µg/ml Aprotinin, 40 µg/ml Bestatin, 1 µg/ml E-64, 20 U/ml DNase). Lysates were thawed, followed by centrifugation at 4 °C and 30,000g for 5 min, and the supernatant was transferred to a new tube followed by RNA quantification (Nanodrop spectrophotometer, ND2000 (Thermo Scientific)).

For total translatome analysis: 200 µg RNA from the total lysates was digested using RNase I (10 U/A260, for 30 min at 4°C). The digested RNA was layered on top a sucrose-cushion (25% sucrose in 20 mM Tris-HCl pH 8.0, 140 mM KCl, 10 mM $MgCl_2$, 0.1 mg/mL Cycloheximide, 1x protease inhibitor tablet) followed by centrifugation for 90 min at 75k RPM and 4°C. Supernatant was removed quickly with vacuum pump and the pellets were re-suspended in 500 µl lysis buffer.

For IP: 200 µl of GFP-binder slurry was washed three times with 1 ml of lysis buffer for 5-10 min, rotating at room temperature, where 1 min centrifugation at 450g was used to pellet the beads. 5 mg of RNA from the total lysate were added to the beads, followed by digestion using RNaseI (10 U/A260) for 30 min at 4°C. Beads were incubated with rotation for 25-30 min at 4°C. Beads were washed twice in 1 ml of the lysis buffer for 1 min, followed by washing twice in 1 ml of wash buffer (0.1 mg/ml Cycloheximide, 20 mM Tris-HCl pH 8.0, 140 mM KCl, 10 mM $MgCl_2$, 1 mM PMSF, 0.01 % NP-40, 2x protease inhibitor tablets, 10% glycerol) for 1 min, then one time in 1 ml of wash buffer for 5 min while rotating. During washing procedure, the tubes were changed two twice.

RNA for either total translatome analysis or IP was isolated by hot-phenol extraction followed by deep sequencing library preparation. Analysis of the deep sequencing data was performed as described earlier (Döring et al., 2017), and as discussed as in section **6.4.** Experiment was done in 2 replicates.

6.6 Isolation of aggregated proteins

Experiments were done as described (Koplin et al., 2010). In summary, cell pellet from 50 OD_{600} units of logarithmically growing cells were suspended in 100 µl lysis buffer ((20 mM Sodium Phosphate pH 6.8, 10 mM DTT, 1 mM EDTA, 0.1% Tween, 1 mM PMSF, protease inhibitor cocktail, 3 mg/ml Zymolyase T20)) and incubated at 25°C for 20 min, while shaking at 750 rpm. The suspended cells were kept on ice, followed by tip sonication (Branson; eight times at level 4 and duty cycle 50%) then centrifuged for 20 min at 200g at 4°C. The supernatant was transferred to a new tube. Supernatants were adjusted to identical protein concentrations using Bradford (Biorad). Aggregated proteins were pelleted at 16,000g for 20 min at 4°C. After removing supernatants, aggregated proteins were washed twice with 600 µl of 2% NP-40 in (20 mM Sodium Phosphate pH 6.8, 1 mM PMSF, and protease inhibitor cocktail) by sonication (six times at level 4 and duty cycle 50%), and collected by centrifugation at 16,000g for 20 min at 4°C. Aggregated proteins were washed in 600 µl NP-40 deficient buffer (20 mM sodium phosphate, pH 6.8, 1 mM PMSF, and protease inhibitor cocktail) by sonication (four times at level 2 and duty cycle 65%), boiled in SDS sample buffer, and separated by SDS-PAGE (14%).

6.7 Quantitative proteomics of the total lysate versus the soluble fraction

Analysis was adapted from (Wallace et al., 2015). In brief, protein aggregates from the wild type and deletion mutant was isolated as described (section **6.6**). Equal volume of the cell lysate before (total cell lysate) and after aggregate isolation (soluble fraction) were loaded into SDS-PAGE followed by trypsin digestion, and dimethyl labeling. Peptides from soluble and total lysate were mixed and quantified by mass-spectrometry analysis.

6.8 Tandem fluorescent timer analysis

The general strategy for introducing *natB* deletion to the tandem fluorescent timer library involves mating of haploid *natB*Δ or the wild type control with the tFT library (Khmelinskii et al., 2014) consisting of 4044 tFT tagged proteins (Knop lab collection, at the ZMBH), followed by diploids selection, sporulation, and selection of double mutant haploids (Tong and Boone, 2007). The design of the library strains adopts a strategy for chromosomal gene tagging that allows generating clones in which only the desired tag sequence is inserted into a specified genomic locus. The strategy is based on a tagging module in which the selection marker URA3, flanked by specific endonuclease cleavage sites, is placed between two copies of the tag sequence such that the marker can be excised by inducing expression of a site-specific endonuclease under galactose inducible promoter. The resulting double-strand break can then be repaired by homologous recombination between the two copies of the tag sequence leaving a single copy of the tag in the genome free from any auxiliary sequences. Seamless tagging is compatible with high-

throughput strain construction using SGA, where the procedure includes two steps: Pining the cells on a media which have galactose as an alternative carbon to induce the expression of the genetically encoded endonuclease, followed by counter selection of the URA3 marker by pinning the cells onto synthetic medium containing 5-fluoroorotic acid (5-FOA) to select for cells that had lost the URA3 marker.

The screen was done in 1536 format using pinning robotics (Singer instruments) with three biological replicates per clone, as follows:

- Library preparation: The tFT library was spotted from glycerol-stock (96-wells) with long pins onto YPD+NAT agar plates and condensed it at the same time to 384-format. The cells were grown at 30°C for 1-2 days. The library was further replicated to yield 1536-format and the cells were left to grow at 30°C for 1-2 days.
- Query preparation: The query strains were spotted onto YPD+G418 agar plates in 384-format, and later condensed into one plate of 1536-format. In addition to *natB* deletion mutant, wild type was used as a reference.
- Mating: The library was mated with the query strains by pinning both to the same YPD plate, free from antibiotic markers, where the library was spotted first for two times (rotor setting: pairs option on, revisit source, recycle, 0.2 mm mix on source, 70% pinning pressure, 0.2 mm mix on target, default pressure) then spotted the query strains on top, for two times using the same settings. The cells were left to grow for 1-2 days at 30°C.
- Diploid selection: The resulting zygotes were pinned onto YPD+G418+NAT agar plates (rotor settings: 0.3 mm mix on source, 70% pinning pressure, 0.2 mm mix on target, default pressure) and left to grow at 30°C for 2 days. The selection was repeated to obtain enough material for sporulation, if necessary.
- Sporulation: Diploid cells were pinned to sporulation medium, where it was stamped two times (rotor settings: pairs option on, revisit source, recycle, 0.3 mm mix on source, 70% pinning pressure, 0.2 mm mix on target, default pressure) and the plates were incubated at 23°C for 5 days.
- Haploid selection 1: As many cells as possible were stamped from the sporulation plates onto SD His/Arg/Lys + Canavanine/Thialysine plates to select for MATa haploids (rotor settings: 0.2 mm mix on source, 70% pinning pressure, 0.2 mm mix on target, default pressure). The cells were left to grow at 30°C for (1-2) days.
- Haploid selection 2: Cells from (haploid selection 1) were pinned onto SD His/Arg/Lys +Canavanine +Thialysine+G418+NAT (with MSG) plates to select for MATa cells which have both the query strains deletion, as well as the tFT tag.
- Endonuclease induction: Cells from (haploid selection 2) plates were pinned onto SD His which has galactose and raffinose as an alternative carbon source for glucose.

- URA3 marker counter-selection: Cells were pinned onto SD His containing 5-FOA to select for cells that have lost the URA3 marker.
- Stamping on imaging plates: For imaging, the cells were finally pinned onto syntheti media agar plates, in the presence of excess Adenine (300 mg/l). The cells were incubated at 30°C for exactly 20 hours before proceeding with the imaging. The plates were imaged using infinite M1000 or Infinite M1000 Pro plate reader (TECAN). To test the effect of heat stress, plates were incubated at 30°C for 1 day then shifted to 37°C for 1 day followed by high throughput fluorescence measurement of colonies in custom temperature control chambers.

Data analysis was performed by Dr. Joseph Barry form the EMBL as described (Khmelinskii et al., 2014). In summary, the fluorescence intensity of sfGFP and mCherry was measured for each colony using infinite M1000 or Infinite M1000 Pro plate reader (TECAN). The median of the fluorescence intensity of sfGFP and mCherry were calculated out of the three replicates per each tFT-tagged protein. Based on the median fluorescence intensities, the ratio of sfGFP and mCherry fluorescence intensity was calculated for each of the tFT tagged proteins. Since colony size can impact the fluorescence intensity, screening plates were also imaged to measure the size of each colony. Fluorescence intensities were normalized to the colony size, and colonies that are smaller/bigger than a preset threshold was filtered out from the analysis. Moreover, screening plates at the second haploid selection stage were also imaged to measure the size of each colony, and colonies that were slowly growing/not growing at the second haploid selection stage, but later showed a better growth in downstream stages were discarded from the analysis. The mCherry/sfGFP values from the *natB* deletion mutant were compared to the corresponding values in the wild type strain.

6.9 Screen for synthetic growth defects in *natB*Δ

Haploid *natB*Δ and wild type control were mated with the yeast non-essential genes deletion library (Bukau lab collection) followed by diploids selection, sporulation, and selection of haploid double mutant (*natB*Δ and gene deletion) (Tong and Boone, 2007). The screen was done in 1536 format using pinning robotics (Singer instruments) with four biological replicates per clone.

- Library preparation: The non-essential genes deletion diploid library was spotted from glycerol-stock (96-wells) with long pins onto YPD+G418 agar plates and condensed it at the same time to 384-format. The cells were grown at 30°C for 1-2 days. The library was further replicated to 1536-format and the cells were left to grow at 30°C for 1-2 days. Diploid cells were pinned to poor sporulation medium, where it was stamped two times (rotor settings: pairs option on, revisit source, recycle, 0.3 mm mix on source, 70% pinning pressure, 0.2 mm mix on target, default pressure) and the plates were incubated at 23°C (or room temperature) for 5 days or longer.

- Query preparation: The query strain was spotted onto SD URA agar plates in 384-format, then condensed into 1536-format. In addition to *natB* deletion mutant, wild type was also used as a reference.
- Mating: The library was mated with the query strains by pinning both to the same YPD plate, free from antibiotic markers, where the library was spotted first for two times (rotor setting: pairs option on, revisit source, recycle, 0.2 mm mix on source, 70% pinning pressure, 0.2 mm mix on target, default pressure) then spotted the query strains on top for two times using the same settings. The cells were left to grow for 1-2 days at 30°C.
- Diploid selection: The resulting zygotes were pinned onto SD (MSG) URA+G418 agar plates (rotor settings: 0.3 mm mix on source, 70% pinning pressure, 0.2 mm mix on target, default pressure) and left to grow at 30°C for 2 days. The selection was repeated to obtain enough material for sporulation, if necessary.
- Sporulation: Diploid cells were pinned to poor sporulation medium, where it was stamped two times (rotor settings: pairs option on, revisit source, recycle, 0.3 mm mix on source, 70% pinning pressure, 0.2 mm mix on target, default pressure) and the plates were incubated at 23°C (or room temperature) for 5 days or longer.
- Haploid selection 1: Stamping as many cells as possible from the sporulation plates onto SD Leu/Arg/Lys + Canavanine/Thialysine plates to select for MATα (rotor settings: 0.2 mm mix on source, 70% pinning pressure, 0.2 mm mix on target, default pressure). The cells were left to grow at 30°C for (1-2) days.
- Haploid selection 2: Cells from (haploid selection 1) were pinned onto SD Leu/Ura/Arg/Lys +Canavanine+Thialysine+G418 (with MSG) plates to select for double mutant MATα.

Double mutants were grown on synthetic media without leucine (for haploid selection) for 2 days. The plates were imaged for colony size measurement. The ratio of colony size between double mutant and single mutants was used as a proxy for double mutant fitness relative to single mutants. Screen was repeated twice, and only significant changes of (double/single) mutant colony size based on one sample t-test (p-value<0.05) were included for further analysis.

6.10 Measuring yeast growth by spotting serial dilutions

Yeast cells were grown to stationary phase, serially diluted (1:10:100:1000:10000:100000), then stamped into YPD or synthetic media plus 2% agar. The plates were first left to dry, then incubated for three days, then imaged.

6.11 Luciferase activity assay

Yeast cells expressing mutant luciferase (Gupta et al., 2011) were grown in synthetic medium to an OD_{600} of (0.8) at 30°C. Cells were treated with 0.1 mg/ml Cycloheximide, and then shifted to 37°C for 90 min, followed by shifting to 45°C for 20 min to heat denature luciferase. Cells were finally shifted to 30°C to allow luciferase refolding. Luciferase activity was measured at specific time points (before heat shock, after 37°C incubation, after 45°C incubation, during refolding: 15 min, 30 min, 60 min, and 120 min after shifting to 30°C). To measure luciferase activity, 100 µl of cells in medium were mixed with 100 µl of 125 µM luciferin and luciferase activity was measured for 10s (Lumat LB 9507 (Berthold Technologies Gmbh & Co. KG)). Measurements were normalized to the optical density OD_{600}. Experiment was done in two replicates.

6.12 Cloning of the *NAA10* gene and mutants

The coding sequence of Naa10 was amplified from phenol-chloroform extracted yeast genome using a primer pair that anneals at the start and end of the coding sequence of the gene, and contain short overhang that contain the restriction sites for SmaI and SalI. The PCR product (insert), and the vector p413CYC1 (Mumberg et al., 1995) were doubled digested with SmaI and SalI according to the supplier instructions. The digested insert and vector were ligated using T4-DNA ligase according to the supplier instructions, followed by transformation into XL1 chemical competent cells, and plated into Ampicillin containing LB-agar plates. Five colonies were used for inoculation of 5 ml LB overnight cultures followed by plasmid purification. The purified plasmids were further sequenced using the respective primers to confirm the sequence identity. Mutants of *NAA10* genes were generated by amplification of the generated plasmid using mismatch primers, followed by digestion of the template DNA using Dpn1, transformation, plasmid purification, and sequencing as described earlier. Wild type and mutant Naa10 were transformed to yeast as described (Section **6.1**), and plated on SD His plates.

6.13 Live cell microscopy

Cells were grown at 30 °C in Synthetic media to an OD_{600} of (0.5 – 0.6). After harvesting by centrifugation, cells were re-suspended in phosphate buffered saline (PBS), and layered on agarose coated slides. Images were acquired using a wide field system (Xcellence IX81, Olympus). All further processing of digital images was performed with ImageJ.

6.14 Purification of GFP-binder

BL21 DE3 Rosetta cells were transformed with a plasmid encoding GFP binder under Isopropyl β-D-1-thiogalactopyranoside (IPTG)-inducible promotor (p2666). In summary, 50 µl of BL21 DE3 Rosetta cells were thawed on ice, followed by addition of at least 5 ng of p2666, followed by incubation on ice for 30

min. The cells were heat shocked at 42°C for 45 sec, and immediately incubated on ice for 2 min. 800 µl of LB media was added to the cells, followed by incubation at 37°C for 1 hour. Cells were plated on LB agar plus 50 µg/ml Kanamycin. Overnight culture (LB plus 50 µg/ml Kanamycin) of the transformed cells was used for inoculation of 10L of LB containing 50 µg/ml Kanamycin at an OD_{600} of (0.05) and grown to an OD_{600} of (0.5) at 37 °C. The culture was shifted to 25 °C followed by addition of IPTG to a final concentration of 1 mM to induce the expression of the GFP-binder. Cells were grown overnight then harvested by centrifugation (4000 rpm, 20 min, 4°C). The cell pellet was re-suspended in 50 mL binding buffer (1x PBS pH 8.0, 0.5 M NaCl, 20 mM Imidazole, 150 µL 5 mg/ml DNaseI, 1 mM PMSF, 20 µg/ml Leupeptin, 20 µg/ml Aprotinin) then lysed twice using the french pressure cell (SLM/Aminco) at 1000 psi, followed by centrifugation for 20 min at 4 °C and 20,000g. The supernatant was applied to an equilibrated 5 ml HisTrap crude column (GE Healthcare Life Sciences) followed by washing with binding buffer. The GFP-binder protein was eluted with binding buffer containing 300 mM Imidazole. Fractions containing the GFP-antibody were pooled, and then concentrated to 5 ml and loaded onto a HiLoad 16/60 Superdex S75 gel filtration column (GE Healthcare Life Sciences). PBS was used as a running buffer, followed by 1 ml fractions collection. Peak fractions were tested for the presence and purity of the GFP-binder by SDS-PAGE and the relevant fractions were pooled. The purified protein was coupled to NHS-activated Sepharose 4 FAST Flow beads (Amersham) according to the manufacturer's protocol and the rest of the protein was kept frozen at -80 °C.

6.15 ^{35}S -Methionine incorporation

Experiment was performed as described (Nillegoda et al., 2010), with a few modifications. In brief, yeast cells were grown in synthetic medium to an OD_{600} of (0.8), washed twice in water, and re-suspended in synthetic dropout medium lacking methionine at a concentration OD_{600} = 6/ml, followed by addition of ^{35}S methionine to a final concentration of 100 µCi/ml. Pulse-labeling was conducted for 10 min at 30°C with shaking. Incorporation of ^{35}S methionine was measured by taking 400 µl of ^{35}S methionine-labeled culture and adding it to an equal volume of ice-cold 20% TCA. Cells were pelleted, washed twice in ice-cold acetone then re-suspended in 200 µl ice-cold extraction buffer (50 mM Tris-HCl pH 7.5, 1 mM EDTA, and complete protease inhibitors). Equal volume of glass beads (500 µm diameter) was added to the cells, followed by vortexing for 40 seconds at 6.0 m/s using (FastPrep 24 (MP Biomedical)). The extracts were quantified for ^{35}S incorporation using Scintillation Counter (Packard 1900 TR β).

7 List of Figures

8 Abbreviations

- **°A:** Angstrom
- **5-FOA:** 5-Fluoroorotic acid hydrate
- **ADP:** Adenosine diphosphate
- **A-site:** Amoinoacyl-tRNA site
- **ATP:** Adenosine triphosphate
- **CLPS:** Chaperones linked to protein synthesi**s**
- **CRP:** Core particle
- **ER:** Endoplasmic reticulum
- **E-site:** Exit-site
- **GDP:** Guanosine diphosphate
- **GET:** Guided entry of TA proteins
- **GO:** gene ontology
- **GTP:** Guanosine triphosphate
- **HSF1:** Heat shock transcription factor
- **HSP:** Heat shock protein
- **IP:** Immunoprecipitation
- **IPTG:** Isopropyl β-D-1-thiogalactopyranoside
- **MAP:** Methionine aminopeptidase
- **MMS:** Methyl methanesulfonate
- **mRNA:** Messenger RNA
- **MS:** Mass spectrometry
- **MSG:** Monosodium Glutamata
- **NAC:** Nascent chain associated complex
- **NAT:** N-terminal acetyltransferases
- **NEF:** Nucleotide exchange factor
- **OD_{600}:** optical density (OD_{600})
- **PBS:** Phosphate buffered saline
- **PIC:** 43S pre-initiation complex
- **P-site:** Peptidyl-tRNA site
- **PTC:** Peptidyl transferase center
- **RAC:** Ribosome associated complex
- **RNA:** Ribonucleic acid
- **RP:** Regulatory particle
- **RPM: Reads per Million**

- ***S.cerevisiae: Saccharomyces cerevisiae***
- **SDS-PAGE:** Sodium dodecyl sulfate polyacrylamide gel electrophoresis
- **sfGFP:** Superfolder green fluorescent protein
- **SILAC:** Stable isotope labeling by amino acids in cell culture
- **SPR:** Signal recognition particle
- **SR:** SRP receptor
- **TC :** Ternary complex
- **tFT:** Tandem Fluorescent timer
- **TRiC/CCT:** TCP1-Ring Complex or Chaperonin Containing TCP1
- Trichloroacetic acid “TCA
- **tRNA:** Transfer RNA

Amino-acids abbreviations:

Full Name	Abbreviation (3 Letter)	Abbreviation (1 Letter)
Alanine	Ala	A
Arginine	Arg	R
Asparagine	Asn	N
Aspartic acid	Asp	D
Cysteine	Cys	C
Glutamic acid	Glu	E
Glutamine	Gln	Q
Glycine	Gly	G
Histidine	His	H
Isoleucine	Ile	I
Leucine	Leu	L
Lysine	Lys	K
Methionine	Met	M
Phenylalanine	Phe	F
Proline	Pro	P
Serine	Ser	S
Threonine	Thr	T
Tryptophan	Trp	W
Tyrosine	Tyr	Y
Valine	Val	V

9 Bibliography

Abe, A., Saeki, K., Yasunaga, T., and Wakabayashi, T. (2000). Acetylation at the N-Terminus of Actin Strengthens Weak Interaction between Actin and Myosin. Biochemical and Biophysical Research Communications 268, 14–19.

Aksnes, H., Drazic, A., Marie, M., and Arnesen, T. (2016). First Things First: Vital Protein Marks by N-Terminal Acetyltransferases. Trends Biochem. Sci. 41, 746–760.

Albanese, V., Yam, A., Baughman, J., and Parnot, C. (2006). Systems analyses reveal two chaperone networks with distinct functions in eukaryotic cells. Cell.

Barlowe, C.K., and Miller, E.A. (2013). Secretory protein biogenesis and traffic in the early secretory pathway. Genetics 193, 383–410.

Bartels, T., Kim, N.C., Luth, E.S., and Selkoe, D.J. (2014). N-alpha-acetylation of α-synuclein increases its helical folding propensity, GM1 binding specificity and resistance to aggregation. PLoS ONE 9, e103727.

Baryshnikova, A., Costanzo, M., and Dixon, S. (2010). Synthetic genetic array (SGA) analysis in Saccharomyces cerevisiae and Schizosaccharomyces pombe. Methods in ….

Becker, A.H., Oh, E., Weissman, J.S., Kramer, G., and Bukau, B. (2013). Selective ribosome profiling as a tool for studying the interaction of chaperones and targeting factors with nascent polypeptide chains and ribosomes. Nat Protoc 8, 2212–2239.

Behnia, R., Panic, B., Whyte, J.R.C., and Munro, S. (2004a). Targeting of the Arf-like GTPase Arl3p to the Golgi requires N-terminal acetylation and the membrane protein Sys1p. Nat Cell Biol 6, 405–413.

Behnia, R., Panic, B., Whyte, J.R.C., and Munro, S. (2004b). Targeting of the Arf-like GTPase Arl3p to the Golgi requires N-terminal acetylation and the membrane protein Sys1p. Nat Cell Biol 6, 405–413.

Ben-Shem, A., Garreau de Loubresse, N., Melnikov, S., Jenner, L., Yusupova, G., and Yusupov, M. (2011). The structure of the eukaryotic ribosome at 3.0 Å resolution. Science 334, 1524–1529.

Bengtson, M.H., and Joazeiro, C.A.P. (2010). Role of a ribosome-associated E3 ubiquitin ligase in protein quality control. Nature 467, 470–473.

Brandman, O., Stewart-Ornstein, J., Wong, D., Larson, A., Williams, C.C., Li, G.-W., Zhou, S., King, D., Shen, P.S., Weibezahn, J., et al. (2012). A ribosome-bound quality control complex triggers degradation of nascent peptides and signals translation stress. Cell 151, 1042–1054.

Brar, G.A., and Weissman, J.S. (2015). Ribosome profiling reveals the what, when, where, and how of protein synthesis. Nat. Rev. Mol. Cell Biol.

Brar, G.A., Yassour, M., Friedman, N., Regev, A., Ingolia, N.T., and Weissman, J.S. (2012). High-resolution view of the yeast meiotic program revealed by ribosome profiling. Science 335, 552–557.

Caesar, R., and Blomberg, A. (2004). The Stress-induced Tfs1p Requires NatB-mediated Acetylation to Inhibit Carboxypeptidase Y and to Regulate the Protein Kinase A Pathway. Journal of Biological Chemistry 279, 38532–38543.

Caesar, R., Warringer, J., and Blomberg, A. (2006a). Physiological Importance and Identification of Novel Targets for the N-Terminal Acetyltransferase NatB. Eukaryotic Cell 5, 368–378.

Caesar, R., Warringer, J., and Blomberg, A. (2006b). Physiological Importance and Identification of Novel Targets for the N-Terminal Acetyltransferase NatB. Eukaryotic Cell 5, 368–378.

Chakrabartty, A., Doig, A.J., and Baldwin, R.L. (1993). Helix capping propensities in peptides parallel those in proteins. Proc. Natl. Acad. Sci. U.S.a. 90, 11332–11336.

Chen, S., Vetro, J.A., and Chang, Y.-H. (2002). The specificity in vivo of two distinct methionine aminopeptidases in Saccharomyces cerevisiae. Arch. Biochem. Biophys. 398, 87–93.

Chen, S.-J., Wu, X., Wadas, B., Oh, J.-H., and Varshavsky, A. (2017). An N-end rule pathway that recognizes proline and destroys gluconeogenic enzymes. Science 355.

Couvillion, M.T., Soto, I.C., Shipkovenska, G., and Churchman, L.S. (2016). Synchronized mitochondrial and cytosolic translation programs. Nature 533, 499–503.

Cox, J., and Mann, M. (2008). MaxQuant enables high peptide identification rates, individualized ppb-range mass accuracies and proteome-wide protein quantification. Nature Biotechnology.

Cox, J., and Mann, M. (2012). 1D and 2D annotation enrichment: a statistical method integrating quantitative proteomics with complementary high-throughput data. BMC Bioinformatics.

De Laureto, P.P., Nikolaev, Y., Oliveira, A.P., and Picotti, P. (2014). Global analysis of protein structural changes in complex proteomes. Nature.

Del Alamo, M., Hogan, D.J., Pechmann, S., and Albanese, V. (2011). Defining the specificity of cotranslationally acting chaperones by systematic analysis of mRNAs associated with ribosome-nascent chain complexes. PLoS ….

Dennis, G., Sherman, B.T., and Hosack, D.A. (2003). DAVID: database for annotation, visualization, and integrated discovery. Genome ….

Dever, T.E., Kinzy, T.G., and Pavitt, G.D. (2016). Mechanism and regulation of protein synthesis in Saccharomyces cerevisiae. Genetics.

Dever, T.E., and Green, R. (2012). The elongation, termination, and recycling phases of translation in eukaryotes. Cold Spring Harbor Perspectives in Biology 4, a013706.

Döring, K., Ahmed, N., Riemer, T., Suresh, H.G., Vainshtein, Y., Habich, M., Riemer, J., Mayer, M.P., O'Brien, E.P., Kramer, G., et al. (2017). Profiling Ssb-Nascent Chain Interactions Reveals Principles of Hsp70-Assisted Folding. Cell 170, 298–311.e20.

Duncan, C.D.S., and Mata, J. (2011). Widespread cotranslational formation of protein complexes. PLoS Genet 7, e1002398.

Duttler, S., Pechmann, S., and Frydman, J. (2013). Principles of cotranslational ubiquitination and quality control at the ribosome. Mol. Cell.

Fairman, R., Shoemaker, K.R., and York, E.J. (1989). Further studies of the helix dipole model: Effects of a free α-NH3+ or α-COO− group on helix stability. Proteins: Structure.

Finley, D., Ulrich, H.D., Sommer, T., and Kaiser, P. (2012). The ubiquitin–proteasome system of Saccharomyces cerevisiae. Genetics.

Forte, G.M.A., Pool, M.R., and Stirling, C.J. (2011). N-terminal acetylation inhibits protein targeting to the endoplasmic reticulum. PLoS Biol 9, e1001073.

Fox, T.D. (2012). Mitochondrial protein synthesis, import, and assembly. Genetics.

Garcia, M., Darzacq, X., Devaux, F., and Singer, R.H. (2007). Yeast mitochondrial transcriptomics. Mitochondria: Practical ….

Gasch, A.P., Spellman, P.T., Kao, C.M., Carmel-Harel, O., Eisen, M.B., Storz, G., Botstein, D., and Brown, P.O. (2000). Genomic expression programs in the response of yeast cells to environmental changes. Mol. Biol. Cell 11, 4241–4257.

Gautschi, M., Just, S., Mun, A., Ross, S., Rucknagel, P., Dubaquie, Y., Ehrenhofer-Murray, A., and Rospert, S. (2003a). The Yeast N -Acetyltransferase NatA Is Quantitatively Anchored to the Ribosome and Interacts with Nascent Polypeptides. Mol. Cell. Biol. 23, 7403–7414.

Gautschi, M., Just, S., Mun, A., Ross, S., Rucknagel, P., Dubaquie, Y., Ehrenhofer-Murray, A., and Rospert, S. (2003b). The Yeast N -Acetyltransferase NatA Is Quantitatively Anchored to the Ribosome and Interacts with Nascent Polypeptides. Mol. Cell. Biol. 23, 7403–7414.

Gautschi, M., Just, S., Mun, A., Ross, S., Rucknagel, P., Dubaquie, Y., Ehrenhofer-Murray, A., and Rospert, S. (2003c). The Yeast N -Acetyltransferase NatA Is Quantitatively Anchored to the Ribosome and Interacts with Nascent Polypeptides. Mol. Cell. Biol. 23, 7403–7414.

Gautschi, M., Lilie, H., Fünfschilling, U., Mun, A., Ross, S., Lithgow, T., Rucknagel, P., and Rospert, S. (2001). RAC, a stable ribosome-associated complex in yeast formed by the DnaK-DnaJ homologs Ssz1p and zuotin. Proc. Natl. Acad. Sci. U.S.a. 98, 3762–3767.

Greenfield, N.J., Stafford, W.F., and Hitchcock-DeGregori, S.E. (1994). The effect of N-terminal acetylation on the structure of an N-terminal tropomyosin peptide and alpha alpha-tropomyosin. Protein Sci. 3, 402–410.

Gupta, R., Kasturi, P., Bracher, A., Loew, C., and Zheng, M. (2011). Firefly luciferase mutants as sensors of proteome stress. Nature.

Guydosh, N.R., and Green, R. (2014). Dom34 rescues ribosomes in 3' untranslated regions. Cell 156, 950–962.

Haar, von der, T. (2008). A quantitative estimation of the global translational activity in logarithmically growing yeast cells. BMC Syst Biol 2, 87.

Hanebuth, M.A., Kityk, R., Fries, S.J., Jain, A., Kriel, A., Albanèse, V., Frickey, T., Peter, C., Mayer, M.P., Frydman, J., et al. (2016). Multivalent contacts of the Hsp70 Ssb contribute to its architecture on ribosomes and nascent chain interaction. Nat Commun 7, 13695.

Holmes, W.M., Mannakee, B.K., and Gutenkunst, R.N. (2014). Loss of N-terminal Acetylation Suppresses A Prion Phenotype By Modulating Global Protein Folding. Nature.

Hong, H., Cai, Y., Zhang, S., Ding, H., Wang, H., and Han, A. (2017). Molecular Basis of Substrate Specific Acetylation by N-Terminal Acetyltransferase NatB. Structure 25, 641–649.e643.

Huang, P., Gautschi, M., Walter, W., Rospert, S., and Craig, E.A. (2005). The Hsp70 Ssz1 modulates the function of the ribosome-associated J-protein Zuo1. Nat. Struct. Mol. Biol. 12, 497–504.

Hwang, C.S., Shemorry, A., and Varshavsky, A. (2010a). N-Terminal Acetylation of Cellular Proteins

Creates Specific Degradation Signals. Science 327, 973–977.

Hwang, C.S., Shemorry, A., and Varshavsky, A. (2010b). N-Terminal Acetylation of Cellular Proteins Creates Specific Degradation Signals. Science 327, 973–977.

Ingolia, N.T., Ghaemmaghami, S., and Newman, J. (2009). Genome-wide analysis in vivo of translation with nucleotide resolution using ribosome profiling. ….

Jain, S., Wheeler, J.R., Walters, R.W., Agrawal, A., and Barsic, A. (2016). ATPase-modulated stress granules contain a diverse proteome and substructure. Cell.

Janke, C., Magiera, M.M., Rathfelder, N., Taxis, C., Reber, S., Maekawa, H., Moreno-Borchart, A., Doenges, G., Schwob, E., Schiebel, E., et al. (2004). A versatile toolbox for PCR-based tagging of yeast genes: new fluorescent proteins, more markers and promoter substitution cassettes. Yeast 21, 947–962.

Jarvis, J.A., Ryan, M.T., Hoogenraad, N.J., Craik, D.J., and Hoj, P.B. (1995). Solution structure of the acetylated and noncleavable mitochondrial targeting signal of rat chaperonin 10. J. Biol. Chem. 270, 1323–1331.

Jenner, L., Melnikov, S., Garreau de Loubresse, N., Ben-Shem, A., Iskakova, M., Urzhumtsev, A., Meskauskas, A., Dinman, J., Yusupova, G., and Yusupov, M. (2012). Crystal structure of the 80S yeast ribosome. Curr. Opin. Struct. Biol. 22, 759–767.

Khmelinskii, A., Blaszczak, E., Pantazopoulou, M., Fischer, B., Omnus, D.J., Le Dez, G., Brossard, A., Gunnarsson, A., Barry, J.D., Meurer, M., et al. (2014). Protein quality control at the inner nuclear membrane. Nature 516, 410–413.

Khmelinskii, A., Keller, P.J., Bartosik, A., Meurer, M., Barry, J.D., Mardin, B.R., Kaufmann, A., Trautmann, S., Wachsmuth, M., Pereira, G., et al. (2012). tandem fluorescent protein timers for in vivo analysis of protein dynamics. Nature Biotechnology 30, 708–714.

Kim, H.-K., Kim, R.-R., Oh, J.-H., Cho, H., Varshavsky, A., and Hwang, C.-S. (2014). The N-Terminal Methionine of Cellular Proteins as a Degradation Signal. Cell 156, 158–169.

Koplin, A., Preissler, S., Ilina, Y., Koch, M., Scior, A., Erhardt, M., and Deuerling, E. (2010). A dual function for chaperones SSB-RAC and the NAC nascent polypeptide-associated complex on ribosomes. The Journal of Cell Biology 189, 57–68.

Leidig, C., Bange, G., Kopp, J., and Amlacher, S. (2013). Structural characterization of a eukaryotic chaperone—the ribosome-associated complex. Nature Structural & ….

Li, X., and Chang, Y.H. (1995). Amino-terminal protein processing in Saccharomyces cerevisiae is an essential function that requires two distinct methionine aminopeptidases. Proc. Natl. Acad. Sci. U.S.a. 92, 12357–12361.

Liszczak, G., Goldberg, J.M., Foyn, H., Petersson, E.J., Arnesen, T., and Marmorstein, R. (2013). Molecular basis for N-terminal acetylation by the heterodimeric NatA complex. Nat. Struct. Mol. Biol. 20, 1098–1105.

Mann, M. (2006). Functional and quantitative proteomics using SILAC. Nat. Rev. Mol. Cell Biol.

Marc, P., Margeot, A., Devaux, F., and Blugeon, C. (2002). Genome-wide analysis of mRNAs targeted to yeast mitochondria. Embo ….

Melnikov, S., Ben-Shem, A., Garreau de Loubresse, N., Jenner, L., Yusupova, G., and Yusupov, M.

(2012). One core, two shells: bacterial and eukaryotic ribosomes. Nat. Struct. Mol. Biol. 19, 560–567.

Monda, J.K., Scott, D.C., Miller, D.J., Lydeard, J., King, D., Harper, J.W., Bennett, E.J., and Schulman, B.A. (2013). Structural conservation of distinctive N-terminal acetylation-dependent interactions across a family of mammalian NEDD8 ligation enzymes. Structure 21, 42–53.

Morano, K.A., Grant, C.M., and Moye-Rowley, W.S. (2012). The response to heat shock and oxidative stress in Saccharomyces cerevisiae. Genetics.

Mumberg, D., Müller, R., and Funk, M. (1995). Yeast vectors for the controlled expression of heterologous proteins in different genetic backgrounds. Gene 156, 119–122.

Myklebust, L.M., Van Damme, P., and Stove, S.I. (2014). Biochemical and cellular analysis of Ogden syndrome reveals downstream Nt-acetylation defects. Human Molecular ….

Nillegoda, N.B., Theodoraki, M.A., Mandal, A.K., Mayo, K.J., Ren, H.Y., Sultana, R., Wu, K., Johnson, J., Cyr, D.M., and Caplan, A.J. (2010). Ubr1 and Ubr2 function in a quality control pathway for degradation of unfolded cytosolic proteins. Mol. Biol. Cell 21, 2102–2116.

Oh, E., Becker, A.H., Sandikci, A., Huber, D., Chaba, R., Gloge, F., Nichols, R.J., Typas, A., Gross, C.A., Kramer, G., et al. (2011). Selective ribosome profiling reveals the cotranslational chaperone action of trigger factor in vivo. Cell 147, 1295–1308.

Pang, Y., Poruri, K., and Martinis, S.A. (2014). tRNA synthetase: tRNA aminoacylation and beyond. Wiley Interdisciplinary ….

Park, E.C., and Szostak, J.W. (1992). ARD1 and NAT1 proteins form a complex that has N-terminal acetyltransferase activity. The EMBO Journal 11, 2087–2093.

Pech, M., Spreter, T., Beckmann, R., and Beatrix, B. (2010). Dual binding mode of the nascent polypeptide-associated complex reveals a novel universal adapter site on the ribosome. Journal of Biological Chemistry 285, 19679–19687.

Pechmann, S., Willmund, F., and Frydman, J. (2013). The ribosome as a hub for protein quality control. Mol. Cell.

Perrot, M., Massoni, A., and Boucherie, H. (2008). Sequence requirements for N α-terminal acetylation of yeast proteins by NatA. Yeast 25, 513–527.

Polevoda, B., and Sherman, F. (2001). NatC Nα-terminal acetyltransferase of yeast contains three subunits, Mak3p, Mak10p, and Mak31p. Journal of Biological Chemistry.

Polevoda, B., Cardillo, T.S., Doyle, T.C., Bedi, G.S., and Sherman, F. (2003). Nat3p and Mdm20p Are Required for Function of Yeast NatB N -terminal Acetyltransferase and of Actin and Tropomyosin. Journal of Biological Chemistry 278, 30686–30697.

Polevoda, B., Hoskins, J., and Sherman, F. (2009). Properties of Nat4, an N -Acetyltransferase of Saccharomyces cerevisiae That Modifies N Termini of Histones H2A and H4. Mol. Cell. Biol. 29, 2913–2924.

Polevoda, B., Brown, S., Cardillo, T.S., Rigby, S., and Sherman, F. (2008a). Yeast Nα-terminal acetyltransferases are associated with ribosomes. J. Cell. Biochem. 103, 492–508.

Polevoda, B., Brown, S., Cardillo, T.S., Rigby, S., and Sherman, F. (2008b). Yeast Nα-terminal acetyltransferases are associated with ribosomes. J. Cell. Biochem. 103, 492–508.

Popp, B., Støve, S.I., Endele, S., Myklebust, L.M., Hoyer, J., Sticht, H., Azzarello-Burri, S., Rauch, A., Arnesen, T., and Reis, A. (2015). De novo missense mutations in the NAA10 gene cause severe non-syndromic developmental delay in males and females. Eur. J. Hum. Genet. 23, 602–609.

Protter, D., and Parker, R. (2016). Principles and properties of stress granules. Trends in Cell Biology.

Ravid, T., and Hochstrasser, M. (2008). Degradation signal diversity in the ubiquitin-proteasome system. Nat. Rev. Mol. Cell Biol.

Reggiori, F., and Klionsky, D.J. (2013). Autophagic processes in yeast: mechanism, machinery and regulation. Genetics 194, 341–361.

Scott, D.C., Monda, J.K., Bennett, E.J., Harper, J.W., and Schulman, B.A. (2011). N-Terminal Acetylation Acts as an Avidity Enhancer Within an Interconnected Multiprotein Complex. Science 334, 674–678.

Selevsek, N., Chang, C.-Y., Gillet, L.C., Navarro, P., Bernhardt, O.M., Reiter, L., Cheng, L.-Y., Vitek, O., and Aebersold, R. (2015). Reproducible and consistent quantification of the Saccharomyces cerevisiae proteome by SWATH-mass spectrometry. Mol. Cell Proteomics 14, 739–749.

Setty, S.R.G., Strochlic, T.I., Tong, A.H.Y., Boone, C., and Burd, C.G. (2004). Golgi targeting of ARF-like GTPase Arl3p requires its Nα-acetylation and the integral membrane protein Sys1p. Nat Cell Biol 6, 414–419.

Shaner, L., Wegele, H., Buchner, J., and Morano, K.A. (2005). The yeast Hsp110 Sse1 functionally interacts with the Hsp70 chaperones Ssa and Ssb. J. Biol. Chem. 280, 41262–41269.

Shao, S., and Hegde, R.S. (2014). Reconstitution of a minimal ribosome-associated ubiquitination pathway with purified factors. Mol. Cell 55, 880–890.

Shao, S., Malsburg, von der, K., and Hegde, R.S. (2013). Listerin-dependent nascent protein ubiquitination relies on ribosome subunit dissociation. Mol. Cell 50, 637–648.

Shemorry, A., Hwang, C.-S., and Varshavsky, A. (2013). Control of Protein Qualityand Stoichiometries by N-Terminal Acetylation and the N-End Rule Pathway. Mol. Cell 50, 540–551.

Shevchenko, A., Tomas, H., Havlis, J., and Olsen, J.V. (2007). In-gel digestion for mass spectrometric characterization of proteins and proteomes. Nat Protoc.

Shieh, Y.-W., Minguez, P., Bork, P., Auburger, J.J., Guilbride, D.L., Kramer, G., and Bukau, B. (2015). Operon structure and cotranslational subunit association direct protein assembly in bacteria. Science 350, 678–680.

Simpson, C.E., and Ashe, M.P. (2012). Adaptation to stress in yeast: to translate or not?

Song, O.-K., Wang, X., Waterborg, J.H., and Sternglanz, R. (2003). An Nα-Acetyltransferase Responsible for Acetylation of the N-terminal Residues of Histones H4 and H2A. Journal of Biological Chemistry 278, 38109–38112.

Starheim, K.K., Gevaert, K., and Arnesen, T. (2012a). Protein N-terminal acetyltransferases: when the start matters. Trends Biochem. Sci.

Starheim, K.K., Gevaert, K., and Arnesen, T. (2012b). Protein N-terminal acetyltransferases: when the start matters. Trends Biochem. Sci. 37, 152–161.

Stoecklin, G., Knop, M., Mogk, A., and Bukau, B. (2015). Systemic control of protein synthesis through

sequestration of translation and ribosome biogenesis factors during severe heat stress. Febs ….

Szklarczyk, D., Franceschini, A., and Kuhn, M. (2010). The STRING database in 2011: functional interaction networks of proteins, globally integrated and scored. Nucleic Acids ….

Teixeira, M.C., Monteiro, P., Jain, P., Tenreiro, S., Fernandes, A.R., Mira, N.P., Alenquer, M., Freitas, A.T., Oliveira, A.L., and Sá-Correia, I. (2006). The YEASTRACT database: a tool for the analysis of transcription regulatory associations in Saccharomyces cerevisiae. Nucleic Acids Research 34, D446–D451.

Tong, A., and Boone, C. (2007). 16 High-Throughput Strain Construction and Systematic Synthetic Lethal Screening in. Methods in Microbiology.

Tyanova, S., Temu, T., Sinitcyn, P., Carlson, A., Hein, M.Y., Geiger, T., Mann, M., and Cox, J. (2016). The Perseus computational platform for comprehensive analysis of (prote)omics data. Nat. Methods 13, 731–740.

Van Damme, P., Hole, K., Pimenta-Marques, A., Helsens, K., Vandekerckhove, J., Martinho, R.G., Gevaert, K., and Arnesen, T. (2011). NatF contributes to an evolutionary shift in protein N-terminal acetylation and is important for normal chromosome segregation. PLoS Genet 7, e1002169.

Van Damme, P., Lasa, M., Polevoda, B., Gazquez, C., Elosegui-Artola, A., Kim, D.S., De Juan-Pardo, E., Demeyer, K., Hole, K., Larrea, E., et al. (2012). N-terminal acetylome analyses and functional insights of the N-terminal acetyltransferase NatB. Proc. Natl. Acad. Sci. U.S.a. 109, 12449–12454.

Varshavsky, A. (2011). The N-end rule pathway and regulation by proteolysis. Protein Science.

Verghese, J., Abrams, J., Wang, Y., and Morano, K.A. (2012). Biology of the heat shock response and protein chaperones: budding yeast (Saccharomyces cerevisiae) as a model system. Microbiol. Mol. Biol. Rev. 76, 115–158.

Verma, R., Oania, R.S., Kolawa, N.J., and Deshaies, R.J. (2013). Cdc48/p97 promotes degradation of aberrant nascent polypeptides bound to the ribosome. Elife 2, e00308.

Wallace, E.W.J., Kear-Scott, J.L., Pilipenko, E.V., Schwartz, M.H., Laskowski, P.R., Rojek, A.E., Katanski, C.D., Riback, J.A., Dion, M.F., Franks, A.M., et al. (2015). Reversible, Specific, Active Aggregates of Endogenous Proteins Assemble upon Heat Stress. Cell 162, 1286–1298.

Wang, X. (2004). Importance of the Sir3 N Terminus and Its Acetylation for Yeast Transcriptional Silencing. Genetics 168, 547–551.

Warner, J.R. (1999). The economics of ribosome biosynthesis in yeast. Trends Biochem. Sci.

Wells, J.N., and Bergendahl, L.T. (2015). Co-translational assembly of protein complexes. Biochemical Society ….

Williams, C.C., Jan, C.H., and Weissman, J.S. (2014). Targeting and plasticity of mitochondrial proteins revealed by proximity-specific ribosome profiling. Science 346, 748–751.

Willmund, F., del Alamo, M., Pechmann, S., Chen, T., Albanèse, V., Dammer, E.B., Peng, J., and Frydman, J. (2013). The cotranslational function of ribosome-associated Hsp70 in eukaryotic protein homeostasis. Cell 152, 196–209.

Wilson, D.N., and Doudna Cate, J.H. (2012). The Structure and Function of the Eukaryotic Ribosome. Cold Spring Harbor Perspectives in Biology 4, a011536–a011536.

Xue, S., and Barna, M. (2012). Specialized ribosomes: a new frontier in gene regulation and organismal biology. Nat. Rev. Mol. Cell Biol. 13, 355–369.

Yam, A.Y.-W., Albanèse, V., Lin, H.-T.J., and Frydman, J. (2005). Hsp110 cooperates with different cytosolic HSP70 systems in a pathway for de novo folding. J. Biol. Chem. 280, 41252–41261.

Yusupova, G., and Yusupov, M. (2014). High-resolution structure of the eukaryotic 80S ribosome. Annu. Rev. Biochem. 83, 467–486.

Zhang, Y., Berndt, U., Gölz, H., and Tais, A. (2012). NAC functions as a modulator of SRP during the early steps of protein targeting to the endoplasmic reticulum. Molecular Biology of ….

10 Acknowledgments

I would like to acknowledge the Helmholtz International Graduate School for Cancer Research at the German Cancer Research Center (DKFZ) at Heidelberg, for supporting my PhD with a three years fellowship.

I would like to acknowledge Prof. Bernd Bukau and Dr. Guenter Kramer for supervising my PhD project, Ulrike Friedrich (PhD student at Bukau lab) for collaborating on this project, and all the members of the Bukau lab for the interesting discussions and feedback.

I would like to acknowledge Dr. Bernd Hessling, Dr. Annette Scharf, Dr. Thomas Ruppert and all members of the Core Facility for Mass Spectrometry & Proteomics (CFMP) at the ZMBH for helping me to perform the quantitative proteomics analysis. I would also like to thank Dr. Bernd Hessling for helping with the quantitative-proteomics analysis of N-terminally acetylated peptides.

I would like to acknowledge the Genomics and Proteomics Core Facility at the DKFZ for deep sequencing of the ribosome profiling samples.

I would like to acknowledge Prof. Michael Knop, Dr. Anton Khmelinskii, and all members of the Knop lab at the ZMBH, for sharing their tandem fluorescent timer library as well as providing feedback throughout the tandem fluorescent timer screen. In addition, I would also like to acknowledge Dr. Joseph Barry (from the EMBL-Heidelberg) for the analysis of the tandem fluorescent timer screen data.

I would like to acknowledge Prof. Dr. Ruedi Aebersold as well as Dr. Ludovic Gillet at ETH-Zurich, for helping us to perform the SWATH-based proteomics analysis.

I would like to acknowledge Prof. Marius Lemberg and Prof. Michael Knop for being members of my thesis advisory committee, and for the interesting discussions and feedback.

In addition, I would also like to thank the secretary team of Bukau lab: Ms. Jutta Rami and Ms. Ina Baro for helping me with finalizing my official documents, as well as the kitchen team of the ZMBH for preparing lab ware, media and reagents, in addition to members of the ZMBH's computer department for helping me with my computer and software.